

# ORS 48<sup>th</sup> International Musculoskeletal Biology Workshop at Sun Valley

## Abstract Book

July 25 – 28, 2019

Sun Valley, Idaho

The ORS 48<sup>th</sup> International Musculoskeletal Biology Workshop appreciates the generous contributions from the following supporters:

Level 1



Level 2



Level 3



*This material is based upon work supported by the National Science Foundation under Grant No. 1930757. Any opinions, findings, and conclusions or recommendations expressed in this material are those of the author(s) and do not necessarily reflect the views of the National Science Foundation.*

The ORS 48<sup>th</sup> International Musculoskeletal Biology Workshop would like to recognize all those who participated in the Mentor Program

### Mentees

Heather Allaway  
Joel Boerckel  
Lauren Boller  
Chike Cao  
Jennifer Coulombe  
Shawon Debnath  
Adam Ferrari  
Michael Friedman  
Matthew Grol  
Nilsson Holguin  
Zixue Jin  
Ha-Neui Kim  
Sarah Little  
Phillip Newton  
Anne Nichols  
Amy Sato  
Steve Schlecht  
Lester Smith  
Vidyani Suryadevara  
Michael Sutton  
Josephine Tauer  
Ericka von Kaeppler  
Christian Wright  
Jinhu Xiong

### Mentors

Teresita Bellido  
Brendan Boyce  
David Burr  
Thomas Carpenter  
Kathleen Derwin  
Virginia Ferguson  
Braden Fleming  
David Fyhrie  
Farshid Guilak  
Chris Hernandez  
Alice Huang  
Lisa Larkin  
Alayna Loiselle  
Helen Lu  
Regis O'Keefe  
Maurizio Pacifici  
Alex Robling  
Javier San Martin  
Rick Sumner  
Marjolein van der Meulen  
Deepak Vashishth  
Jennifer Westendorf  
Lianping Xing  
Elizabeth Zimmerman






## Schedule-At-A-Glance

**Wednesday, July 24, 2019**

3:00 PM – 5:30 PM	Registration Open	Limelight B Promenade
7:00 PM – 10:00 PM	<b>Netowrking Reception</b> <i>With support provided by:</i> 	Dr. Robling's Condo

**Thursday, July 25, 2019**

**Limelight B**

<i>General contributions provided to the workshop by:</i>	     <p>This material is based upon work supported by the National Science Foundation under Grant No. 1930757. Any opinions, findings, and conclusions or recommendations expressed in this material are those of the author(s) and do not necessarily reflect the views of the National Science Foundation.</p>
---	---

7:00 AM – 8:00 AM	<b>Breakfast</b>
-------------------	------------------

8:00 AM - 9:15 AM	<b>Welcome &amp; Plenary Session: The Remodeling in Bone (RIB) Award and Presentation</b> Rib Awardee: David Burr, PhD ( <i>Indiana University School of Medicine</i> ) How Basic Science Can Result in Clinical Insights
-------------------	---

9:30 AM - 10:00 AM	<b>Blue Ribbon Sun Valley Posters</b> Chair: Teresita Bellido, PhD ( <i>Indiana University</i> )
	<b>Disruption of LINC Complex in Stem Cells Results in Decreased Osteogenesis and Trabecular Architecture</b> Scott Birks ( <i>University of Boise</i> )
	<b>Regulation of Tendon Formation by Ca<sup>2+</sup> Signaling Through CaV1.2 L-type Voltage-gated Calcium Channel</b> Chike Cao, PhD ( <i>Weill Cornell Medicine</i> )
	<b>Disruption of Notch Signaling Targeted to the Myeloma Bone Marrow Microenvironment Simultaneously Inhibits Tumor Growth and Prevents Bone Loss Without Inducing Gut Toxicity</b> Adam Ferrari, BS, MS ( <i>Indiana University School of Medicine</i> )
	<b>The Fibrodysplasia Ossificans Progressiva-causing ACVR1[R206H] and ACVR1[R258G] Mutations Exhibit Distinct Skeletal Phenotypes In Neonatal Mice</b> Lily Huang ( <i>Regeneron Pharmaceuticals, Inc.</i> )
	<b>Isolation of Differentially Activated Tendon Cell Populations</b> Anne Nichols, PhD ( <i>University of Rochester</i> )

10:15 AM - 12:00 PM	<b>Tendon Biology and Disease</b> Chair: Alayna Loiselle, PhD ( <i>University of Rochester Medical Center</i> )
	<b>Mechanisms of Tendon Regeneration</b> Alice Huang, PhD ( <i>Icahn School of Medicine at Mount Sinai</i> )
	<b>Cellular Basis of Tendon Regeneration</b> Alayna Loiselle, PhD ( <i>University of Rochester Medical Center</i> )
	<b>Engineering Tissue Integration</b> Helen H. Lu, PhD ( <i>Columbia University</i> )

2:00 PM – 4:00 PM	Volleyball	Volleyball Court
-------------------	------------	------------------

7:30 PM - 8:00 PM	<b>Blue Ribbon Sun Valley Posters</b> Chair: Alexander Robling, PhD ( <i>Indiana University</i> )
	<b>Effects of Diet Alterations, With or With Out Gut Microbial Transplants, on Bone Strength and Density</b> Sarah Little, MS ( <i>Texas A&amp;M University</i> )
	<b>Sclerostin Antibody Rescues Hypophosphatemia and Increases Bone Mass in Hyp Mouse Model</b> Ryan Ross, PhD ( <i>Rush University Medical Center</i> )
	<b>The Role of AGEs Accumulation and RAGEs Signaling in Intervertebral Disc Degeneration</b> Simon Tang, PhD ( <i>Washington University in St Louis</i> )
	<b>IL-4 is Protective Against Murine Post-Traumatic Osteoarthritis</b> Ericka von Kaeppler, BS ( <i>Stanford School of Medicine</i> )
	<b>The Primary Cilium and Osteoclastogenesis</b> Michael Sutton, BSE, MS ( <i>Columbia University</i> )

8:00 PM - 10:00 PM	<b>Poster Session</b>
	<b>Alice L. Jee Award Winners</b>
	<b>Impact of Long-acting Reversible Contraceptives on Femoral Bone Density and Mechanical Properties During Simulated Microgravity</b> Heather Allaway, PhD ( <i>Texas A&amp;M University</i> )
	<b>Osteocytes Remodel Bone by TGF-beta-induced YAP/TAZ Signaling</b> Joel Boerckel, PhD ( <i>University of Pennsylvania</i> )
	<b>A Novel Cryo-sectioning Method for Histological Assessment of Bone Remodeling in Nanocrystalline Hydroxyapatite Scaffolds</b> Lauren Boller, BS ( <i>Vanderbilt University</i> )
	<b>Regulation of Tendon Formation by Ca<sup>2+</sup> Signaling Through CaV1.2 L-type Voltage-gated Calcium Channel</b> Chike Cao, PhD ( <i>Weill Cornell Medicine</i> )
	<b>3D Peri-Lacunar Bone Mineral Density Assessment: A Novel Approach</b> Jennifer Coulombe, BS ( <i>University of Colorado</i> )
	<b>Differential Musculoskeletal Response to Unloading in Diversity Outbred Mouse Founder Strains</b> Michael Friedman, PhD ( <i>Virginia Commonwealth University</i> )
	<b>Anabolic Effect of Nitric Oxide on Bone Formation Revealed by Genetic Deficiency of Argininosuccinate Lyase</b> Zixue Jin, PhD ( <i>Baylor College of Medicine</i> )
	<b>Effects of Diet Alterations, With or With Out Gut Microbial Transplants, on Bone Strength and Density</b> Presenter Sarah Little, MS ( <i>Texas A&amp;M University</i> )

8:00 PM – 10:00 PM	<b>Isolation of Differentially Activated Tendon Cell Populations</b> Anne Nichols, PhD ( <i>University of Rochester</i> )
	<b>Advanced Approaches to Bone Biofabrication</b> Lester Smith, PhD ( <i>IUPUI/IUSM</i> )
	<b>The Primary Cilium and Osteoclastogenesis</b> Michael Sutton, BSE, MS ( <i>Columbia University</i> )
	<b>Osteocyte-specific Deletion of the Auxiliary <math>\alpha_2\delta_1</math> Voltage Sensitive Calcium Channel Subunit Results in Impaired Skeletal Strength and Decreases in Both Lean and Fat Masses</b> Christian Wright, PhD ( <i>Indiana University</i> )
	<b>Older Mice Attenuate Compression-induced Intervertebral Disc Degeneration by Suppressing Serpina1 via Wnt Signaling</b> Nilsson Holguin, PhD ( <i>IUPUI</i> )
	<b>Distinct Muscle-specific Ubiquitin Ligases Regulating Bone Microarchitecture in their Unique Ways</b> Vidyani Suryadevara, PhD ( <i>IUPUI</i> )
	<b>Osteoarthritis Award Winner</b>
	<b>IL-4 is Protective Against Murine Post-Traumatic Osteoarthritis</b> Ericka von Kaeppler, BS ( <i>Stanford School of Medicine</i> )
	<b>Charles H. Turner Young Investigator Bone Research Award Winner</b>
	<b>Disruption of Notch Signaling Targeted to the Myeloma Bone Marrow Microenvironment Simultaneously Inhibits Tumor Growth and Prevents Bone Loss Without Inducing Gut Toxicity</b> Adam Ferrari, BS, MS ( <i>Indiana University School of Medicine</i> )
	<b>Submitted Poster Presenters</b>
	<b>Using the Genetic Control of Bone Mineralization for Bone Tissue Engineering</b> Jean-Philippe Berteau, PhD ( <i>College of Stanten Island</i> )
	<b>Disruption of LINC Complex in Stem Cells Results in Decreased Osteogenesis and Trabecular Architecture</b> Scott Birks ( <i>University of Boise</i> )
	<b>Identification of Multiple Maturational Trajectories: A Longitudinal Assessment of Skeletal Age</b> Melanie Boeyer, MS ( <i>University of Missouri</i> )
	<b>Optimization of Sclerostin and Dkk1 Neutralizing Antibody Ratio to Maximize Anabolic Action in the Skeleton</b> Roy Byung-Jun Choi, Msc ( <i>Indiana University School of Medicine</i> )
	<b>Bone-derived Sclerostin has Endocrine Actions in Adipocyte Precursors and Pancreatic Beta-cells</b> Jesus Delgado-Calle, PhD ( <i>Indiana University School of Medicine</i> )
	<b>Pretreatment with Anti-Sclerostin Antibody Protects from Disuse-Induced Bone Loss in the Proximal Tibia of Unloaded Male Rats</b> Jon Paul Elizondo, BS ( <i>Texas A&amp;M University</i> )
	<b>Structural and Compositional Analysis of Bone and its Relevance to Mechanical Properties</b> Pratima Labroo, PhD ( <i>PolarityTE</i> )
	<b>Complete Transcriptomic and Pseudotemporal Analysis of a New Chondro-Osseous Progenitor in Bone Formation</b> Julio Mejia, BS ( <i>Baylor College of Medicine</i> )
	<b>Constitutive Activation of MEK1 in Osteoprogenitors Increases Strength of Mouse Bone Despite Impairing Mineralization</b> Jeffrey Nyman, PhD ( <i>Vanderbilt University Medical Center</i> )
	<b>ACL Femoral Enthesis Degeneration: A Factor to Consider in ACL Reconstruction</b> Daniella Patton, MS ( <i>University of Michigan</i> )

8:00 PM – 10:00 PM	Sclerostin Antibody Rescues Hypophosphatemia and Increases Bone Mass in Hyp Mouse Model Ryan Ross, PhD ( <i>Rush University Medical Center</i> )
	Vitamin D Receptor Signaling Prevents the Adverse Actions of Glucocorticoid Excess in Bone, Skeletal Muscle, and the Heart, by Interfering with the AtroGene Pathway Amy Sato, PhD ( <i>Indiana University School of Medicine</i> )
	Sensate Long Segment Regeneration Scaffolds Can Document Load Changes following Dynamization John Szivek, PhD ( <i>University of Arizona</i> )
	The Role of AGEs Accumulation and RAGEs signaling in Intervertebral Disc Degeneration Simon Tang, PhD ( <i>Washington University in St Louis</i> )

7:00 AM – 8:00 AM	Breakfast	
7:30 AM – 8:00 AM	Regeneron Breakfast Session	
	Cracking the Code of Rare Diseases: Understanding Mechanisms and Developing Therapies Presenter: Aris Economides, PhD	
8:00 AM – 9:00 AM	ASBMR/Harold M. Frost Young Investigator Award Presentations Chair: Teresita Bellido, PhD ( <i>Indiana University</i> )	
	Identification of a Novel Periosteal Stem Cell Population that Mediates Intramembranous Bone Formation Shawnon Debnath, PhD ( <i>Weill Cornell Medicine, Cornell University</i> )	
	Single and Combinatorial Gene Therapy Strategies for Treatment of Post-Traumatic and Genetic Forms of Osteoarthritis Matthew Grol, PhD ( <i>Baylor College of Medicine</i> )	
	Deletion of the Mitochondrial Deacetylase Sirt3 Suppresses Osteoclast Fusion and Increases Bone Mass in Old Mice Ha-Neui Kim, PhD ( <i>University of Arkansas for Medical Sciences</i> )	
9:15 AM - 12:00 PM	Major Methodologies: Material Properties and Tissue Quality - State of the Art Chair: David Burr, PhD ( <i>Indiana University</i> )	
	Introduction – What are the Physical Attributes of Bone Tissue Properties? David Burr, PhD ( <i>Indiana University</i> )	
	Measuring Bone's Structure and Mechanical Behavior at Multiple Length Scales Elizabeth Zimmerman, PhD ( <i>Shriners' Hospital for Children</i> )	
	Measuring Multi-Scale Relationships between Bone Structure, Chemistry and Function and Their Importance to Skeletal Fragility Virginia Ferguson, PhD ( <i>University of Colorado</i> )	
	Does Loss and Modification of Collagenous and Non-Collagenous Proteins Affect Fracture Risk? Tools, Assays and Disease Models Deepak Vashishth, PhD ( <i>Rensselaer Polytechnic Institute</i> )	
	Reducing Fracture Risk by Acellular Manipulation of Bone Tissue Properties David Burr, PhD ( <i>Indiana University</i> )	
1:00 PM – 2:30 PM	Career Development Workshop	
	Career Transitions: Planning and Negotiating for Career Advancement Chair: Marjolein van der Meulen, PhD ( <i>Cornell University</i> ) <ul style="list-style-type: none"> <li>• Mentoring: including transition from mentee to mentor</li> <li>• Resources: start up and facilities, budgets, personnel</li> <li>• Personnel: staffing a lab including recruiting graduate students, technicians &amp; staff, postdocs</li> <li>• PI vs team science: maintaining your own projects and collaborating successfully</li> <li>• Transition considerations and concerns: intangibles and other considerations.</li> <li>• Transitions within industry</li> </ul>	
6:00 PM – 8:00 PM	Awards and Recognition Banquet	Lodge Terrace



7:00 AM – 8:00 AM	Breakfast
7:30 AM – 8:00 AM	<b>Ultragenyx Breakfast Session</b> <b>Understanding Bone Remodeling in XLH: Insight into Restoring Phosphate Homeostasis</b> <i>Presenter: Javier San Martin. MD</i>
8:00 AM – 9:00 AM	<b>ASBMR/Harold M. Frost Young Investigator Award Presentations</b> Chair: Alexander Robling, PhD ( <i>Indiana University</i> ) <b>Serum Bone-Derived Extracellular Vesicles are Associated with Bone Loss with Antiretroviral Therapy in Adults with HIV</b> Erika Marques de Menezes, PhD ( <i>University of California - San Francisco</i> ) <b>Innervation Controls Epiphyseal Stem Cell Niche Performance</b> Phillip Newton, PhD ( <i>Karolinska Institute</i> ) <b>Intra-articular Ablation of Periostin Attenuates Post-traumatic Osteoarthritis in Mice via Canonical Wnt and NFkB Pathways</b> Muhammad Farooq Rai, PhD ( <i>Washington University in St. Louis School of Medicine</i> )
9:15 AM - 12:00 PM	<b>Epigenetics and Musculoskeletal Disease</b> Chair: Regis J. O'Keefe, MD, PhD ( <i>Washington University</i> ) <b>Brief Overview of Epigenetics</b> Regis J. O'Keefe, MD, PhD ( <i>Washington University</i> ) <b>Histone Deacetylase 3 in Cartilage Development and Osteoarthritis</b> Jennifer Westendorf, PhD ( <i>Mayo Clinic</i> ) <b>Defining DNMT3b and Downstream Targets in the Pathogenesis of Osteoarthritis</b> Regis J. O'Keefe, MD, PhD ( <i>Washington University</i> ) <b>Genome-wide DNA Methylation Changes in Mice under Simulated Microgravity Conditions</b> Mario Fraga ( <i>University of Oviedo</i> )
1:00 PM – 2:30 PM	<b>Career Development Workshop</b> <b>Bringing Discoveries to Market: Navigating the FDA</b> Chair: Jose Moreno, PhD ( <i>FDA</i> ) The workshop will provide the audience with an overview of the various mechanisms available to obtain FDA feedback regarding the potential regulatory pathway ahead for any products resulting from their research efforts. This information is of special interest for researches applying to the Small Business Innovation Research (SBIR) and Small Business Technology Transfer (STTR) funding programs, where such regulatory information can have a larger impact in the funding process. Attendees will gain key knowledge regarding the current regulatory pathways for device, drug, biological and combination products, and the mechanisms available to present the results of their research efforts to FDA.

7:30 PM - 9:30 PM	<b>Rare Diseases of Phosphate Handling and Tissue Mineralization: Too Much or Too Little</b> Chair: Javier San Martin ( <i>Ultragenyx, Inc.</i> )
	<b>Introduction to Phosphate Metabolism</b> Javier San Martin ( <i>Ultragenyx, Inc.</i> )
	<b>From Therapeutics Target Identification to Drug Development, with an Anti-FGF23 Antibody, Burosumab</b> Javier San Martin ( <i>Ultragenyx, Inc.</i> )
	<b>Targeting a Unique Pathophysiology for Improved Outcomes in X-linked Hypophosphatemia</b> Thomas Carpenter, MD ( <i>Yale University</i> )
	<b>Pathogenic Mechanisms and Therapeutic Targets for Multiple Osteochondroma, a Pediatric Musculoskeletal Disorder</b> Maurizio Pacifici, PhD ( <i>Children's Hospital of Philadelphia</i> )

7:00 AM – 8:00 AM	Breakfast & Registration
7:50 AM – 8:00 AM	<b>ORS Membership Presentation</b> <i>Presenter: Christopher Hernandez, PhD</i>
8:00 AM - 9:00 AM	<b>ASBMR/Harold M. Frost Young Investigator Award Presentations</b> <i>Chair: Teresita Bellido, PhD (Indiana University)</i>
	<b>Vitamin D Receptor Signaling Prevents the Adverse Actions of Glucocorticoid Excess in Bone, Skeletal Muscle, and the Heart, by Interfering with the Atroгене Pathway</b> <i>Amy Sato, PhD (Indiana University School of Medicine)</i>
	<b>Could Many Non-Contact Anterior Cruciate Ligament Injuries be a Result of Fatigue-Damage Accumulation?</b> <i>Stephan Schlecht, PhD (University of Michigan)</i>
	<b>Osteocalcin Deficiency Rescues Glucose Metabolism in a Model of Severe Osteogenesis Imperfecta</b> <i>Josephine Tauer, PhD (McGill University)</i>
	<b>Stimulation of Piezo1 by Mechanical Signals Promotes Bone Anabolism</b> <i>Jinhu Xiong, PhD (University of Arkansas for Medical Sciences)</i>
9:15 AM - 12:00 PM	<b>Musculoskeletal Regenerative Medicine Meets the Clinic</b> <i>Chair: Lisa Larkin, PhD (University of Michigan)</i>
	<b>Bridge Enhanced ACL Repair: From Concept to Clinical Trial</b> <i>Braden Fleming, PhD (Rhode Island Hospital/Warren Alpert Medical School of Brown University)</i>
	<b>Rotator Cuff Healing: Gaps in Knowledge, Progress and Opportunities</b> <i>Kathleen Derwin, PhD (Cleveland Clinic)</i>
	<b>A Tissue Engineering Approach to Repair Volumetric Muscle Loss</b> <i>Lisa Larkin, PhD (University of Michigan)</i>
12:30 PM – 5:00 PM	<b>Guided Hikes</b>  <b>Pioneer Cabin</b> <i>(rigorous, 8 miles round-trip, led by David Burr)</i>  <b>TBD Location</b> <i>(shorter and easy, led by Sue Bloomfield)</i>  Attendees meet at the back door of the Sun Valley Resort Inn at 12:30 PM
7:30 PM - 9:30 PM	<b>Targeting Musculoskeletal Tissues</b> <i>Chair: Brendan Boyce, MD (University of Rochester Medical Center)</i>
	<b>Introduction to Targeting Strategies</b> <i>Brendan Boyce, MD (University of Rochester Medical Center)</i>
	<b>Targeting Chloroquine and Hydroxychloroquine to Bone to Increase Bone Mass</b> <i>Brendan Boyce, MD (University of Rochester Medical Center)</i>
	<b>Genome Engineering of New Stem Cell Therapies for Arthritis</b> <i>Farshid Guilak, PhD (Washington University)</i>
	<b>Bone-targeting Bortezomib in Pre-clinical Myeloma Studies</b> <i>Lianping Xing, PhD (University of Rochester Medical Center)</i>

General contributions  
provided to the  
workshop by:



This material is based upon work supported by the National Science Foundation under Grant No. 1930757. Any opinions, findings, and conclusions or recommendations expressed in this material are those of the author(s) and do not necessarily reflect the views of the National Science Foundation.

7:00 AM – 8:00 AM

Breakfast

8:00 AM - 9:15 AM

**Welcome & Plenary Session: The Remodeling in Bone (RIB) Award and Presentation**  
Rib Awardee: David Burr, PhD (*Indiana University School of Medicine*)  
How Basic Science Can Result in Clinical Insights

9:30 AM - 10:00 AM

**Blue Ribbon Sun Valley Posters**

Chair: Teresita Bellido, PhD (*Indiana University*)

**Disruption of LINC Complex in Stem Cells Results in Decreased Osteogenesis and Trabecular Architecture**

Scott Birks (*University of Boise*)

**Regulation of Tendon Formation by Ca<sup>2+</sup> Signaling Through CaV1.2 L-type Voltage-gated Calcium Channel**

Chike Cao, PhD (*Weill Cornell Medicine*)

**Disruption of Notch Signaling Targeted to the Myeloma Bone Marrow Microenvironment Simultaneously Inhibits Tumor Growth and Prevents Bone Loss Without Inducing Gut Toxicity**

Adam Ferrari, BS, MS (*Indiana University School of Medicine*)

**The Fibrodysplasia Ossificans Progressiva-causing ACVR1[R206H] and ACVR1[R258G] Mutations Exhibit Distinct Skeletal Phenotypes In Neonatal Mice**

Lily Huang (*Regeneron Pharmaceuticals, Inc.*)

**Isolation of Differentially Activated Tendon Cell Populations**

Anne Nichols, PhD (*University of Rochester*)

10:15 AM - 12:00 PM

**Tendon Biology and Disease**

Chair: Alayna Loiselle, PhD (*University of Rochester Medical Center*)

**Mechanisms of Tendon Regeneration**

Alice Huang, PhD (*Icahn School of Medicine at Mount Sinai*)

**Cellular Basis of Tendon Regeneration**

Alayna Loiselle, PhD (*University of Rochester Medical Center*)

**Engineering Tissue Integration**

Helen H. Lu, PhD (*Columbia University*)

2:00 PM – 4:00 PM

Volleyball

Volleyball Court

7:30 PM - 8:00 PM	<b>Blue Ribbon Sun Valley Posters</b> Chair: Alexander Robling, PhD ( <i>Indiana University</i> )
	<b>Effects of Diet Alterations, With or With Out Gut Microbial Transplants, on Bone Strength and Density</b> Sarah Little, MS ( <i>Texas A&amp;M University</i> )
	<b>Sclerostin Antibody Rescues Hypophosphatemia and Increases Bone Mass in Hyp Mouse Model</b> Ryan Ross, PhD ( <i>Rush University Medical Center</i> )
	<b>The Role of AGEs Accumulation and RAGEs Signaling in Intervertebral Disc Degeneration</b> Simon Tang, PhD ( <i>Washington University in St Louis</i> )
	<b>IL-4 is Protective Against Murine Post-Traumatic Osteoarthritis</b> Ericka von Kaeppler, BS ( <i>Stanford School of Medicine</i> )
	<b>The Primary Cilium and Osteoclastogenesis</b> Michael Sutton, BSE, MS ( <i>Columbia University</i> )

8:00 PM - 10:00 PM	<b>Poster Session</b>
	<b>Alice L. Jee Award Winners</b>
	<b>Impact of Long-acting Reversible Contraceptives on Femoral Bone Density and Mechanical Properties During Simulated Microgravity</b> Heather Allaway, PhD ( <i>Texas A&amp;M University</i> )
	<b>Osteocytes Remodel Bone by TGF-beta-induced YAP/TAZ Signaling</b> Joel Boerckel, PhD ( <i>University of Pennsylvania</i> )
	<b>A Novel Cryo-sectioning Method for Histological Assessment of Bone Remodeling in Nanocrystalline Hydroxyapatite Scaffolds</b> Lauren Boller, BS ( <i>Vanderbilt University</i> )
	<b>Regulation of Tendon Formation by Ca<sup>2+</sup> Signaling Through CaV1.2 L-type Voltage-gated Calcium Channel</b> Chike Cao, PhD ( <i>Weill Cornell Medicine</i> )
	<b>3D Peri-Lacunar Bone Mineral Density Assessment: A Novel Approach</b> Jennifer Coulombe, BS ( <i>University of Colorado</i> )
	<b>Differential Musculoskeletal Response to Unloading in Diversity Outbred Mouse Founder Strains</b> Michael Friedman, PhD ( <i>Virginia Commonwealth University</i> )
	<b>Anabolic Effect of Nitric Oxide on Bone Formation Revealed by Genetic Deficiency of Argininosuccinate Lyase</b> Zixue Jin, PhD ( <i>Baylor College of Medicine</i> )
	<b>Effects of Diet Alterations, With or With Out Gut Microbial Transplants, on Bone Strength and Density</b> Presenter Sarah Little, MS ( <i>Texas A&amp;M University</i> )
	<b>Isolation of Differentially Activated Tendon Cell Populations</b> Anne Nichols, PhD ( <i>University of Rochester</i> )
	<b>Advanced Approaches to Bone Biofabrication</b> Lester Smith, PhD ( <i>IUPUI/IUSM</i> )
	<b>The Primary Cilium and Osteoclastogenesis</b> Michael Sutton, BSE, MS ( <i>Columbia University</i> )
	<b>Osteocyte-specific Deletion of the Auxiliary <math>\alpha_2\delta_1</math> Voltage Sensitive Calcium Channel Subunit Results in Impaired Skeletal Strength and Decreases in Both Lean and Fat Masses</b> Christian Wright, PhD ( <i>Indiana University</i> )
	<b>Older Mice Attenuate Compression-induced Intervertebral Disc Degeneration by Suppressing Serpina1 via Wnt Signaling</b> Nilsson Holguin, PhD ( <i>IUPUI</i> )
	<b>Distinct Muscle-specific Ubiquitin Ligases Regulating Bone Microarchitecture in their Unique Ways</b> Vidyani Suryadevara, PhD ( <i>IUPUI</i> )

8:00 PM - 10:00 PM	<b>Osteoarthritis Award Winner</b>
	<b>IL-4 is Protective Against Murine Post-Traumatic Osteoarthritis</b> Ericka von Kaeppler, BS ( <i>Stanford School of Medicine</i> )
	<b>Charles H. Turner Young Investigator Bone Research Award Winner</b>
	<b>Disruption of Notch Signaling Targeted to the Myeloma Bone Marrow Microenvironment Simultaneously Inhibits Tumor Growth and Prevents Bone Loss Without Inducing Gut Toxicity</b> Adam Ferrari, BS, MS ( <i>Indiana University School of Medicine</i> )
	<b>Submitted Poster Presenters</b>
	<b>Using the Genetic Control of Bone Mineralization for Bone Tissue Engineering</b> Jean-Philippe Berteau, PhD ( <i>College of Staten Island</i> )
	<b>Disruption of LINC Complex in Stem Cells Results in Decreased Osteogenesis and Trabecular Architecture</b> Scott Birks ( <i>University of Boise</i> )
	<b>Identification of Multiple Maturational Trajectories: A Longitudinal Assessment of Skeletal Age</b> Melanie Boeyer, MS ( <i>University of Missouri</i> )
	<b>Optimization of Sclerostin and Dkk1 Neutralizing Antibody Ratio to Maximize Anabolic Action in the Skeleton</b> Roy Byung-Jun Choi, Msc ( <i>Indiana University School of Medicine</i> )
	<b>Bone-derived Sclerostin has Endocrine Actions in Adipocyte Precursors and Pancreatic Beta-cells</b> Jesus Delgado-Calle, PhD ( <i>Indiana University School of Medicine</i> )
	<b>Pretreatment with Anti-Sclerostin Antibody Protects from Disuse-Induced Bone Loss in the Proximal Tibia of Unloaded Male Rats</b> Jon Paul Elizondo, BS ( <i>Texas A&amp;M University</i> )
	<b>Structural and Compositional Analysis of Bone and its Relevance to Mechanical Properties</b> Pratima Labroo, PhD ( <i>PolarityTE</i> )
	<b>Complete Transcriptomic and Pseudotemporal Analysis of a New Chondro-Osseous Progenitor in Bone Formation</b> Julio Mejia, BS ( <i>Baylor College of Medicine</i> )
	<b>Constitutive Activation of MEK1 in Osteoprogenitors Increases Strength of Mouse Bone Despite Impairing Mineralization</b> Jeffrey Nyman, PhD ( <i>Vanderbilt University Medical Center</i> )
	<b>ACL Femoral Enthesis Degeneration: A Factor to Consider in ACL Reconstruction</b> Daniella Patton, MS ( <i>University of Michigan</i> )
	<b>Sclerostin Antibody Rescues Hypophosphatemia and Increases Bone Mass in Hyp Mouse Model</b> Ryan Ross, PhD ( <i>Rush University Medical Center</i> )
	<b>Vitamin D Receptor Signaling Prevents the Adverse Actions of Glucocorticoid Excess in Bone, Skeletal Muscle, and the Heart, by Interfering with the AtroGene Pathway</b> Amy Sato, PhD ( <i>Indiana University School of Medicine</i> )
	<b>Sensate Long Segment Regeneration Scaffolds Can Document Load Changes following Dynamization</b> John Szivek, PhD ( <i>University of Arizona</i> )
	<b>The Role of AGEs Accumulation and RAGEs signaling in Intervertebral Disc Degeneration</b> Simon Tang, PhD ( <i>Washington University in St Louis</i> )

## From Basic Science to Clinical Treatment

David B. Burr, PhD, Indiana Center for Musculoskeletal Health, Indiana University School of Medicine, Indianapolis, IN

This is a story about how asking fundamental questions that initially have no apparent translational value can provide information that contributes to our understanding of clinically-relevant phenomena. Years ago we began by asking a very basic – and apparently useless – question: ***Why is human bone osteonal, whereas these structures in the bones of other animals are few or non-existent?*** We proposed that one function of osteons was to stop cracks and allow for repair. To prove this required that we prove that microcracks in bone were a naturally occurring physiological phenomenon. Harold Frost had originally posited in 1960 [1] that microcracks occur naturally in bone in response to cyclic mechanical loading, and developed a histological technique to clearly demonstrate it, but by the early 1980's very few people outside of the engineering fields believed that bone microdamage was physiological. We were able to validate Frost's en bloc basic fuchsin technique to demonstrate microdamage [2,3] [Fig. 1], and performed a series of experiments to demonstrate that microdamage not only occurred naturally, but

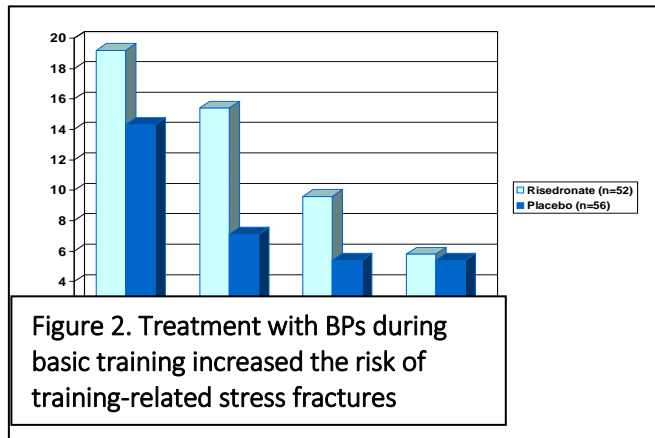


**Figure 1. Microcrack demonstrated using en bloc basic fuchsin staining**

was specifically targeted for repair [4,5]. Subsequently, using a rat model in which osteons did not occur under normal circumstances, others proved that generating microcracks in bone would initiate a remodeling process to remove the cracks [6]. These groups showed that osteocyte signaling was the central mechanism that allowed the bone “to know” that repair was required, and to initiate the processes to remove the damage and renew the bone [7]. The process of targeted remodeling has now been proven many times, and is well accepted. Therefore, early studies were able to show that (1) microdamage occurs naturally; (2) microcracking in bone performs a physiologic as well as mechanical function; and (3) osteocyte apoptosis was the cellular signal to initiate

bone remodeling and repair. Although the idea of targeted remodeling and the exact nature of the cellular signaling mechanisms were not fully understood, by 1990 many accepted the idea that bone microcracking occurred, and that if left unrepaired, microcracks could lead to stress fractures.

Discussions at the Sun Valley Workshop in 1991 were critically important to understanding how anti-remodeling agents that were being developed for the treatment of osteoporosis (but were not yet approved) could represent a risk for the development of stress fractures. Subsequently, we posed a series of experiments to address a second, very basic question: ***What is the purpose of bone remodeling, and what happens if remodeling is entirely suppressed?*** This series of experiments using a non-osteoporotic canine model demonstrated clearly that suppressing bone remodeling by 70% or more using bisphosphonates (BPs) increased bone volume and density, a benefit for the treatment of osteoporosis, but was detrimental to the bone tissue matrix [8-11]. This change to matrix properties reduced bone toughness, making it easier to initiate and grow cracks in bone, and posed a potential risk for creating stress fractures from unrepaired damage. Of course, bone is not loaded quasi-statically in real life, and we subsequently demonstrated that treatment with alendronate (ALN) for 3 years reduced the fatigue life of bone by 3-fold. This led to a more translational question: ***Is the risk of fracture, particularly stress fractures, increased if bone remodeling and repair are suppressed?*** A study using Israeli soldiers during basic training showed that even short term treatment with ALN was associated with an increase in stress fracture risk [12] [Fig. 2]. Although not statistically significant, this suggested that longer-term treatment with BPs could lead to stress fractures.



In 2006, the first report surfaced of unusual subtrochanteric and diaphyseal fractures of the femur. These were dubbed atypical femoral fractures, or AFFs [Fig. 3]. It became apparent over time that these were stress fractures, although different in some morphological respects from athletic or military stress fractures. These were associated with prolonged suppression of bone turnover by BPs that presumably prevented the repair of microdamage. But the pathogenesis of AFFs was not known: *Were AFFs caused by the normal accumulation of*

*unrepaired microdamage over time, or was damage accumulation accelerated by changes to bone matrix caused by the bisphosphonates?* Studies before and after the initial observation of AFFs demonstrated that suppression of bone remodeling allowed the accumulation of advanced glycation end-products

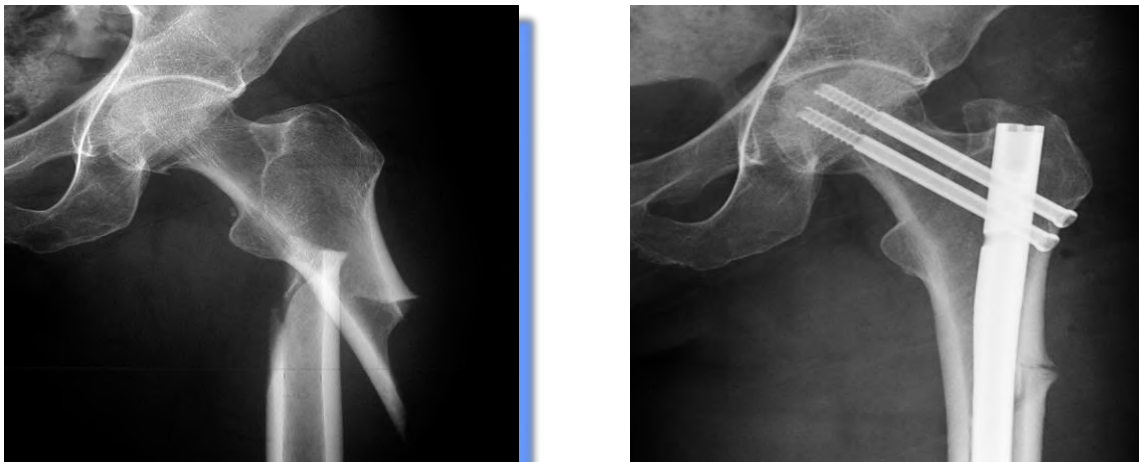
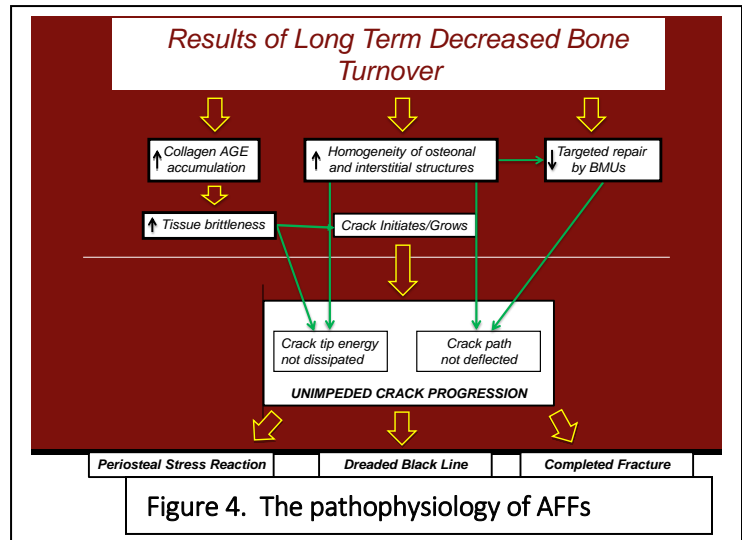


**Figure 3. AFFs begin in the lateral femoral cortex and are characterized by a transverse fracture line, a medial spike, and a periosteal reaction on the lateral cortex**

(AGEs). These intra-fibrillar cross links restricted the ductility of collagen fibers, making the bone tissue more brittle, thereby increasing the initiation and growth of cracks. Thus, in vitro experiments, as well as pre-clinical studies in animal models, were able to demonstrate that the likely cause of AFFs involved changes to bone matrix that allowed the accumulation of bone damage, which could not be repaired because the remodeling mechanism was suppressed [13] [Fig. 4]. This has led to a change in clinical practice in which physicians do not use BPs for preventative treatment, as they did previously, and are now more likely to consider a drug holiday after 5 years of BP treatment.



Thus the bisphosphonate story provides an allegory for how any scientific question – even very basic questions that have no apparent or immediate utility – can provide answers that ultimately inform patient treatment, and improve medical care. The evolution of these ideas was developed at the Sun Valley Workshops, by the people and in discussion with the people who attended. And for that, I thank the Workshop and its many participants over the past 35 years.



#### References:

1. Frost HM. (1960) Bull. Henry Ford Hosp 8:25-35.
2. Burr DB, Stafford T. (1990) Clin Orthop Rel Res 260:305-308.
3. Burr DB, Hooser M. (1995) Bone 17: 431-433.
4. Burr DB et al., (1985) J Biomech 18:189-200.
5. Mori S, Burr DB (1993) Bone 14:103-109.
6. Bentolila V et al. (1998) Bone 23:275-281.
7. Verborgt O et al. (2000) J Bone Miner Res 15:60-67.
8. Mashiba T et al. (2000) J Bone Miner Res 15:613-620
9. Mashiba T et al. (2001) Bone 28:524-531.
10. Allen MR et al. (2006) Bone 39:872-879.
11. Allen MR et al. (2008) Osteoporos Int 19:329-337.
12. Milgrom C et al. (2004) Bone 35:418-424.
13. Ettinger B et al. (2013) Bone 55:495-500.

# Disruption of LINC complex in stem cells results in decreased osteogenesis and trabecular architecture

Scott Birks<sup>1</sup>, Stacie Loiate<sup>1</sup>, Destiny Francis<sup>2</sup>, Sarah Manske, PhD<sup>2</sup>, Gunes Uzer, PhD<sup>1</sup>

<sup>1</sup>Boise State University, Boise, ID, <sup>2</sup>University of Calgary, Calgary, AB, Canada

**INTRODUCTION:** Mesenchymal stem cells (MSCs) are multipotent stem cells within bone marrow that support bone modeling at load bearing sites by differentiating into osteoblasts. We recently reported LINC (Linker of Nucleoskeleton and Cytoskeleton) complexes connecting the nucleus to the cytoskeleton play an integral role in MSC response to mechanical challenge by regulating nuclear access of  $\beta$ catenin (1). In this way, depleting LINC complexes results in increased adipogenic bias of MSCs (2). Therefore, we hypothesize that disabling LINC complex function *in vitro* and *in vivo* will negatively impact osteogenesis in MSCs.

**METHODS:** *In vitro*, a dominant negative form of the nesprin KASH domain (DNK) was overexpressed as previously described (2). Osteogenic differentiation was assessed at day 7 by measuring alkaline phosphatase (ALP) mRNA levels via qPCR. For *in vivo* studies, a tamoxifen inducible Cre/Lox mouse model was generated with Cre-mediated disruption of LINC complexes in skeletal MSCs. Briefly, male Tg(Prrx1-cre/ERT2,-EGFP) mice (The Jackson Laboratory) were crossed with female Tg(<sup>HSAfllox</sup>CAG-LacZ/EGFP-KASH2) mice (Didier Hodzic, Washington University School of Medicine in St. Louis) to produce offspring with Cre-mediated EGFP-KASH2 overexpression. Cre expression driven by the Prrx1 promoter was chosen as the Prrx1 gene is shown to be active in bone progenitor cells (3). LINC complex disruption by EGFP-KASH2 overexpression inhibits endogenous nesprin-SUN binding within the nuclear envelope, delocalizing nesprin from the nucleus; thus, disconnecting the nucleus from cytoskeleton (4). Tamoxifen administration began at 7 weeks using +Cre/+LacZ or +Cre/-LacZ male mice and bone endpoints for microCT were collected at 7, 9, and 12 weeks (n=3/group). All procedures approved by Boise State University Institutional Animal Care and Use Committee.

**RESULTS AND DISCUSSION:** As seen in Figure 1, MSCs plated on plastic expressing DNK showed a 61% (p=0.09) decrease in mRNA ALP levels compared to empty plasmid controls. Shown in Table 1, compared to +Cre/-LacZ controls: bone fraction (BV/TV) in +Cre/+LacZ groups was decreased 26% (p=0.1), trabecular separation (Tb. Sp.) was increased by 73% (p=0.09), trabecular number (Tb.N.) was decreased by 35% (p<0.05), and trabecular thickness (Tb.Th.) did not change. Our findings suggest LINC deficiency negatively effects osteogenesis *in vitro* and results in inferior trabecular architecture *in vivo*. We are currently investigating a tamoxifen independent Prrx1-Cre mouse line along with a pre-osteoblastic Osx-Cre strain to study LINC depletion effects on bone growth without the estrogenic effects of tamoxifen (5). Completion of this data will lead to greater understanding of how disrupting LINC-mediated mechanosignaling of bone progenitor cells effects skeletal health *in vivo*.

## REFERENCES:

1. Uzer, G., et al. Sun-mediated mechanical LINC between nucleus and cytoskeleton regulates  $\beta$ catenin nuclear access. Journal of Biomechanics, 2018; 74, 32-40. doi:http://dx.doi.org/10.1016/j.jbiomech.2018.04.013
2. Uzer G, Thompson WR, Sen B, et al. Cell Mechanosensitivity to Extremely Low Magnitude Signals is Enabled by a LINCed Nucleus. Stem cells (Dayton, Ohio). 2015; 33(6):2063-2076. doi:10.1002/stem.2004.
3. Ouyang Z, Chen Z, Ishikawa M, et al. Prx1 and 3.2 kb Col1a1 promoters target distinct bone cell populations in transgenic mice. Bone. October 2013;S8756-3282(13)00426-210.1016/j.bone.2013.10.016. doi:10.1016/j.bone.2013.10.016.
4. Razafsky D, Hodzic D. Temporal and Tissue-Specific Disruption Of LINC Complexes In Vivo. Genesis (New York, NY : 2000). 2014; 52(4):359-365. doi:10.1002/dvg.22755.
5. Zhong ZA, Sun W, Chen H, et al. Optimizing tamoxifen-inducible Cre/lox system to reduce tamoxifen effect on bone turnover in long bones of young mice. Bone. 2015; 81:614-619. doi:10.1016/j.bone.2015.07.034.

	+Cre/+LacZ	+Cre/-LacZ (control)
BV/TV	0.19±0.04	0.25±0.005
Tb. Sp. (mm)	0.29±0.07	0.17±0.016
Tb.N.	3.82±0.8*	5.87±0.4
Tb.Th. (mm)	0.056±0.002	0.056±0.0006

Table 1 Micro-CT bone morphometry measurements for 9-week mice.

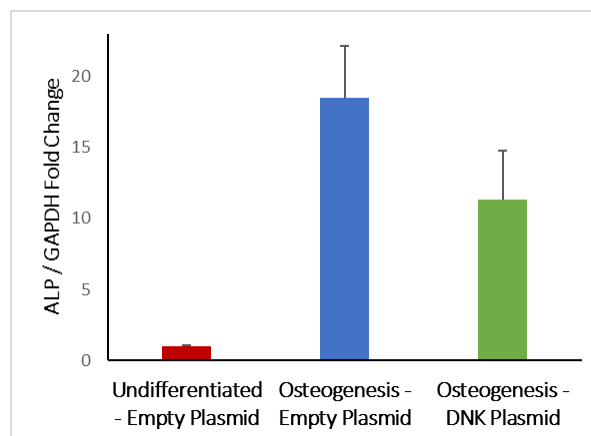


Figure 1 qPCR results probing for alkaline phosphatase expression in undifferentiated MSCs, differentiated MSCs transfected with an empty plasmid, and differentiated MSCs transfected with a DNK plasmid.

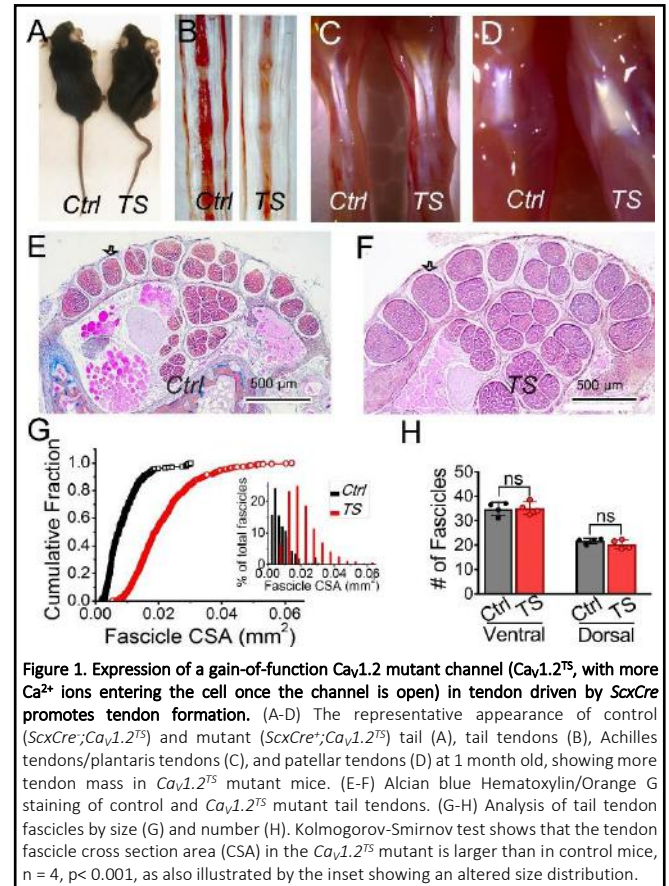
# Regulation of tendon formation by $\text{Ca}^{2+}$ signaling through $\text{Ca}_v1.2$ L-type voltage-gated calcium channel

Chike Cao<sup>1</sup>, Scott A. Rodeo<sup>2</sup>, Christopher L. Mendias<sup>3</sup>, Geoffrey S. Pitt<sup>1</sup>

<sup>1</sup>Cardiovascular Research Institute, Weill Cornell Medical College, New York, NY, USA, 10021; <sup>2</sup>Sports Medicine and Shoulder Service, Hospital for Special Surgery, New York, NY, USA, 10021; <sup>3</sup>Hospital for Special Surgery and Department of Physiology and Biophysics, Weill Cornell Medical College, New York, NY, USA, 10021

Tensile-bearing tendons are highly prone to acute injury and chronic degeneration from overuse, processes called tendinopathies. Therapeutic options for tendinopathies remain few due to limited knowledge about the basic biology underlying tendon development and postnatal tendon growth. While  $\text{Ca}^{2+}$  signals have been implicated in tendon mechanotransduction, acting as second messengers to convert mechanical load to biochemical signals,  $\text{Ca}^{2+}$  signaling details in tendon and the source(s) of the increase in intracellular  $\text{Ca}^{2+}$  in tendon fibroblasts are largely unknown.

$\text{Ca}_v1.2$ , an L-type voltage-gated  $\text{Ca}^{2+}$  channel, allows the influx of  $\text{Ca}^{2+}$  upon cell membrane depolarization and plays critical roles in many physiological processes including neuronal excitability, cardiac contractility, vascular tone, and gene expression. Using a  $\text{Ca}_v1.2$  reporter mouse, we found that  $\text{Ca}_v1.2$  was highly expressed in the developing limb tendons from early embryonic stages (E13.5) and expression remained strong postnatally in tendons and ligaments, suggesting important roles for  $\text{Ca}_v1.2$  channels during tendon development and adult tendon/ligament homeostasis. Consistent with those discoveries, we found that driving expression of a transgenic gain-of-function G406R mutant  $\text{Ca}_v1.2$  ( $\text{Ca}_v1.2^{\text{TS}}$ ) specifically in tendon with *Scleraxis-Cre* (*ScxCre*) leads to a marked increase in tendon mass, including the patellar tendon, Achilles tendon, tail tendons, and trunk tendons. Histological analysis revealed that *ScxCre;Ca\_v1.2^{\text{TS}}* mice at 1 month of age have thicker tail tendon fascicles with a broader size distribution as well as more tendon fibroblasts compared to those of *Cre* negative control littermates. There was no difference in the number of fascicles in both ventral and dorsal sides of the tail. Further, electron microscopic analysis showed that patellar tendons of *ScxCre;Ca\_v1.2^{\text{TS}}* mice displayed an increase in the diameter of collagen fibrils. Taken together, these studies demonstrate that increasing  $\text{Ca}^{2+}$  signaling through  $\text{Ca}_v1.2$  promotes tendon fibroblast proliferation and extracellular matrix collagen synthesis. Our results suggest that enhancing  $\text{Ca}_v1.2$  signaling may be a novel and effective therapeutic strategy for treating tendinopathies.



# Disruption of Notch Signaling targeted to the myeloma bone marrow microenvironment simultaneously inhibits tumor growth and prevents bone loss without inducing gut toxicity

Adam Ferrari, Kevin McAndrews, Jessica Nelson, James Bell, Venkatesan Srinivasan, Frank H. Ebetino, Robert K. Boeckman Jr, G. David Roodman, Teresita Bellido, Jesus Delgado-Calle

Communication between myeloma (MM) cells and cells of the bone marrow via Notch signaling promotes tumor growth/survival and stimulates bone resorption. Systemic inhibition of Notch, using  $\gamma$ -secretase inhibitors (GSIs), decreases MM growth and reduces bone destruction, but the clinical use of GSIs is limited due to dose-limiting severe gut toxicity.

To circumvent GSI side effects, we generated a bone specific Notch inhibitor (BT-GSI) by conjugating GSI-XII to a targeting molecule (BT) with high bone affinity using an acid hydrolyzable linker. *In vitro*, BT-GSI was inactive unless pre-incubated at low pH, and exhibited equal inhibition of Notch target genes in MM cells as unconjugated GSI. *Ex vivo*, BT-GSI decreased Notch expression and reduced MM growth in bone organ cultures that reproduce acidic conditions in the MM-bone microenvironment. *In vivo*, treatment with BT-GSI (5mg/kg/3x/wk, i.p.) for 2 wks decreased Notch signaling in bone more efficiently than unconjugated GSI (10mg/kg/5x/wk, i.p.) in naïve mice. In addition, BT-GSI increased cancellous bone mass (30%) and decreased bone resorption by 40%, without affecting bone formation. In contrast, these parameters remained unchanged by GSI. Next, we examined *in vivo* the impact of BT-GSI on MM growth and bone disease in a preclinical model of established MM. 8-wk-old immunodeficient mice were injected intratibially with  $10^5$  JJN3 human MM (hMM) cells or saline. hMM injected mice exhibited detectable serum levels of the tumor biomarker human K-light chain (40 ng/mL) and visible osteolytic disease (osteolytic area 1.7 mm<sup>2</sup>) 3 wks after hMM inoculation. Then, hMM-injected mice were randomized based on tumor levels to two subgroups to receive either BT-GSI (10mg/kg/3x/wk) or vehicle (DMSO) for 3 wks. Saline-injected mice received vehicle injections. BT-GSI selectively decreased Notch gene expression in bone, but had no effect in the brain or gut. Further, BT-GSI did not increase the expression of Adipsin in the gut, a biomarker of gut toxicity, nor showed evidence of gut toxicity at necropsy. Mice treated with BT-GSI exhibited a 45% decrease in tumor burden (168 vs 254 ng/mL human K-light chain) and 50% less osteolytic area compared to vehicle treated mice bearing hMM (4.4 vs 10.2 mm<sup>2</sup>). Moreover, BT-GSI decreased serum CTX by 30%, but did not affect serum P1NP. Importantly, equimolar administration of the unconjugated BT molecule did not alter MM growth nor prevented bone loss in mice with established MM.

In conclusion, these results show that bone-targeted Notch inhibition reduces MM growth and preserves bone mass in mice with established MM. Because BT-GSI shows bone specific Notch inhibition and lacks gut toxicity, it should circumvent the deleterious side effects that limit GSI use in patients. Thus, BT-GSI is a promising approach to inhibit MM growth and to prevent bone loss in MM patients.

## The fibrodysplasia ossificans progressiva-causing ACVR1[R206H] and ACVR1[R258G] mutations exhibit distinct skeletal phenotypes in neonatal mice.

Lily Huang<sup>1</sup>, John B. Lees-Shepard<sup>1</sup>, Lili Wang<sup>1</sup>, Xialing Wen<sup>1</sup>, Qian Zhang<sup>1</sup>, Vincent Idone<sup>1</sup>, Kalyan Nannuru<sup>1</sup>, Christopher Schoenherr<sup>1</sup>, Andrew J. Murphy<sup>1</sup> and Aris N. Economides<sup>1, 2</sup> and Sarah Hatsell<sup>1</sup>

<sup>1</sup>Regeneron Pharmaceuticals Inc., 777 Old Saw Mill River Road Tarrytown, NY 10591. <sup>2</sup>Regeneron Genetics Center 777 Old Saw Mill River Road Tarrytown, NY 10591

Fibrodysplasia Ossificans Progressiva (FOP), is a rare, autosomal-dominant disorder characterized by seemingly episodic yet cumulative heterotopic ossification (HO) of ligaments, tendons, and select skeletal muscle. It arises from mutations in the cytoplasmic domain of the type I BMP receptor ACVR1. The vast majority of cases carry a mutation that alters Arg206 to a His (R206H). However, other FOP-causing variants of ACVR1 have been described, leading to variations in the severity of HO as well as other manifestations. The two most severe cases described to date arise from ACVR1[R258G] and they exhibit much more severe developmental skeletal and non-skeletal defects and potentially a more robust post-natal HO than that observed in ACVR1[R206H]-bearing FOP patients. We have modeled ACVR1[R258G] in the mouse by engineering the corresponding Cre-regulated 'conditional-ON' allele – *Acvr1*<sup>[R258G]FLEX/+</sup> – similar to the previously described *Acvr1*<sup>[R206H]FLEX/+</sup> mouse (Hatsell, Idone et al. 2015). As observed with *Acvr1*<sup>[R206H]FLEX/+</sup>; *Gt(ROSA26)Sor*<sup>CreERT2/+</sup> mice, body-wide 'activation' of the FOP allele in adult *Acvr1*<sup>[R258G]FLEX/+</sup>; *Gt(ROSA26)Sor*<sup>CreERT2/+</sup> mice (using tamoxifen) resulted in progressive HO, evident radiographically as early as 2 weeks post-induction. When recombination was driven by early-embryonic expression of Cre-recombinase (using Nanog-Cre), both ACVR1[R206H] and ACVR1[R258G] muteins exhibited skeletal deformities and neonatal lethality. However, the skeletal phenotype presented more severely in mice possessing the *Acvr1*[R258G] variant than the *Acvr1*[R206H] variant. These findings are consistent with the increased severity of ACVR1[R258G] relative to ACVR1[R206H] in human FOP. Experiments are presently underway to determine whether ACVR1[R258G] exhibits enhanced ligand-dependent signaling, ligand-independent signaling, and/or neoresponsiveness to other TGFβ or BMP family ligands, and to explore whether any of the yet-to-be-defined differences can account for the increased severity of ACVR1[R258G].

## Isolation of differentially activated tendon cell populations

Anne E.C. Nichols, PhD<sup>1</sup>, Alayna E. Loiselle, PhD<sup>1</sup>

<sup>1</sup>Center for Musculoskeletal Research, University of Rochester Medical Center, Rochester, NY, USA

**Introduction:** Tendon disorders and injuries are common but there are few therapeutic options available due in part to a lack of understanding of fundamental tendon cell biology. Though tendon cells have traditionally been seen as a homogenous population, we have recently demonstrated that expression of the tendon marker Scleraxis (Scx) and/or the small calcium binding protein S100a4 marks several subpopulations of cells within the murine flexor digitorum longus (FDL) tendon *in vivo*, and that both populations contribute to tendon repair<sup>1</sup>. To date, *in vitro* models of tendon cell behavior have not accounted for this cellular heterogeneity and there are therefore conflicting reports regarding the response of tendon cells to various stimuli. With an increasing appreciation for the heterogeneity of tendon cells, we can now determine how these various populations interact, which populations are present in tendon cell cultures *in vitro*, and whether the isolation method affects cell function or the cell populations present. To begin to address these questions, we first investigated how the two most common isolation methods (explant and collagenase digest) affect cell proliferation, and the expression of tendon markers and markers associated with fibroblast activation. We then utilized genetic lineage tracing methods to identify which *in vivo* tendon cell populations are represented *in vitro*.

**Methods:** Cells from FDL tendons were isolated either by collagenase digest (0.075% collagenase II) or migration from tendon explants. Cells were maintained in Fibroblast Growth Medium-2 (Lonza) and serially passaged upon reaching 70% confluence. At each passage, cells were counted, imaged, and collected for gene expression analysis. To determine the different populations present, tendon cells were isolated from S100a4-Cre; Ai9 and Scx-CreER; Ai9 mice (injected with tamoxifen [100 mg/kg] for three days, five days prior to isolation). In the cells derived from Scx-CreER; Ai9 mice, only cells that expressed Scx prior to isolation are labeled red (Scx-lin+), whereas in the S100a4-Cre; Ai9 mice, any cell that has previously or is currently expressing S100a4 is labeled red (S100a4-lin+). Cultures were imaged every two days and the number of lin+ vs. non-lineage (lin-) cells was quantified.

**Results:** A substantial decrease in proliferation was observed in explant cells vs. collagenase digested cells as indicated by increased doubling time (Fig. 1A). Explanted cells had decreased expression of tendon-related genes and a concomitant upregulation of fibroblast activation genes compared to those isolated by collagenase digest (Fig. 1B). In terms of differential lineage enrichment, explant cultures began as ~50% lin+ and lin- for both Scx and S100a4, and both increased in the proportion of lin+ cells over time. In contrast, the proportion of Scx and S100a4 lin+ and lin- cells isolated via collagenase digest remained consistent over time (Fig. 2). The Scx-lin+ labeling regimen suggests the increase in Scx-lin+ cells seen in explanted cells is due to increased proliferation of these cells relative to the lin- cells, while the increase in S100a4-lin+ cells may be attributed to either increased proliferative capacity of these cells or *de novo* expression of S100a4 in additional cells following isolation. Despite the fact that more Scx-lin+ cells were present in explant culture vs. collagenase digested cultures, explant cells had decreased expression of Scx. Combined with the gene expression data, this suggests that activation of resident tendon cells involves downregulation of Scx.

**Discussion:** Here, we demonstrate that loss of tension and migration through an intact extracellular matrix (explant culture) results in an activated cell phenotype relative to cells from which all matrix cues have been removed (collagenase digest), indicating an important role for cell-matrix cues in regulating tendon cell function. To our knowledge, this is the first study to document increased expression of fibroblast activation markers in tendon cells. While the majority of cells in culture are derived from known resident tendon cells populations (Scx-lin+ and S100a4-lin+), we identified an additional novel population of resident tendon cells (Scx-lin-; S100a4-lin-) whose presence is highly dependent on isolation method. Future studies will determine the specific mechanisms involved in matrix-mediated tendon cell activation, the terminal fate of activated tendon cells both *in vitro* and *in vivo*, as well as the functional relationship between the lineage and non-lineage resident tendon cells identified in this study.

**References:** <sup>1</sup>Best 2019 (FASEB)

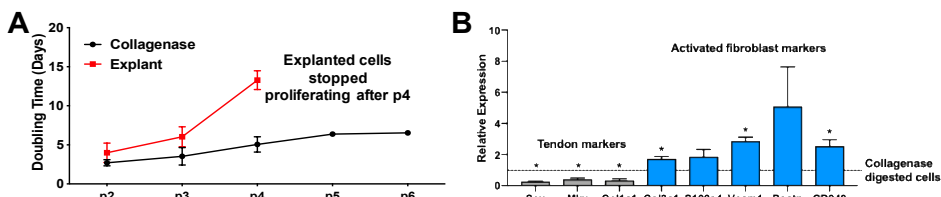


**Figure 1.** Explanted tendon cells were less proliferative (A) and had decreased expression of tendon markers (gray bars) combined with increased expression of fibroblast activation marker genes (blue bars) compared to collagenase digested cells (B). \*p<0.05 compared to collagenase digested cells (n=2).

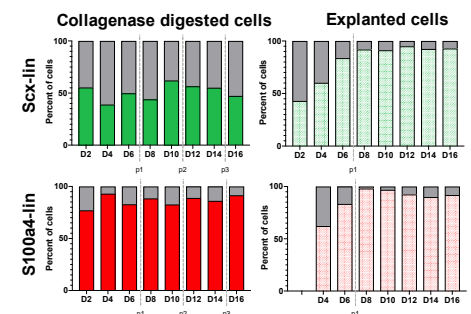


**Figure 2.** Collagenase digested cultures contained both lineage (colored bars) and non-lineage cells (gray bars) in non-varying proportions over time. In contrast, while both Scx-lin+ and S100a4-lin+ cells comprised only ~50% of explanted cells initially, both lineage populations increased to represent >80% of cells present by day 8.

## **Mechanisms of Tendon Regeneration**

*Alice H. Huang, PhD<sup>1</sup>*

*<sup>1</sup>Icahn School of Medicine at Mount Sinai, New York, NY, USA*

Adult tendon heals via fibrosis (scarring), and this failure to re-establish native tendon structure is likely the leading cause of injury recurrence. To date, most models of tendon injury are models of poor, fibrotic healing, which limits the ability to identify regenerative mechanisms. We recently established a novel model of tendon regeneration in neonatal mice following full transection. We showed that regeneration is mediated by recruitment of tenocytes into the injury site leading to full recovery of functional properties. In contrast, adult injury heals by permanent scar and aberrant differentiation of tenocytes to cartilage. While our research largely focuses on the regenerative potential of intrinsic neonatal vs adult tenocytes and putative stem cell populations, the immune environment is also a critical determinant of healing. It is well-established that the neonatal immune system is immature and studies in other tissue and animal models suggest a link between maturity of the immune system and regenerative capacity. Our work in this exciting new area suggests that the neonatal immune response to tendon injury is characterized by rapid polarization to a type 2 phenotype (vs sustained type 1 inflammation in adult) that is driven by distinctive T cell and monocyte populations.

## Cellular Mechanisms of Fibrotic Tendon Healing and Opportunities for Regeneration

Alayna E. Loisel, PhD<sup>1</sup>

<sup>1</sup>University of Rochester Medical Center, Rochester, NY, USA

Effective surgical repair of tendon injuries is limited due to a propensity for scar tissue mediated healing rather than regeneration of native tendon structure. This fibrotic scar tissue results in impaired tendon function due to extracellular matrix (ECM) disorganization and inferior mechanical properties, relative to healthy tendon. Our understanding of the mechanisms that govern fibrotic healing in tendon remains limited, and this gap in knowledge has resulted in a paucity of therapeutic targets to improve clinical outcomes. We and others have recently demonstrated heterogeneity of the resident tendon cell population, in contrast to the previous assumption that the tendon was composed of a uniform population of cells that responded uniformly to injury. Our current work seeks to understand the relative contributions of these cell populations to the healing process, and to delineate the discrete and overlapping functions of these populations. Moreover, we are investigating how resident tendon cell populations and extrinsic cell populations interact to modulate terminal cell fate and to mediate the healing process. Enhancing our understanding of the cellular environment can also facilitate the identification of promising therapeutic targets. For example, we have recently identified S100a4 (S100 calcium binding protein A4) as a key driver of fibrotic tendon healing. S100a4-haploinsufficiency decreases scarring and accelerates improvements in mechanical properties, relative to WT. We originally focused on S100a4 due to its expression in resident tendon cells. However, the beneficial effects of S100a4 are mediated primarily through cell non-autonomous signaling function, and we have identified inhibition of S100a4 signaling as a novel therapeutic approach to promote regenerative tendon healing.



## Engineering Tissue Integration

*Helen H. Lu, PhD<sup>1</sup>*

*<sup>1</sup>Columbia University, Department of Biomedical Engineering, New York, NY, USA*

Heterotypic and homotypic cellular interactions are essential processes for tissue repair and homeostasis, and they are of particular significance at the interface between soft and hard tissues. To test the hypothesis that heterotypic cellular interactions (osteoblasts, fibroblasts, chondrocytes) mediates the regeneration and maintenance of key interfaces such as the fibrocartilaginous ligament-bone enthesis or the osteochondral interface, we have designed 2D and 3D biomaterial-based co-culture and tri-culture models and used them to explore the role of paracrine signaling and cell-cell contact on chondrogenesis. Currently we are studying the contributions of stem cells and cells from the immune system in this complex tissue regeneration process. Findings from these studies will be presented and discussed.

## Effects of Diet Alterations, With or With Out Gut Microbial Transplants, on Bone Strength and Density

Sarah E. Little, MS<sup>1</sup>, Ayland C. Letsinger<sup>1</sup>, Jon P. Elizondo, MS<sup>1</sup>, Heather C.M. Allaway, PhD<sup>1</sup>, Harry A. Hogan, PhD<sup>1</sup>, J. Timothy Lightfoot, PhD<sup>1</sup>, and Susan A. Bloomfield, PhD<sup>1</sup>

<sup>1</sup>Texas A&M University, College Station, TX

High fat feeding has been demonstrated to negatively impact bone quality and bone strength, with exercise as protective against these negative effects<sup>1,2</sup>. However, these studies have employed isocaloric diets to examine low versus high fat diets, rather than a model of over-feeding. Our model of over-feeding utilizes a high fat diet with 20% fructose water and has been shown to reduce voluntary wheel running by ~50-70%<sup>3</sup>. Further, gut microbiota have been strongly linked to bone outcomes, using several models, including germ-free mice, colonized mice, and pro-biotic and pre-biotic supplementation<sup>2,4,5</sup>. A clear mechanism linking alterations in gut microbiota, diet composition and energy content and bone has not yet been elucidated in the literature. As such, we hypothesized that fecal microbiota transplantations (FMT) from healthy, chow-fed mice in combination with a change in diet will reverse the negative impacts of high fat feeding on bone quality and strength.

**METHODS:** 6-week old C57Bl/6 mice (n=10/group) were randomized to normal chow, low-fat (LF) or high fat, high sugar (HFS) diet *ad libitum* for 13 weeks (Tab. 1). After 13 weeks, HFS mice were subsequently randomized to one of three groups: LF diet with fecal metabolic transplants from the LF mice, LF diet with sham FMT using PBS, or HFS diet with FMT from the LF mice for 4 weeks (Tab. 2). All animals were singly housed and had access to a wheel for the duration of the study. Animals were sacrificed at 23 weeks of age. Wheel running distance, duration and speed was assessed daily. Body weight and composition and food and water intake were assessed weekly. Femoral neck strength testing was performed to assess maximal strength (N) using published methods<sup>6</sup>. Statistical analyses were performed using a two-way ANOVA (factors = diet, treatment). Tukey's *post-hoc* test was employed when appropriate. Pearson's correlations were used to examine the relationship between femoral neck strength and six study outcomes. Significance was assessed using an  $\alpha$  of 0.05.

**RESULTS:** Total body weight (TBW) and fat mass (FM) at sacrifice were higher in HFS/HFS+ mice, compared to all other groups ( $p<0.001$ ), though % change in TBW and FM from Week 13-17 revealed loss of both TBW and FM in HFS/LF+ and HFS/LF groups, as compared with LF/LF and HFS/HFS+ mice ( $p<0.001$ ). Total caloric intake from Week 13-17 was reduced in HFS/LF+ and HFS/LF mice compared with LF/LF and HFS/HFS+, with HFS/HFS+ consuming greater calories per day than all other groups ( $p<0.018$ ). Wheel running indices reveal an increase (% change from Week 13-17) in duration, distance and speed in HFS/LF+ and HFS/LF mice compared with LF/LF and HFS/HFS+ mice ( $p<0.011$ ). HFS/HFS+ mice showed greater femoral neck strength as compared to HFS/LF and HFS/LF+ mice ( $p<0.003$ ), with no difference compared to LF/LF mice ( $p=0.077$ ). When normalized to total body weight, however, LF/LF mice had the greatest femoral neck strength compared to all other groups ( $p<0.016$ ). Whole femur bone mineral density (BMD, g/cm<sup>2</sup>) was higher in HFS/HFS+ compared to all other groups ( $p<0.023$ ), though when normalized to body weight, LF/LF mice had the highest BMD ( $p<0.029$ ). Significant correlations were found between femoral neck strength and % change in TBW ( $r=0.559$ ,  $p<0.001$ ), % change in FM ( $r=0.538$ ,  $p<0.001$ ), and % change in running distance ( $r=-0.420$ ,  $p=0.008$ ).

**CONCLUSIONS:** A change in diet from HFS to LF led to decreased total body weight, fat mass, and caloric intake and increased running distance, duration and speed, with no apparent additive effect from the presence of "healthy" gut microbes. Femoral neck strength was significantly reduced in these groups, as compared with no change from the HFS diet. This is likely due to the abrupt decrease in caloric intake and increase in exercise, resulting in a negative energy balance. When controlling for body weight, however, control (LF/LF) mice had stronger femoral necks, suggesting that HFS feeding may impair bone strength.

## REFERENCES:

1. Styner M, Pagnotti GM, McGrath C, Wu X, Sen B, Uzer G, Xie Z, Zong X, Styner MA, Rubin CT, Rubin J. Exercise Decreases Marrow Adipose Tissue Through  $\beta$ -Oxidation in Obese Running Mice. *Journal of Bone and Mineral Research*. 2017 Aug;32(8):1692-702.
2. McCabe LR, Irwin R, Tekalur A, Evans C, Schepper JD, Parameswaran N, Ciancio M. Exercise prevents high fat diet-induced bone loss, marrow adiposity and dysbiosis in male mice. *Bone*. 2018 Mar 29.

3. Vellers HL, Letsinger AC, Walker NR, Granados JZ, Lightfoot JT. High fat high sugar diet reduces voluntary wheel running in mice independent of sex hormone involvement. *Frontiers in physiology*. 2017 Aug 25;8:628.

4. Yan J, Charles JF. Gut microbiome and bone: to build, destroy, or both?.*Current osteoporosis reports*. 2017 Aug 1;15(4):376-84.

5. Weaver CM. Diet, gut microbiome, and bone health. *Current osteoporosis reports*. 2015 Apr ;13(2):125-30.

6. Peng Z, Tuukkanen J, Zhang H, Jamsa T, Vaananen HK: The mechanical strength of bone in different rat models of experimental osteoporosis. *Bone* 15:523-532, 1994.

**FUNDING:** This study was funded by the Omar Smith Endowment via Dr. J. Timothy Lightfoot.

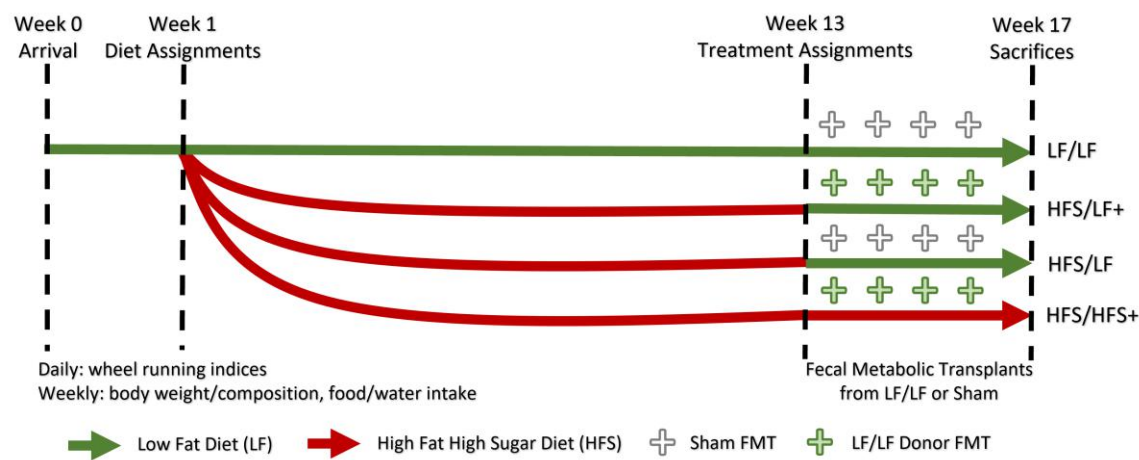


**Figure 1.** Experimental Design Timeline

Macronutrient	Low Fat Diet	High Fat Diet
Carbohydrate	39.5%	35%
Protein	25.2%	20%
Fat	4%	45%
Fiber/Ash	23.3%	0%
Fructose in H <sub>2</sub> O	0%	20%

**Table 1.** Diet composition of experimental diets.

Group ID	Design	Treatment
LF/LF	Low Fat Diet to Low Fat Diet + Sham FMT	Control
HFS/LF+	High Fat High Sugar Diet/Low Fat Diet + FMT	Diet + Microbes
HFS/LF	High Fat High Sugar Diet/Low Fat Diet + Sham FMT	Diet Only
HFS/HFS+	High Fat High Sugar Diet/High Fat High Sugar Diet + FMT	Microbes Only

**Table 2.** Summary of experimental groups.

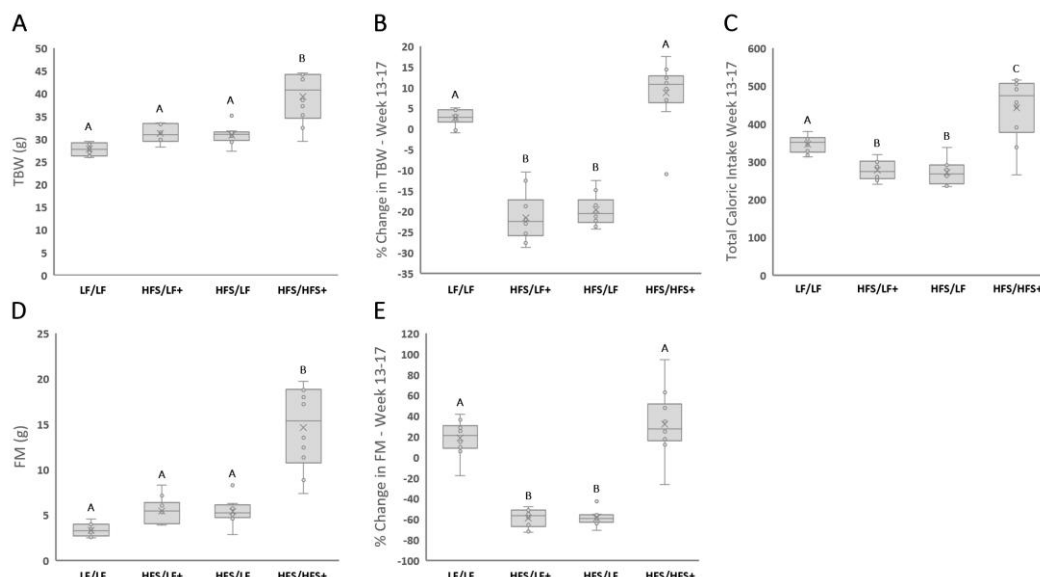


**Figure 2. Body weight, caloric intake and fat mass.** A) Total body weight (TBW, g) at sacrifice. HFS/HFS+ mice had the highest total mass. B) % change in TBW from Week 13-17. HFS/LF+ and HFS/LF mice experienced ~20% loss of total mass. C) Total caloric intake from Week 13-17. HFS/LF+ and HFS/LF mice consumed the fewest calories, while HFS/HFS+ consumed the most. D) Fat mass (FM) at sacrifice. HFS/HFS+ mice had the highest fat mass. E) % change in FM from Week 13-17. HFS/LF+ and HFS/LF mice experiences ~59% reduction in fat mass. Significance assessed using Tukey's *post-hoc* test and  $\alpha$  of 0.05.

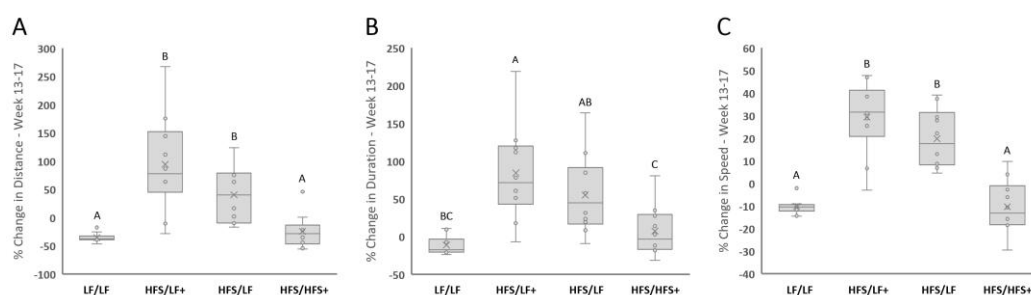


**Figure 3. Wheel running indices.** A) % change in distance from Week 13-17. HFS/LF+ and HFS/LF mice experienced ~95% and ~40% increase in meters run per day, respectively. B) % change in duration from Week 13-17. HFS/LF+ and HFS/LF mice experienced ~84% and ~55% increase in minutes run per day, respectively. C) % change in speed from Week 13-17. HFS/LF+ and HFS/LF mice experienced ~29% and ~19% increase in meters run per minute, respectively. Significance assessed using Tukey's *post-hoc* test and  $\alpha$  of 0.05.

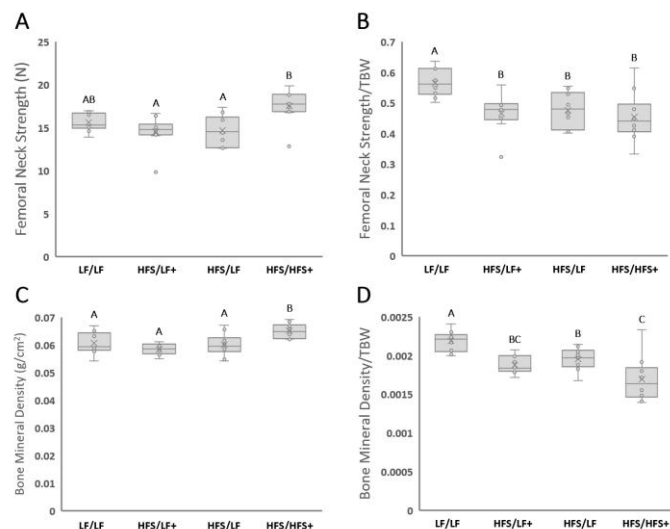


**Figure 4. Femoral neck strength and bone mineral density.** A) Femoral neck strength (N). HFS/HFS+ mice had the greatest absolute strength. B) Femoral neck strength/TBW (N/g). LF/LF mice showed the strongest femoral necks per gram of TBW. C) Whole femur bone mineral density (BMD, g/cm<sup>3</sup>). HFS/HFS+ mice had the greatest BMD. D) Whole femur BMD normalized to TBW. LF/LF mice had the highest BMD per gram of TBW. Significance assessed using Tukey's *post-hoc* test and  $\alpha$  of 0.05.

## Sclerostin antibody rescues hypophosphatemia and increases bone mass in *Hyp* mouse model

Ryan D. Ross, PhD; Kelsey Carpenter, MS - Rush University Medical Center, Chicago, IL USA

X-linked hypophosphatemia (XLH) is the most common form of vitamin-D resistant rickets caused by a loss-of-function mutation in the phosphate regulating gene with homology to endopeptidase located on the X chromosome (PHEX). This mutation leads to elevated fibroblast growth factor 23 (FGF23) levels which subsequently impair phosphate reabsorption in the kidney and inhibit skeletal mineralization. XLH is commonly diagnosed in children who exhibit shortened stature and leg bowing. XLH patients also present with decreased bone mass and are at an increased fracture risk.

Sclerostin, a protein produced primarily in osteocytes, suppresses bone formation by antagonizing Wnt-signaling and is elevated at both the gene level in *Hyp* mice (2,3), the XLH murine homolog, and in the circulation of XLH patients (4). Sclerostin's role in the pathophysiology of XLH has not yet been investigated. We hypothesize that sclerostin is a key regulator of phosphate metabolism and skeletal mineralization and that suppression of sclerostin via sclerostin antibody (Scl-Ab) can improve both metabolic and skeletal pathologies of XLH.

Male hemizygous and female heterozygous *Hyp* mice and wild type littermates were used for this study. Mice were randomly assigned to biweekly subcutaneous injections of either 25 mg/kg Scl-Ab or vehicle (saline) treatment starting at 4-weeks of age until sacrifice at 8 weeks of age. Right femurs were collected for micro-computed tomography ( $\mu$ CT, Scanco  $\mu$ CT50). Cortical area was assessed at the midpoint of the femoral diaphysis, while trabecular bone volume fraction (BV/TV) was assessed at the distal femoral metaphysis, just proximal to the growth plate. Cortical osteoid surface per bone surface (OS/BS) was assessed in histological sections from the distal femur following Goldner's Trichrome staining for unmineralized osteoid. Serum was collected for analysis of circulating phosphate (Biovision) and fibroblast growth factor 23 (FGF23) levels (Immuntopics). Data was compared separately for males and females using a two-way analysis of variance (ANOVA) with genotype and treatment as the independent factors. When main effects were significant post-hoc analysis was performed using an independent student's T-test. A significance threshold of  $p < 0.05$  was set for all primary endpoints.

Scl-Ab treatment increased serum phosphate in treated wild-type and *Hyp* mice of both sexes, with significant treatment effects noted in both males and females (Fig 1a). Scl-Ab treatment significantly suppressed circulating levels of intact FGF23 (Fig 1b). Cortical area and trabecular BV/TV increased with Scl-Ab treatment in both sexes (Fig 2a and 2b, respectively). Scl-Ab treatment significantly reduced the OS/BS in males, with a trend towards significance in the females. The current study demonstrates that short-term treatment of growing *Hyp* mice with Scl-Ab leads to significant improvement in circulating phosphate and bone structure. Surprisingly, there was also a significant reduction in the circulating levels of intact or active FGF23 following Scl-Ab treatment, suggesting that sclerostin influences FGF23 production.

**REFERENCES:** (1) TM Carpenter et al. J Bone Miner Res 2011 26(7): 1381-1388. (2) GJ Atkins et al. J Bone Miner Res 2011 26(7): 1425-1436. (3) LV Zelenchuk et al. Bone 2015 72:23-33. (4) T. Palomo et al. J Clin Endocrinol Metab 2014 99(5):E920-925. **ACKNOWLEDGEMENTS:** Sclerostin antibody provided by Amgen Inc, Thousand Oaks, CA and UCB. Brussels, Belgium.

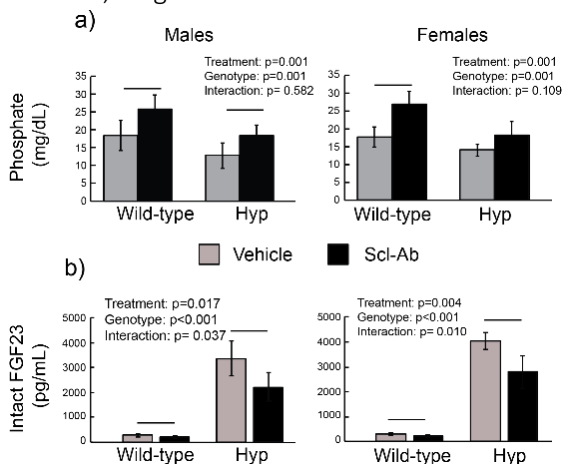


**Figure 1:** Circulating a) phosphate and b) intact FGF23 in male (left) and female (right) mice.

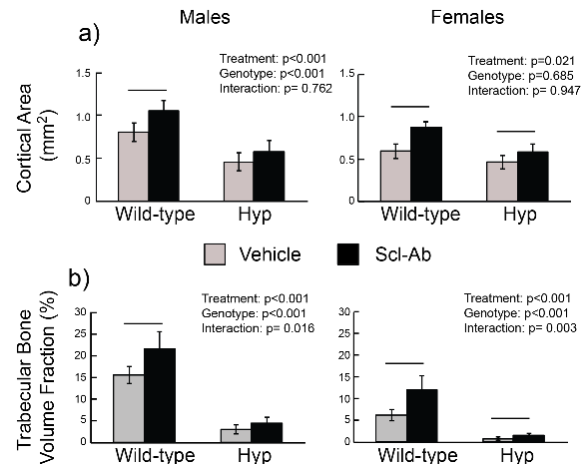


**Figure 2:** a) Cortical area at the femoral mid-diaphysis and b) trabecular BV/TV at the distal femoral metaphysis in male (left) and female (right) mice.

# The Role of AGEs and RAGEs Signaling in Intervertebral Disc Inflammation and Degeneration

Simon Y. Tang<sup>1,2,3</sup>

<sup>1</sup>Washington University in St. Louis, Dept. of Biomedical Engineering, <sup>2</sup>Dept. of Orthopaedic Surgery, <sup>3</sup>Dept. of Mechanical Engineering

**DISCLOSURES:** The authors have nothing to disclose.

**INTRODUCTION:** Lower back pain (LBP), often caused by intervertebral disc (IVD) degeneration, is the leading cause of disability in the US [1]. Understanding the mechanisms IVD degeneration is thus critical for developing therapeutic strategies for treating LBP. Diabetes mellitus is a significant risk factor for IVD degeneration [2,3], and diabetics are susceptible to the accumulation of advanced glycation end-products (AGEs). AGEs diminish the mechanical performance of skeletal tissues including bone and cartilage [4,5]. We have previously shown that AGEs and the upregulation of Receptor for AGEs (RAGE) signaling by High Motility Group Box 1 (HMGB1) increases expression of proteases and inflammatory cytokines, and deteriorates the structure and mechanics of the murine intervertebral disc [6, 7]. Here, we investigate the necessity of RAGE signaling in the AGEs- and HMGB1- mediated degeneration of the intervertebral disc using a global deletion of RAGE in nine-week old mice.

**METHODS:** All animal experiments were done with approval from the Washing University Animal Studies Committee approval. Mice with a global deletion of the RAGE (RAGE KO) [8] along with C57BL/6 WT age and gender matched controls were allowed to age to nine weeks of age (n = 6). The mice were euthanized and 3 lumbar functional spine units (FSU), containing an intact vertebrae-disc-vertebrae structure, from each animal were dissected under aseptic conditions per IACUC approval. The FSU samples were cultured in 2mL of DMEM:F12 supplemented with 20% fetal bovine serum and 1% penicillin-streptomycin. Media was changed every 48 hours. After an initial 48-hour conditioning period, the FSUs from both groups (RAGE KO or WT) are then split further into three groups treated with 100nM of HMGB1 administered once at day 1, 200g/mL of AGEs, or control media throughout the culture period. These samples were then cultured for 21 days. Disc height was measured using a laser micrometer, proteoglycan were measured using biochemical fluorescent assays, and mechanical properties were determined using cyclical dynamic compression [9]. All quantitative analyses were normalized to either the RAGE KO or the WT control groups. Finally, samples were processed for histology and stained with Safranin-O/Fast Green.

## RESULTS:

**A:** Compositional analyses of the IVDs showed that RAGE KO animals significantly blunts the AGEs- and HMGB1- loss of proteoglycans in the IVD ( $p < 0.001$ ;  $p < 0.001$ ). **B:** Likewise, the disc heights in RAGE KO animals for either groups were significantly less than the AGEs- and HMGB1- treated IVDs ( $p < 0.001$ ;  $p < 0.001$ ). **C&D:** Mechanical analyses showed that RAGE KO IVDs had improved stiffness and Tan Delta values at 5% strain levels compared to the WT treated groups ( $p < 0.05$  for all comparisons). **E-G:** Histological analyses show that the RAGE KO IVDs remain structurally intact despite the AGEs- and HMGB-1 treatment.

## DISCUSSION:

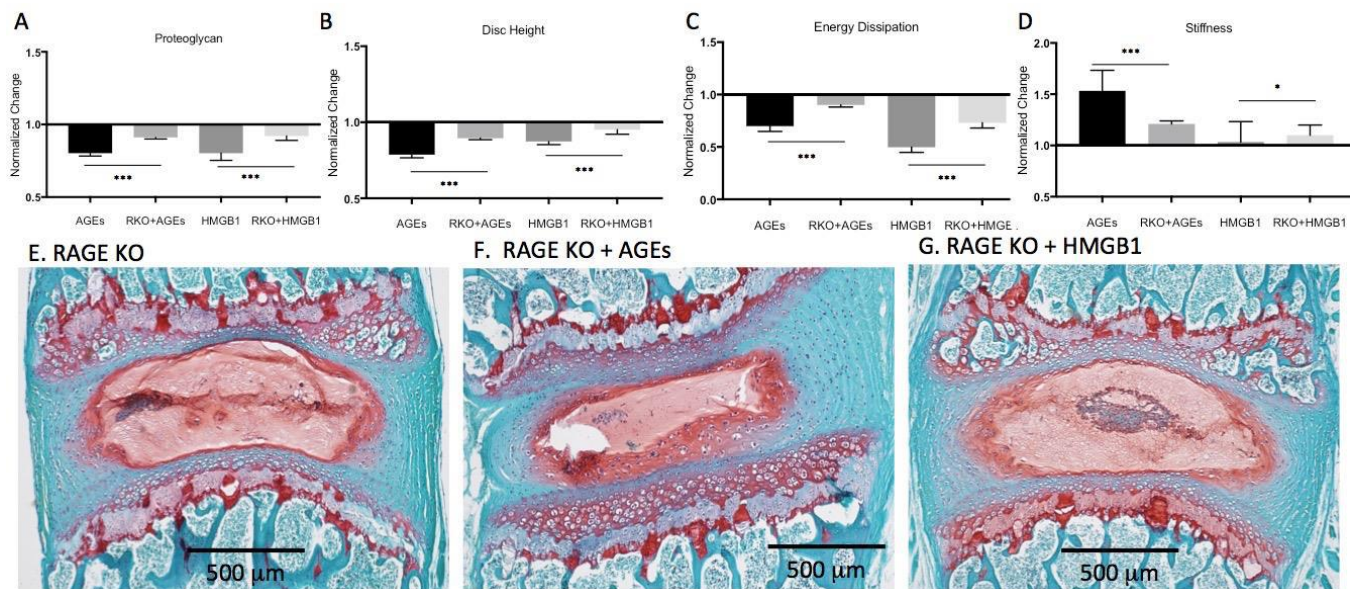
Diabetes increases AGEs accumulation and impairs the mechanical behavior of IVD tissues [10,11]. In this study, the deletion of RAGE appears to have mitigated the adverse effects of AGEs and HMGB1 treatment. We have previously shown that AGEs accumulation and RAGE signaling is elevated in the IVDs of diabetic animals [7]. Furthermore, the AGEs rich environment can stimulate a milieu of inflammatory cytokines including elevated TNF $\alpha$ , NFkB, IL1, as well as depressed TIMPs and increased MMPs that may contribution to inflammation and pain in the IVD. The inhibition of the RAGE pathway may be a viable therapeutic strategy to arrest degeneration and alleviating inflammation relating to pain.

## SIGNIFICANCE:

The deletion of RAGE blunts the AGEs- and HMGB1- mediated degeneration of the IVD and may be a viable therapeutic strategy in diabetes related low back pain and disc degeneration.

**REFERENCES:** [1] Dagenais S et al 2008, [2] Kim RP et al 2001, [3] Ardic F et al 2003, [4] Vlassara H et al 2002, [5] Ahmed N et al 2005 [6] Liu JW et al BMES 2016 [7] Liu JW et al ORS 2017 [8] Liu JW et al 2015 [9] Bierhaus et al 2003. [10] Fields A et al 2015, [11] Illien-Junger S et al 2013.

**ACKNOWLEDGEMENTS:** We would like to acknowledge the Washington University Musculoskeletal Research Center (P30 AR057235), the Washington University Summer Engineering Fellowship, NIH K01 AR069116 and NIH R21AR069804. The authors acknowledge the contributions of Jennifer W Liu in conducting the experiments.



## IL-4 is protective against murine post-traumatic osteoarthritis

Ericka von Kaeppler<sup>1,2</sup>, Harini Raghu<sup>1,2</sup>, Michelle S. Bloom<sup>1,2</sup>, Qian Wang<sup>1,2</sup>, Heidi H. Wong<sup>1,2</sup>, William H. Robinson<sup>1,2</sup>

<sup>1</sup>Stanford University School of Medicine, Palo Alto, CA, <sup>2</sup>VA Palo Alto Health Care System, Palo Alto, CA

evonk@stanford.edu

**Disclosures:** E. von Kaeppler: None. H. Raghu: None. M.S. Bloom: None. Q. Wang: None. H. Wong: None. W.H. Robinson: 8; Associate editor for Arthritis & Rheumatology.

**INTRODUCTION:** Osteoarthritis (OA), the leading cause of joint failure, is characterized by breakdown articular cartilage and remodeling of the underlying bone in synovial joints. Despite the high prevalence and debilitating effects of OA, no disease-modifying drugs currently exist. Increasing evidence implicates a key role for “low-grade” inflammation in the development of OA, though precise mechanisms remain unclear. A better understanding of contributory inflammatory pathways in degenerative joint disease could transform care for individuals with OA. The cytokine IL-4 has been widely implicated in atopic diseases and has known effects on many cell types found in synovial joints. However, the role of IL-4 in the pathogenesis of OA is poorly defined. Preliminary data showed that IL-4 is downregulated in the synovial membranes of individuals with OA, suggesting that IL-4 is protective against the pathogenesis of OA.

**METHODS:** We tested our hypothesis that IL-4 protects against OA pathogenesis by surgically-inducing osteoarthritis by destabilization of the medial meniscus (DMM) in mice that were globally deficient for either IL-4 (*IL-4<sup>-/-</sup>*) or the signaling mediator STAT6 (*STAT6<sup>-/-</sup>*), had a myeloid-specific deficiency in the IL-4 receptor subunit, IL-4R $\alpha$  (*LysMCre-IL-4R $\alpha$ <sup>-/-</sup>*), or were wildtype (WT). Five months post-surgery, tibio-femoral joints were collected, and Safranin-O stained joint sections were scored according to established metrics for OA severity. To further investigate mechanisms underlying this pathway, two myeloid cell types, macrophages and osteoclasts, were cultured, stimulated *in vitro* and assayed for functional and gene expression changes. Peripheral blood mononuclear cell (PBMC)-derived macrophages were harvested and cultured in the presence of recombinant IL-4. Phagocytic capacity of stimulated macrophages was measured by incubating macrophages with cartilage debris that was covalently labeled with PHrodo-Red dye, a dye that emits fluorescence only after internalization into acidified phago-lysosomes. qPCR was used to characterize gene expression (*Tnfa*, *CD206*) in stimulated, cartilage exposed macrophages. Osteoclasts were harvested from bone marrow of WT, *IL-4<sup>-/-</sup>* and *LysMCre-IL-4R $\alpha$ <sup>-/-</sup>* mice and stimulated with recombinant IL-4. Osteoclast differentiation and activation was assayed by measuring tartrate resistant acid phosphatase (TRAP) activity in culture supernatants and by measuring gene expression with qPCR (*Nfatc1*, *Tnfrsf11a*, *Acp5*, *Ctsk*, *Mmp9*, *Calcr*, *Car2*).

All animal studies were performed under protocols approved by the Stanford Administrative Panel on Laboratory Animal Care (APLAC) and VA Palo Alto Animal Component of Research Protocol (ACORP) committee, and in accordance with the guidelines of the US National Institutes of Health.

**RESULTS:** Following DMM, *IL-4<sup>-/-</sup>*, *STAT6<sup>-/-</sup>*, and *LysMCre-IL-4R $\alpha$ <sup>-/-</sup>* mice (n=10, per group) developed exacerbated cartilage damage, osteophyte formation, and synovitis relative to WT controls (n=10). The semi-quantitative disease severity score was statistically significantly higher in *IL-4<sup>-/-</sup>*, *STAT6<sup>-/-</sup>*, and *LysMCre-IL-4R $\alpha$ <sup>-/-</sup>* mice as compared to WT by two-tailed t-test. *In vitro*, IL-4 stimulated macrophages phagocytosed cartilage debris significantly more than unstimulated macrophages. Additionally, in the presence of cartilage debris, IL-4 stimulated macrophages significantly upregulated the alternative macrophage activation (M2) marker *CD206* and significantly downregulated the expression of classical macrophage activation (M1) marker *Tnfa*. *In vitro*, IL-4 stimulation of WT bone marrow-derived osteoclasts significantly reduced TRAP production and inhibited expression of all markers of osteoclast differentiation (*Nfatc1*, *Tnfrsf11a*, *Acp5*) and activation (*Ctsk*, *Mmp9*, *Calcr*, and *Car2*). IL-4 stimulation of *LysMCre-IL-4R $\alpha$ <sup>-/-</sup>* bone marrow-derived osteoclasts did not reduce TRAP production, nor inhibit expression of all markers of osteoclast differentiation (*Nfatc1*, *Tnfrsf11a*, *Acp5*) and activation (*Ctsk*, *Mmp9*, *Calcr*, and *Car2*).

**DISCUSSION:** The exacerbated OA phenotype observed in IL-4-deficient mice supports our hypothesis that IL-4 is protective against OA development. Further, the exacerbated OA phenotype observed in STAT6 deficient mice and in myeloid-specific IL-4R $\alpha$  deficient mice suggests that the IL-4 protective mechanism is mediated through STAT6 signaling in myeloid cell-types. *In vitro*, IL-4 stimulated macrophage M2 polarization and enhanced macrophage phagocytosis of cartilage debris. These data suggested that joint-resident IL-4 might promote an immunomodulatory microenvironment in



which joint-resident macrophages more efficiently clear pro-inflammatory wear-and-tear debris. Additionally, *in vitro*, IL-4 inhibits differentiation and activation of WT bone marrow-derived osteoclasts, but not *LysMCre-IL-4R $\alpha$ <sup>-/-</sup>* bone marrow-derived osteoclasts. These data suggest that the IL-4R $\alpha$  receptor subunit is necessary for osteoclast inhibition by IL-4. These data suggest that IL-4 might promote an anti-osteoclastogenic microenvironment that prevents pathologic activation of subchondral bone osteoclasts in a healthy joint. Taken together, these *in vivo* and *in vitro* results support a role for IL-4 modulation of myeloid cell types in the maintenance of joint health.

**SIGNIFICANCE/CLINICAL RELEVANCE:** (1-2 sentences): Our findings suggest that IL-4 plays a key role in protection against the development of post-traumatic OA, in part, through modulation of myeloid cell types, such as macrophages and osteoclasts. These findings identify a potential novel therapeutic candidate for the treatment of OA.

## The Primary Cilium and Osteoclastogenesis

Michael M. Sutton, MS<sup>1</sup>, Christopher R. Jacobs, PhD<sup>1</sup>

<sup>1</sup>Columbia University, New York, NY

**Introduction:** Osteoporosis, presently affecting more than 200 million people worldwide, is a metabolic bone disease characterized by low bone density and deterioration of bone architecture that ultimately increases the risk of fragility fractures. The physical impairment is compounded by the insufficiency of prophylaxis and treatment options devoid of negative side effects<sup>1,2</sup>. As a result, there is a need to discover better therapeutic solutions to address this disease. Our lab and others have established the osteocyte primary cilium – a mechanosensing, antenna-like organelle – as a promising pharmaceutical target to exploit the body's natural anabolic response to physical loading to maintain bone health<sup>4</sup>. However, little is known about the potential impact of targeting the primary cilium in relation to osteoclasts, the bone resorbing cell. In this work, we share results from preliminary examination of the primary cilium specifically within the context of osteoclasts.

**Methods:** We cultured RAW 264.7 cells (an immortal cell line that is a mixture of monocytes/macrophages) in DMEM supplemented with 10% FBS and 1% P/S, and added 30 ng/mL of macrophage colony stimulating factor (m-CSF); this factor drives the equilibrium of the cell mixture towards macrophages, the precursor of osteoclasts. We then seeded these cells onto glass-bottom dishes and performed double immunocytochemistry (Figure 1A). Next, we cultured the cells in  $\alpha$ MEM supplemented with 10% FBS and 1%P/S and added 33 ng/mL of m-CSF and 66 ng/mL of receptor activator of nuclear factor-Kappa B ligand (RANKL); this is the activating molecule of osteoclastogenesis. We seeded these cells onto glass-bottom dishes and, after ten days, performed ICC again (Figure 1B and 1C).

**Results:** After three independent stains of undifferentiated RAW 264.7 cells, we counted a total of 248 cells and noted a 51% cilia incidence, concluding that osteoclast precursors do in fact possess primary cilia, which was previously unknown. These primary cilia appear spatially aligned as protrusions from the cell's centrosome, as expected. In the osteoclast differentiation study, we again did three independent stains. As a result of a low differentiation percentage, only 41 osteoclasts were counted, none of which had clear or distinct primary cilia. Some stains, however, appear as though macrophages in the process of fusing may still express primary cilia.

**Discussion:** In vertebrates, cilia are found on quiescent cells and on proliferating cells in the G1 phase of the cell cycle; in dividing cells, they are resorbed before S phase or during G2<sup>3</sup>. It is not yet clear to what extent the fusion of macrophages during osteoclastogenesis is related to cell division and cilia resorption on the molecular scale. The primary question that now exists is if, and by what mechanism, macrophage primary cilia regulate osteoclast formation and function.

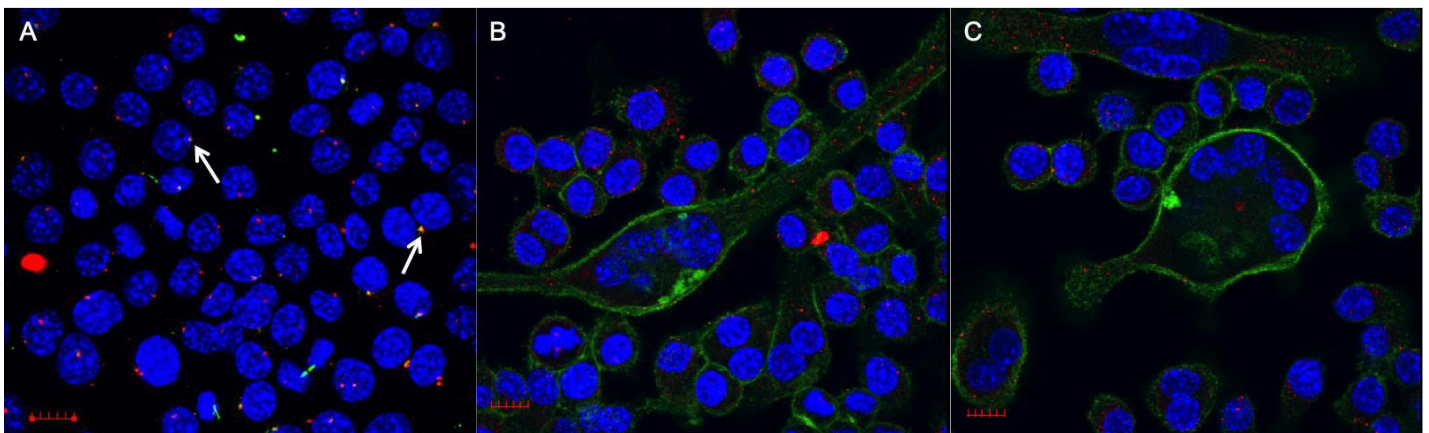


Figure 1: Maximum projection of confocal image z-stack. A) Primary cilia were found on pre-differentiated RAW 264.7 cells. Blue = DAPI (nuclei), green = acetylated alpha-tubulin (primary cilia), and red =  $\gamma$ -tubulin (centrosomes). Arrows indicate centrosome/primary cilia overlay. B,C) Primary cilia were absent on differentiated RAW 264.7 cells. Distinct multinuclear and actin staining demonstrate differentiated osteoclasts. Blue = nuclei, green = actin, and red = primary cilia. Scalebar = 10  $\mu$ m.

# Impact of long-acting reversible contraceptives on femoral bone density and mechanical properties during simulated microgravity

Heather C.M. Allaway, PhD<sup>1</sup>, Jon P. Elizondo<sup>1</sup>, Harry A. Hogan, PhD<sup>1</sup>, Susan A. Bloomfield, PhD<sup>1</sup>

<sup>1</sup>Texas A&M University, College Station, Texas

Premenopausal women, including female astronauts, routinely use hormonal contraception to suppress ovarian function and menstrual cycling<sup>[1-3]</sup>. Combined oral contraceptive (COC, ethinyl estradiol and progestin) use has been demonstrated to suppress bone turnover and reduce bone mineral density (BMD) gain with exercise<sup>[4,5]</sup>. Long-acting, reversible contraceptive (LARC, progestin-only) use provides many practical advantages over COC. It is well known that the LARC DepoProvera causes a dramatic loss of BMD due to severe hypoestrogenism<sup>[6-8]</sup>; however, newer, implantable LARC options do not cause the development of severe hypoestrogenism<sup>[9,10]</sup> and the impact on bone health varies depending on ethnicity, site of testing, and duration of use<sup>[7, 11-14]</sup>. Limited data is available regarding the interaction of exogenous estrogens and progestins at the bone cellular level. It is known that inadequate estradiol concentrations suppress expression of estrogen<sup>[15]</sup> and progesterone receptors<sup>[16]</sup> on osteoblasts and osteocytes, which facilitate the uncoupling of bone turnover. Additionally, in vitro work has demonstrated a dose response effect of progesterone on osteoblast function, such that osteoblast differentiation is optimal at luteal phase concentrations with suppression at higher, supraphysiologic progesterone doses<sup>[17]</sup>.

**Hypothesis:** We hypothesize that LARC use will blunt decrements in BMD and mechanical properties associated with hindlimb unloading (HU).

**Methods:** Virgin, female Sprague-Dawley rats (n=50; 16-18 wk-old) were singly housed and randomly assigned to placebo (PL) and LARC groups, via slow-release etonogestrel pellet (0.00ug/d vs 0.30ug/d; Innovative Research of America, Sarasota, FL) implanted under the skin. Animals were further randomized into weight bearing (WB) and HU subgroups (n=11-14/subgroup), with HU initiated a week following pellet insertion and lasting for 6 weeks (Figure 1). Following tissue collection, the left femur was scanned ex vivo with peripheral quantitative computed tomography (pQCT) at the distal femoral metaphysis (DFM) and the midpoint of the femoral diaphysis (FD). The femur was subsequently under-went a 3-point-bending load-to-failure test (Instron 3345, Norwood, MA) with a 1000N load cell at 2.54 mm/min. Univariate and repeated measures 2-way ANOVA and Non-Parametric (NP) statistical analyses were used.

**Results:** There was a time\*loading group interaction ( $p<0.01$ ) for body weight and food consumption. Animals did not differ with respect to body weight until the final week where HU lead to a reduction in weight in the PL animals ( $p<0.05$ ). All animals consumed the same amount of food until the second week of HU, when food consumption increased for HU animals, regardless of pellet type (LARC or PL;  $p<0.05$ ). There was a loading group main effect ( $p<0.001$ ) for soleus weight, such that HU reduced soleus size compared to WB animals. At the DFM, pQCT revealed pellet type ( $p=0.013$ ) and loading group ( $p=0.001$ ) main effects for total and cortical BMD (Figure 2). PL groups had greater total and cortical BMD than LARC groups, independent of loading group. WB groups had greater total and cortical BMD than HU groups, independent of pellet type. There was a significant effect (NP  $p=0.010$ ) for cancellous area. There was a trend ( $p<0.071$ ) for total and cortical area, cortical thickness, and periosteal circumference at the DFM, such that LARC had greater areas, thickness, and circumference than PL groups. At the FD, pQCT revealed a pellet type\*loading group interaction ( $p<0.030$ ) for total BMD, marrow area, and periosteal and endosteal circumference (Figure 3). The LARC-WB group had a greater total BMD than the LARC-HU group. The LARC-HU group had a greater marrow area and endosteal circumference than the PL-HU group. The PL-WB group had a greater periosteal circumference than the PL-HU group. Total bone area and cortical thickness were significantly different (NP  $p<0.030$ ) among groups. There was a loading group effect ( $p=0.001$ ; Figure 4) for cortical area at the FD, such that the WB groups had a larger area than the HU groups, regardless of pellet type. There was a trend ( $p=0.065$ ) for cortical BMD at the FD, such that LARC-HU had a lower BMD compared with PL-WB. Cross sectional moment of inertia at the FD was significantly different among groups (NP  $p<0.020$ ; Figure 4). Mechanical testing found no significant effects ( $p>0.110$ ) for yield load, post-yield displacement, work-to-fracture, and stiffness. There was a loading group effect ( $p=0.009$ ; Figure 4) for maximum load, such that the WB groups had a greater maximal load than the HU groups, regardless of pellet type. There were no significant effects ( $p>0.190$ ) on elastic modulus, yield stress, or ultimate stress.

**Conclusions:** LARC implantation had neutral or positive effects on BMD and bone geometry response to unloading, however, the changes were site specific. At the DFM there were no interaction effects of LARC on the HU response. Pellet type and loading group had independent impacts on BMD and area measures at the DFM. At the DFD there were interaction effect of pellet type and loading groups. The observed increase in marrow area and endosteal circumference indicate a potential alteration in cellular activity at the diaphysis. LARC implantation did not change the mechanical or material properties of the femur.

This work is supported by the Translational Research Institute for Space Health through Cooperative Agreement NNX16AO69A.

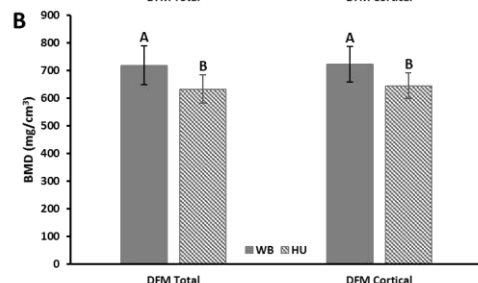
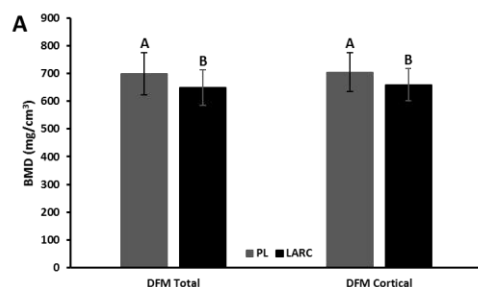
## References:

- [1] R.T. Jennings, E.S. Baker, Gynecological and reproductive issues for women in space: a review, *Obstet Gynecol Surv* 55(2) (2000) 109-16.
- [2] A.E. Ronca, E.S. Baker, T.G. Bavendam, K.D. Beck, V.M. Miller, J.S. Tash, M. Jenkins, Effects of sex and gender on adaptations to space: reproductive health, *J Womens Health (Larchmt)* 23(11) (2014) 967-74.
- [3] K. Daniels, J.C. Abma. Current contraceptive status among women aged 15-49: United States, 2015-2017. NCHS Data Brief, no327. Hyattsville, MD: National Center for Health Statistics. 2018.
- [4] D.B. Burr, T. Yoshikawa, D. Teegarden, R. Lyle, G. McCabe, L.D. McCabe, C.M. Weaver, Exercise and oral contraceptive use suppress the normal age-related increase in bone mass and strength of the femoral neck in women 18-31 years of age, *Bone* 27(6) (2000) 855-63.
- [5] J.M. Weaver, D. Teegarden, R.M. Lyle, G.P. McCabe, L.D. McCabe, W. Proulx, M. Kern, D. Sedlock, D.D. Anderson, B.M. Hillberry, M. Peacock, C.C. Johnston, Impact of exercise on bone health and contraindication of oral contraceptive use in young women, *Med Sci Sports Exerc* 33(6) (2001) 873-80.
- [6] S. Freeman, L.P. Shulman, Considerations for the use of progestin-only contraceptives, *J Am Acad Nurse Pract* 22(2) (2010) 81-91.
- [7] S. Pongsatha, M. Ekmahachai, N. Suntornlinsiri, N. Morakote, S. Chaovitsaree, Bone mineral density in women using the subdermal contraceptive implant Implanon for at least 2 years, *Int J Gynaecol Obstet* 109(3) (2010) 223-5.
- [8] B.A. Cromer, K.S. Berg-Kelly, J.P. Van Groningen, B.S. Seimer, L. Ruusuvaara, Depot medroxyprogesterone acetate (Depo-Provera) and levonorgestrel (Norplant) use in adolescents among clinicians in Northern Europe and the United States, *J Adolesc Health* 23(2) (1998) 74-80.
- [9] H.B. Croxatto, Mechanisms that explain the contraceptive action of progestin implants for women, *Contraception* 65(1) (2002) 21-7.
- [10] L. Makarainen, A. van Beek, L. Tuomivaara, B. Asplund, H. Coelingh Bennink, Ovarian function during the use of a single contraceptive implant: Implanon compared with Norplant, *Fertil Steril* 69(4) (1998) 714-21.
- [11] L. Bahamondes, C. Monteiro-Dantas, X. Espejo-Arce, A.M. Dos Santos Fernandes, J.F. Lui-Filho, M. Perrotti, C.A. Petta, A prospective study of the forearm bone density of users of etonorgestrel- and levonorgestrel-releasing contraceptive implants, *Hum Reprod* 21(2) (2006) 466-70.
- [12] R. Beerthuizen, A. van Beek, R. Massai, L. Makarainen, J. Hout, H.C. Bennink, Bone mineral density during long-term use of the progestagen contraceptive implant Implanon compared to a non-hormonal method of contraception, *Hum Reprod* 15(1) (2000) 118-22.
- [13] W. Modesto, N. Dal Ava, I. Monteiro, L. Bahamondes, Body composition and bone mineral density in users of the etonogestrel-releasing contraceptive implant, *Arch Gynecol Obstet* 292(6) (2015) 1387-91.
- [14] C. Monteiro-Dantas, X. Espejo-Arce, J.F. Lui-Filho, A.M. Fernandes, I. Monteiro, L. Bahamondes, A three-year longitudinal evaluation of the forearm bone density of users of etonogestrel- and levonorgestrel-releasing contraceptive implants, *Reprod Health* 4 (2007) 11.
- [15] S.N. Swift, J.M. Swift, S.A. Bloomfield, Mechanical loading increases detection of estrogen receptor-alpha in osteocytes and osteoblasts despite chronic energy restriction, *J Appl Physiol* (1985) 117(11) (2014) 1349-55.
- [16] K.M. Nicks, T.W. Fowler, D. Gaddy, Reproductive hormones and bone, *Curr Osteoporos Rep* 8(2) (2010) 60-7.
- [17] M. Schmidmayr, U. Magdolen, J. Tubel, M. Kiechle, R. Burgkart, V. Seifert-Klauss, Progesterone enhances differentiation of primary human osteoblasts in long-term cultures. The influence of concentration and cyclicity of progesterone on proliferation and differentiation of human osteoblasts in vitro, *Geburtshilfe und Frauenheilkund* 68(7) (2008) 722-728.

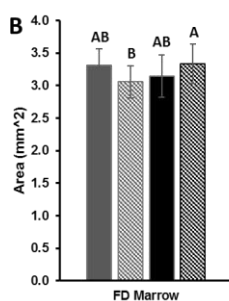
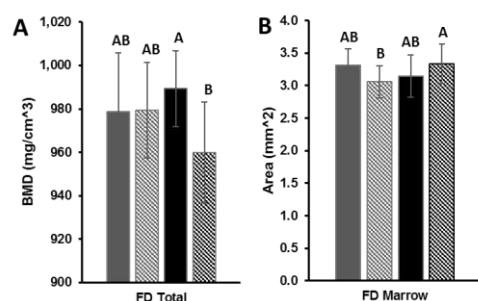
## Figures:



Figure 1: Experimental Design Timeline.



**Figure 2: Distal femoral metaphysis bone mineral density.** A) Total and cortical BMD by pQCT grouped by pellet type. The PL group had greater total and cortical BMD than the LARC group independent of loading group randomization. B) Total and cortical BMD by pQCT grouped by loading group. The WB group had greater total and cortical BMD than the HU group independent of pellet type randomization. Bars associated with each BMD measure with different letters are significantly different.



**Figure 3: Femoral diaphysis bone mineral density, marrow areal, and periosteal and endosteal circumference.** A) Total BMD by pQCT. The LARC-WB group had a greater total BMD than the LARC-HU group. B) Marrow area by pQCT. The LARC-HU group had a greater marrow area than the PL-HU group. C) Periosteal and endosteal circumference by pQCT. The PL-WB group had a greater periosteal circumference than the PL-HU group, while the LARC-HU group had a greater endosteal circumference than the PL-HU group. Bars associated with each measure with different letters are significantly different (Tukey's post-hoc test with alpha of 0.05).

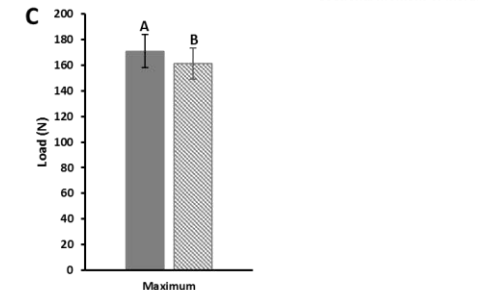
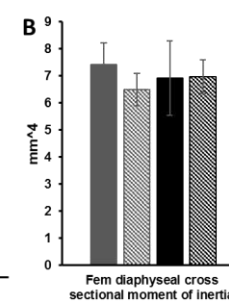
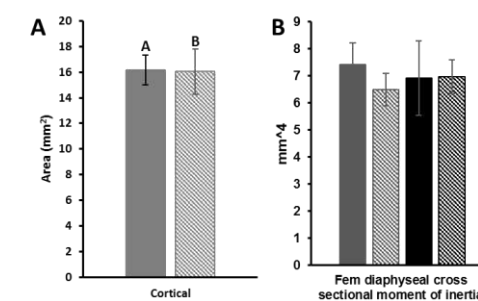
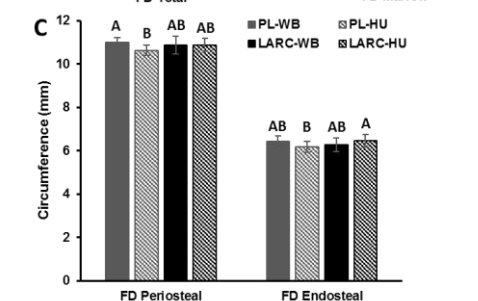


**Figure 4: Femoral diaphysis cortical area, cross sectional moment of inertia and maximum load.** A) Cortical area by pQCT grouped by loading group. The WB group had a greater cortical area than the HU group. B) Cross sectional moment of inertia by pQCT is significantly different among groups based on medians (non-parametric testing). C) Maximum load by 3pt bending load-to-failure testing grouped by loading group. The WB group had a greater maximal load than the HU group. Bars associated with each measure with different letters are significantly different.

# Osteocytes remodel bone by TGF- $\beta$ -induced YAP/TAZ signaling

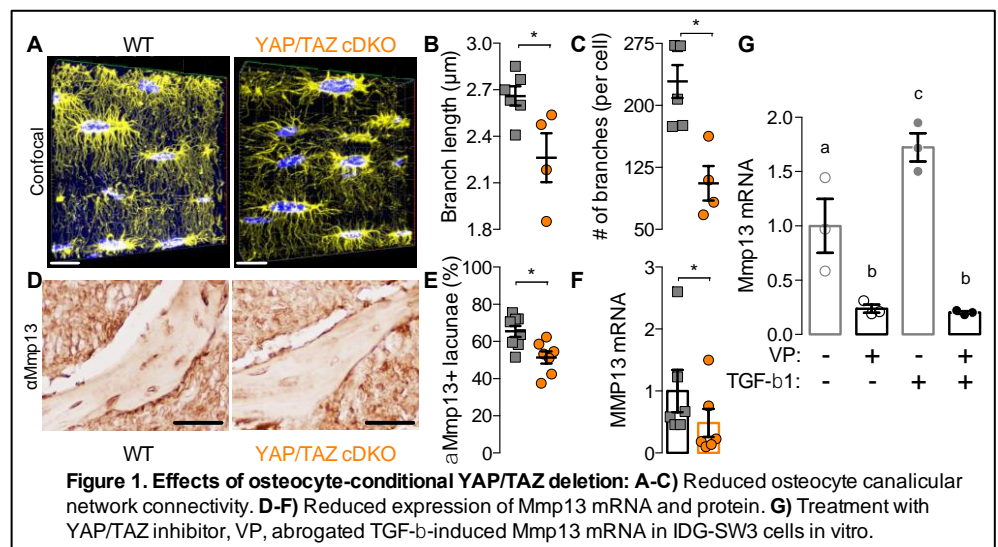
Christopher D. Kegelman<sup>1</sup>, Jennifer C. Coulombe<sup>2</sup>, Kelsey M. Jordan<sup>1</sup>, Alexander G. Robling<sup>3</sup>, Virginia L. Ferguson<sup>2</sup>, Teresita M. Bellido<sup>3</sup>, and Joel D. Boerckel<sup>1</sup>

<sup>1</sup>University of Pennsylvania, Philadelphia, PA; <sup>2</sup>University of Colorado, Boulder, CO; <sup>3</sup>Indiana University School of Medicine, Indianapolis, IN

**INTRODUCTION:** Osteocytes are matrix-entombed cells in bone that form an interconnected network of processes called canaliculi, which enable osteocytes to coordinate bone formation and resorption. Osteocytes indirectly regulate osteoblast and osteoclast activity but also directly resorb and deposit bone matrix through perilacunar/canalicular remodeling. However, the molecular mechanisms by which osteocytes control bone remodeling remain unclear. We previously reported that the transcriptional co-activators Yes-associated protein (YAP) and Transcriptional co-activator with PDZ-motif (TAZ) are important in bone.<sup>1</sup> Here, we tested the hypothesis that YAP and TAZ regulate osteocyte-mediated bone remodeling by conditional ablation of both YAP and TAZ from mouse osteocytes.

**METHODS:** We generated a conditional loss-of-function mouse model with dual deletion of YAP and TAZ through Cre-recombination under control of the 8kb-DMP1 promoter. All animal experiments were approved by the IACUC. We employed a breeding strategy to produce allele-dosage dependent deletion of YAP and/or TAZ, but only double homozygotes (YAP<sup>fl/fl</sup>;TAZ<sup>fl/fl</sup>;DMP1-Cre, hereafter cDKO) had a significant deficit in long bone growth. These were further compared with YAP<sup>fl/fl</sup>;TAZ<sup>fl/fl</sup> (WT) littermates. At 12 weeks of age, long bones (i.e., femurs and tibiae) from both WT and cDKO were harvested for analysis. The right femur was scanned by microCT (vivaCT80) and tested in three-point bending to failure. Femurs were then decalcified, processed for histology and second harmonic generation imaging, and immunostained for Mmp13, Mmp14, and Cathepsin K. Messenger RNA was isolated from contralateral limbs and evaluated by qPCR. Right tibiae were used to visualize the osteocyte-network via Ploton silver nitrate staining. Left tibiae underwent non-destructive X-ray microscopy imaging (Zeiss 520 Versa; 0.6  $\mu$ m voxels) to quantify osteocyte lacunar shape and orientation. Methyl-methacrylate-embedded bones from a separate cohort of 3-week-old mice, injected with Calcein and Alizarin Complexone at 26 and 28 days, respectively, were processed for dynamic bone histomorphometry. Comparisons were made using Student's t-tests, with data log-transformed to achieve homoscedasticity, when necessary. A p-value less than 0.05 was considered significant.

**RESULTS & DISCUSSION:** YAP/TAZ deletion reduced bone mass and dysregulated matrix collagen content and organization, which together impaired bone mechanical properties. YAP/TAZ deletion reduced osteoblast number and activity and increased osteoclast activity, likely by indirect osteocyte coordination since osteoblastic recombination was negligible. Further, YAP/TAZ deletion directly impaired osteocyte canalicular network remodeling, reducing process density, length, and branching, but did not alter lacunar size, shape, or orientation. Recent studies identify TGF- $\beta$  signaling as a key inducer of perilacunar/canalicular remodeling through expression of matrix-remodeling enzymes.<sup>2</sup> Consistent with these data, YAP/TAZ deletion in vivo decreased osteocyte expression of matrix proteases Mmp13, Mmp14, and Cathepsin K. YAP/TAZ deletion also reduced peri-osteocyte mineral deposition and reduced Col1a1 expression in vivo. Mechanistically, pharmacologic inhibition of YAP/TAZ transcriptional activity in osteocyte-like cells in vitro abrogated TGF- $\beta$ -induced protease gene expression. Together, these data show that osteocyte YAP and TAZ act downstream of TGF- $\beta$  to control bone matrix accrual, organization, and mechanical properties by regulating both direct perilacunar/canalicular remodeling and indirect osteoblast/osteoclast activity.



**REFERENCES:** [1] Kegelman+ FASEB J, 2018 [2] Dole+ Cell Reports, 2017



# A novel cryo-sectioning method for histological assessment of bone remodeling in nanocrystalline hydroxyapatite scaffolds

Lauren A. Boller, BS<sup>1</sup>, Stefanie M. Shiels, PhD<sup>2</sup>, Joseph C. Wenke, PhD<sup>2</sup>, Scott A. Guelcher, PhD<sup>1,3</sup>

<sup>1</sup>Vanderbilt University, Nashville, TN, <sup>2</sup>U.S. Army Institute of Surgical Research, Fort Sam Houston, TX, <sup>3</sup>Vanderbilt University Medical Center, Nashville, TN

**Introduction:** Over 1.6 million bone grafting procedures are performed annually in the United States (1). Autograft is the gold standard for bone grafting due to its inherent osteoinductive, osteoconductive, and osteogenic properties. However, significant challenges including donor site morbidity, limited quantity, and failure to integrate are associated with its use. Synthetic bone grafts have evolved as a substitute for autograft. The ideal biomaterial for regenerative bone grafts promotes cellular proliferation and osteogenesis and degrades to non-toxic breakdown products at a rate that complements new tissue formation. We have previously developed a reactive oxygen species-degradable lysine-based poly (thioketal urethane) (PTKUR) ceramic composite for bone tissue engineering applications (2). Preliminary in vitro studies utilizing nanocrystalline hydroxyapatite-poly (thioketal urethane) (nHA-PTKUR) show that mineralization and osteogenic differentiation of human mesenchymal stem cells increases with nHA loading (Figure 1). Given these data, we aimed to investigate the ability of nHA-PTKUR composites to mediate different cellular responses in vivo at different nHA loadings. We hypothesized that varying the weight% of nHA within the composites would promote a fundamentally distinct cellular response with low concentrations of nHA eliciting a fibrocartilage and granulation tissue response and large concentrations of nHA eliciting an osteogenic response.

**Methods:** 40 mature Sprague-Dawley rats (250-450g) were used in this study. 3D-printed nHA-PTKUR tissue engineered bone constructs were fabricated to recapitulate the trabecular architecture of the femoral head (3). Under sterile conditions, a plate was fixed to the femur with threaded K-wire, and a 2 mm segment of bone was removed, and the scaffold was implanted. 4 groups were evaluated in this study: 0% nHA (PTKUR control), 15% nHA, 35% nHA, and 45% nHA. Animals were randomly assigned to treatment groups and were placed into either 4-week or 8-week outcome groups. Within the 8-week group, at 2 and 4 weeks, animals were injected with calcein green and xylenol orange fluorophores. At their designated time point, animals were euthanized and the femur was harvested for histology, immunohistochemistry, and dynamic histomorphometry. Femurs were flash-frozen in liquid nitrogen and subsequently processed using Kawamoto's film method (4). Cryo-sections (5  $\mu$ m) were processed for H&E, Safranin O, Tartrate-Resistant Acid Phosphatase (TRAP), and Von Kossa staining. Immunohistochemistry (IHC) for CD31 and CD68 was also performed.

**Results:** H&E staining showed increased new bone in the defect space (Fig2A) in groups containing nHA at both 4 and 8 weeks. Osteoblast like cells were seen around the edges of the scaffold (Fig2B). Von Kossa staining (Fig2C) and dynamic histomorphometry (Fig2D) confirmed H&E results, showing new bone formation within the defect space in the presence of nHA at both time points. Additionally, in the presence of nHA, Safranin O showed positive staining of cartilage within the defect space and inside and along the edges of the scaffold (Fig2E). In all groups, TRAP staining showed osteoclasts present within the host bone, but not within the defect space (Fig2F). CD31 positive cells were seen in the defects of all groups, especially within regions of granulation tissue (Fig2G). CD68 positive cells were also seen in all groups, particularly around the edges of the scaffolds (Fig2H). Residual scaffold was seen in all groups.

**Conclusions:** Histological techniques are a significant challenge, and are often limited to plastic or paraffin sectioning in large animal models. In this study, we utilized Kawamoto's film method to obtain cryo-sections of an engineered scaffold in a rat femur model. Histological observations suggest increased new bone formation in the presence of nHA. The advantages of cryo-sectioning include short processing time (<1day), soft and hard tissue preservation without decalcification, the ability to clearly identify cell populations, and the ability to use sections for histology, IHC, and dynamic histomorphometry all allowing for a better understanding of what happens at the cellular level within bioengineered scaffolds.

**References:** 1) O'Keefe et al., *Tissue Eng Part B Rev* 17, 389-392 (2011). 2) McGough et al., *Tissue Eng Part A* (2018). 3) Vanderburgh et al., *Adv Healthcare Mat* 22 (2017). 4) Kawamoto et al., *Methods Mol Bio* 1130, 149-164 (2014).

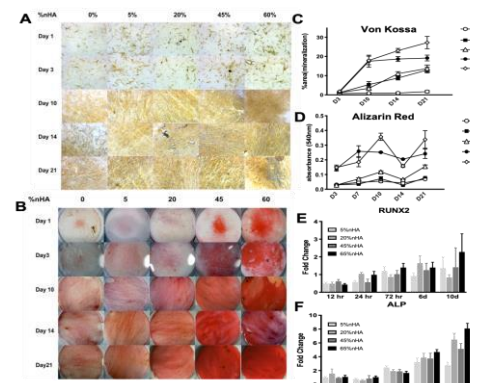


Figure 1: Effects of nHA loading on osteogenic differentiation. (A) Von Kossa and (B) Alizarin Red staining. Quantification of (C) Von Kossa and (D) Alizarin Red. Expression of (E) RUNX2 and (F) ALP measured by qRT-PCR.

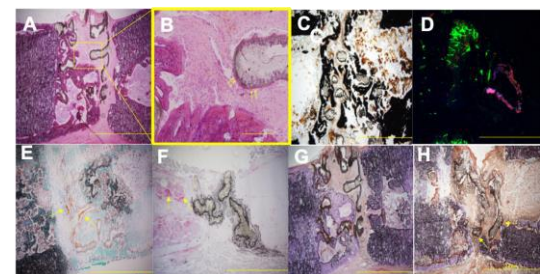


Figure 2: Representative histology. (A) H&E (4X), (B) H&E (10X), (C) Von Kossa (4X), (D) Dynamic Histomorphometry (4X), (E) Safranin O (4X), (F) TRAP (4X), (G) CD31 (4X), (H) CD68 (4X).

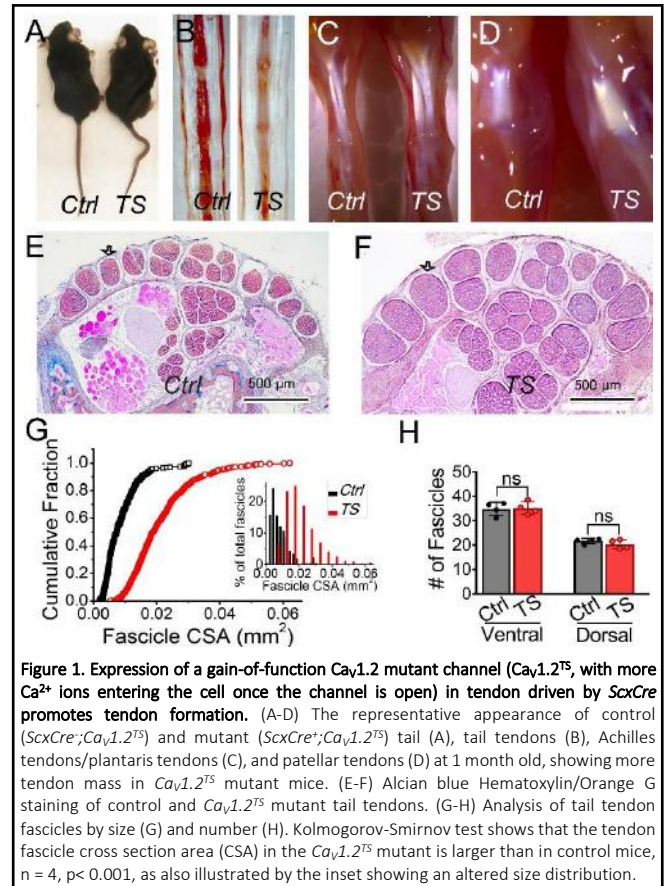
# Regulation of tendon formation by $\text{Ca}^{2+}$ signaling through $\text{Ca}_v1.2$ L-type voltage-gated calcium channel

Chike Cao<sup>1</sup>, Scott A. Rodeo<sup>2</sup>, Christopher L. Mendias<sup>3</sup>, Geoffrey S. Pitt<sup>1</sup>

<sup>1</sup>Cardiovascular Research Institute, Weill Cornell Medical College, New York, NY, USA, 10021; <sup>2</sup>Sports Medicine and Shoulder Service, Hospital for Special Surgery, New York, NY, USA, 10021; <sup>3</sup>Hospital for Special Surgery and Department of Physiology and Biophysics, Weill Cornell Medical College, New York, NY, USA, 10021

Tensile-bearing tendons are highly prone to acute injury and chronic degeneration from overuse, processes called tendinopathies. Therapeutic options for tendinopathies remain few due to limited knowledge about the basic biology underlying tendon development and postnatal tendon growth. While  $\text{Ca}^{2+}$  signals have been implicated in tendon mechanotransduction, acting as second messengers to convert mechanical load to biochemical signals,  $\text{Ca}^{2+}$  signaling details in tendon and the source(s) of the increase in intracellular  $\text{Ca}^{2+}$  in tendon fibroblasts are largely unknown.

$\text{Ca}_v1.2$ , an L-type voltage-gated  $\text{Ca}^{2+}$  channel, allows the influx of  $\text{Ca}^{2+}$  upon cell membrane depolarization and plays critical roles in many physiological processes including neuronal excitability, cardiac contractility, vascular tone, and gene expression. Using a  $\text{Ca}_v1.2$  reporter mouse, we found that  $\text{Ca}_v1.2$  was highly expressed in the developing limb tendons from early embryonic stages (E13.5) and expression remained strong postnatally in tendons and ligaments, suggesting important roles for  $\text{Ca}_v1.2$  channels during tendon development and adult tendon/ligament homeostasis. Consistent with those discoveries, we found that driving expression of a transgenic gain-of-function G406R mutant  $\text{Ca}_v1.2$  ( $\text{Ca}_v1.2^{TS}$ ) specifically in tendon with *Scleraxis-Cre* (*ScxCre*) leads to a marked increase in tendon mass, including the patellar tendon, Achilles tendon, tail tendons, and trunk tendons. Histological analysis revealed that *ScxCre;Ca\_v1.2^{TS}* mice at 1 month of age have thicker tail tendon fascicles with a broader size distribution as well as more tendon fibroblasts compared to those of *Cre* negative control littermates. There was no difference in the number of fascicles in both ventral and dorsal sides of the tail. Further, electron microscopic analysis showed that patellar tendons of *ScxCre;Ca\_v1.2^{TS}* mice displayed an increase in the diameter of collagen fibrils. Taken together, these studies demonstrate that increasing  $\text{Ca}^{2+}$  signaling through  $\text{Ca}_v1.2$  promotes tendon fibroblast proliferation and extracellular matrix collagen synthesis. Our results suggest that enhancing  $\text{Ca}_v1.2$  signaling may be a novel and effective therapeutic strategy for treating tendinopathies.





### 3D Peri-Lacunar Bone Mineral Density Assessment: A Novel Approach

Jennifer C. Coulombe, BS<sup>1</sup>, Zachary K. Mullen, PhD<sup>2</sup>, Virginia L. Ferguson, PhD<sup>1</sup>

<sup>1</sup>Department of Mechanical Engineering, University of Colorado, Boulder CO, United States; <sup>2</sup>Department of Applied Mathematics, University of Colorado, Boulder CO, United States.

Though several studies have explored peri-lacunar remodeling by osteocytes [1–3], bone material quality in the osteocyte's local environment is poorly understood. One synchrotron-based study suggested that bone mineral density is graded with distance from the lacunae, implicating the lacunar-canalicular network as a key regulator in bone mineral homeostasis [4]. Moreover, osteocyte projections (dendrites) within canaliculae are predominately oriented perpendicular to the major axis of the generally elliptical-shaped cells. Here we propose an X-ray microscope (XRM)-based imaging approach to measure the peri-lacunar bone mineral density that leverages improved sample sizes (e.g., numbers of lacunae) and greater accessibility than synchrotron techniques. We hypothesize that peri-lacunar density will be greatest perpendicular to the primary axis of ellipsoidal lacunae and greater than intensities proximal to spherical lacunae.

To evaluate osteocyte lacunae morphometry and peri-lacunar bone mineral density, the anterior-medial tibia, 7 mm from the tibiofibular junction of one female, 12-month-old Balb/C mouse was imaged using nano-computed tomography (nanoCT, Zeiss XRadia 520 Versa: 20×, 40V, 3.0W, 0.32  $\mu\text{m}$  and 3,201 projections). Six lacunae with matched volumes were selected within the region of interest. Intensity values scale with bone mineral density distributions [5], where higher intensities correspond to increased density. Using Dragonfly Pro 4.0 (Object Research Systems (ORS) Inc, Montreal, QC) and custom python code based on previous studies of lacunar morphometry [6-8], each lacuna was evaluated for volume, surface area, aspect ratio, phi, theta, oblateness, stretch, primary orientation. Additionally, all x, y, z coordinates and intensity values for voxels within 5  $\mu\text{m}$  of lacunae edges ( $n > 10\text{k}$  voxels per lacunae) were collected. Angles were binned according to quantile creating regions A, B, C, and D (Fig. 1A). Oblateness was binned from -0.75 to -0.25 (Spherical), -0.25 to 0.25 (Elongated), and 0.25 to 0.75 (Oblate) (Fig. 1B). Intensity differences were tested by repeated measures ANOVA on angular regions and oblateness with Tukey's Post Hoc in R v3.5.5. Significance reported for  $p < 0.05$ .

Intensity values of bone tissue maintained consistent values surrounding spherical lacunae. However, elongated lacunae had significantly greater intensities in regions perpendicular to the lacunae's primary axis (C, D) as compared to regions adjacent to the axis (C vs. A: +2.8%, D vs. A: +2.4%, and D vs. B: +1.2%). Oblate lacunae also demonstrated significantly greater intensities in regions D vs. A (+1.1%). Notably, oblate lacunae had a significantly greater intensity in region D than for elongated lacunae (+1.1%). Preliminary analysis using linear regression demonstrated that both distance from lacunae and angle from primary axis are significant predictors of intensity ( $p < 0.001$ ), where high intensities are observed closer to the lacunae and at more extreme angles of incidence. Moreover, our analysis is readily extendable to enable assessment of up to hundreds of osteocyte lacunae in a single imaged region.

The importance of distance as a predictor of peri-lacunar mineral intensity is consistent with the findings from synchrotron-based analyses. Our work looks to include the effects of angles of incidence and oblateness on these intensity measures. More homogenous intensity values around spherical lacunae may indicate reduced osteocyte maintenance of bone material such as observed with aging, senescence, or empty lacuna. Future work will investigate the ability of osteocytes to adapt their microenvironment by altering the peri-lacunar bone mineral density distribution in response to factors such as aging, mechanical loading, and disrupted LCNs (e.g., with genetic variation). Additionally, these predictors will be incorporated into a hierarchical linear model for intensity as a function of angle and distance while accounting for osteocyte morphology and the presence of localized spatial autocorrelation. In sum, this study demonstrated a novel XRM technique to evaluate 3D peri-lacunar intensity distributions as they relate to lacunar morphology.

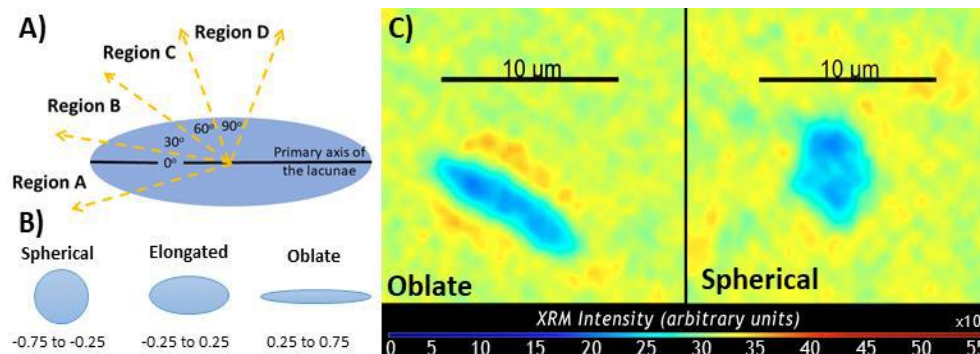


**Figure 1:** A) Angular regions for ANOVA analysis, each section spans 30°. B) Binned oblateness measures. C) Two representative images of osteocyte lacunae (blue) with comparable volumes but different morphologies and their surrounding bone material density (displayed as intensity). The Oblate example has a volume of 95  $\mu\text{m}^3$  and oblateness value of +0.8 compared to a Spherical example with a volume of 75  $\mu\text{m}^3$  and oblateness of -0.4.

References: 1. Wysolmerski, JJ., Bonekey Rep. (2012); 2. Qing, H et al., J Bone Miner Res. (2012); 3. Qing, H and Bonewald, LF., Int J Oral Sci (2009); 4. Dallas, SL, Prideaux, and Bonewald, LF., Endo Rev, (2013); 5. Burghardt, AJ et al., Calcif Tissue Int. (2008); 6. Mader, KS et al., Bone, (2013); 7. Heveran, CH et al., Bone, (2018); 8. McCreddie, BR et al., J. Biomech (2004)

## Differential Musculoskeletal Response to Unloading in Diversity Outbred Mouse Founder Strains

MA Friedman, CR Maroni, A Abood, Y Zhang, CR Farber, HJ Donahue

Mechanical unloading of the musculoskeletal system, experienced by astronauts in space or during prolonged bed rest, decreases bone and muscle volume and strength by up to 3% per month<sup>1</sup>. Variation in lean mass, bone mass and risk of osteoporosis are largely influenced by genetics; however, it remains unclear how genetic variation affects the musculoskeletal response to unloading. Diversity outbred mice (DO) are a genetically diverse outbred population of mice which allow for high-resolution genetic mapping and are an ideal model to study the effects of genetic variability on the musculoskeletal response to unloading<sup>2</sup>. We examined the phenotypic and transcriptomic response to unloading in the 8 DO founder strains C57Bl/6J, A/J, 129S1/SvImJ, NOD/ShiLtJ, NZO/HILtJ, CAST/EiJ, PWK/PhJ and WSB/EiJ after 3 weeks of single limb immobilization (SLI). We hypothesized that there would be differential, strain-dependent effects of unloading across these strains.

At 16 weeks, 6 male mice of each strain had the left limb immobilized in a cast for 3 weeks. The unaltered right limb was used as a control. Femoral bone geometry was analyzed by micro-CT. Mechanical properties were tested by 3-point bending. Quadriceps and gastrocnemius muscle samples were analyzed for markers of muscle atrophy and protein synthesis in 5 of the 8 strains. Two-way RM ANOVAs with Tukey's tests were used to test for significant group differences ( $p < 0.05$ ). RNA-seq was performed on RNA isolated from tibiae in 7 of the strains. Raw reads were aligned to the reference mouse genome GRCM38, and transcript assembly and quantification was conducted. Differential Gene Expression analysis was completed, and enriched Gene Ontology terms were identified.

All strains had significantly decreased femoral BV/TV in immobilized versus control limbs, but they had significantly different magnitudes of bone loss ranging from 7% to 37% (Fig 1). C57 was the only strain showing a significant loss of bone strength. Quadriceps mass loss ranged from 4% to 45%, and gastrocnemius mass loss ranged from 1% to 33%. C57 and CAST strains had the greatest BV/TV loss while NOD and NZO strains had the greatest muscle loss. Only NOD and CAST strains had greater expression of atrophy genes. NOD mice had decreased protein synthesis. RNA-seq revealed many significantly differentially expressed genes in immobilized tibiae (Fig 2). Interestingly, immobilized bones displayed upregulation of osteogenic genes involved in bone formation (*col1a1*, *bglap*, *sparc*), indicating a change in bone remodeling. This response differed across strains.

The results indicate that different strains respond to unloading from SLI differently, and this could be explained by genetic differences. The timing of when bones and muscles were evaluated could explain how some strains had significant bone or muscle loss but lesser changes in gene expression. Future work will examine gene expression earlier or in different tissues. These results suggest DO mice will be a powerful model for examining effects of genetics on musculoskeletal response to unloading.

References: 1. Lang T et al. J Bone Miner Res 19, 2004. 2. Svenson KL et al. Genetics 190:2, 2012.

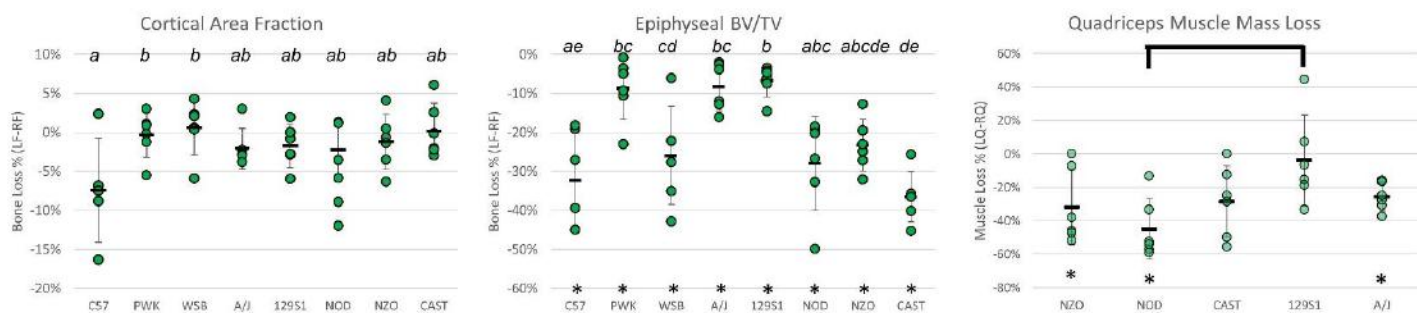


Figure 1. Percent loss (immobilized – control) of cortical area fraction, epiphyseal BV/TV and quadriceps muscle mass after 3 weeks of single limb immobilization. Groups that do not share a letter or are connected by a bar are significantly different. \*Significant difference between immobilized and control limbs for this strain.

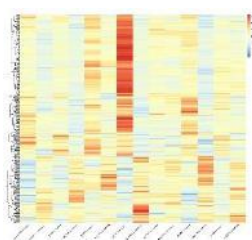


Figure 2. Overall comparison between immobilized (casted) and contralateral uncasted limbs in all strains. The figure represents expression of 414 differentially expressed genes, with expression level represented by color intensity. Each gene is represented by a row in the plot. Every 2 columns represent the casted and uncasted limbs of each strain of mice. The heatmap provides evidence that transcriptional response differs as a function of genetic background.

## Anabolic effect of nitric oxide on bone formation revealed by genetic deficiency of argininosuccinate lyase

Zixue Jin, PhD<sup>1</sup>, Jordan Kho, PhD<sup>1</sup>, Brian Dawson, BS<sup>1</sup>, Monica Grover, MBBS<sup>2</sup>, Donna J Palmer, DVM<sup>1</sup>, Philip Ng, PhD<sup>1</sup>, and Brendan Lee, MD, PhD<sup>1</sup>.

<sup>1</sup>Department of Molecular and Human Genetics, Baylor College of Medicine, Houston, TX, 77030.

<sup>2</sup>Stanford school of medicine, Department of Pediatric Endocrinology, Stanford, CA, 94305.

Nitric oxide (NO) is an important signaling molecule that influences a wide range of biological processes, including bone metabolism. NO is enzymatically produced by three nitric oxide synthases (nNOS, iNOS and eNOS) from L-arginine. NOS knock out (KO) mice have been used to study NO function; however, analyses have been limited by the potential redundancy of the three NOS isoforms. Argininosuccinate lyase (ASL) is the only mammalian enzyme capable of generating arginine, the sole precursor for NOS-dependent NO synthesis. Moreover, we recently showed that ASL is also required for channeling extracellular arginine to NOS for NO production. Hence, deletion of ASL leads to a cell-autonomous deficiency of NOS-dependent NO production due to combined loss of endogenous arginine production and extracellular arginine channeling. ASL deficiency is thus a Mendelian model for cell-autonomous, NOS-dependent NO deficiency.

Here, we show that ASL deletion led to decreased NO production and impaired osteoblast differentiation in ASL knockdown osteoblastic cell lines and hypomorphic *Asl* mice (*Asl*<sup>Neo/Neo</sup>) derived primary osteoblasts. Osteoblast-lineage specific *Asl* knockout mice (*Osteocalcin Cre; Asl*<sup>f/f</sup>) resulted in decreased bone mass, which was due to reduced bone formation. To understand the molecular mechanisms that underlie the osteoblast phenotype, we performed RNA sequencing analyses of WT and *Asl*<sup>Neo/Neo</sup> mice derived osteoblasts. RNA sequencing further confirmed that pathways involved in osteoblast function were dysregulated in *Asl* deficient osteoblasts. Importantly, RNA sequencing revealed that genes involved in glycolysis were significantly downregulated in *Asl*<sup>Neo/Neo</sup> mice derived osteoblasts. Using seahorse system, we found that glycolysis rate, which is essential for osteoblast differentiation was significantly suppressed in *Asl* deficient osteoblasts. Caveolin 1 (Cav-1) has been reported to be an endogenous negative regulator of NO synthesis. Accordingly, *Cav-1* mRNA and protein levels were increased in *Asl* deficient osteoblasts. Therefore, we hypothesized that ablation of *Cav-1* might rescue NO production and low bone mass in *Asl*<sup>Neo/Neo</sup> mice. Indeed, we observed that bone mass, NO production, as well as glycolysis were restored in *Asl*<sup>Neo/Neo</sup>; *Cav*<sup>+/-</sup> mice compared to *Asl*<sup>Neo/Neo</sup> mice. Finally, to evaluate the effect of ASL deficiency (ASLD) on human osteoblast, we generated induced pluripotent stem cells (iPSCs) from an ASLD individual carrying compound heterozygous *Asl* mutations (c.557G>A and c.857A>G). We also established two isogenic control iPSCs lines with heterozygous *Asl* mutations (c.557G>A or c.857A>G) by correcting one of the variants. Consistently, the capacity of iPSCs differentiation into osteoblasts was impaired as shown by decreased osteoblast marker genes expression, mineralization and glycolytic genes expression from iPSCs generated from ASLD patient compared to the two isogenic controls. Taken together, our results suggest that NO promotes osteoblast function, in part by enhancing glycolysis pathway.

## Effects of Diet Alterations, With or With Out Gut Microbial Transplants, on Bone Strength and Density

Sarah E. Little, MS<sup>1</sup>, Ayland C. Letsinger<sup>1</sup>, Jon P. Elizondo, MS<sup>1</sup>, Heather C.M. Allaway, PhD<sup>1</sup>, Harry A. Hogan, PhD<sup>1</sup>, J. Timothy Lightfoot, PhD<sup>1</sup>, and Susan A. Bloomfield, PhD<sup>1</sup>

<sup>1</sup>Texas A&M University, College Station, TX

High fat feeding has been demonstrated to negatively impact bone quality and bone strength, with exercise as protective against these negative effects<sup>1,2</sup>. However, these studies have employed isocaloric diets to examine low versus high fat diets, rather than a model of over-feeding. Our model of over-feeding utilizes a high fat diet with 20% fructose water and has been shown to reduce voluntary wheel running by ~50-70%<sup>3</sup>. Further, gut microbiota have been strongly linked to bone outcomes, using several models, including germ-free mice, colonized mice, and pro-biotic and pre-biotic supplementation<sup>2,4,5</sup>. A clear mechanism linking alterations in gut microbiota, diet composition and energy content and bone has not yet been elucidated in the literature. As such, we hypothesized that fecal microbiota transplantations (FMT) from healthy, chow-fed mice in combination with a change in diet will reverse the negative impacts of high fat feeding on bone quality and strength.

**METHODS:** 6-week old C57Bl/6 mice (n=10/group) were randomized to normal chow, low-fat (LF) or high fat, high sugar (HFS) diet *ad libitum* for 13 weeks (Tab. 1). After 13 weeks, HFS mice were subsequently randomized to one of three groups: LF diet with fecal metabolic transplants from the LF mice, LF diet with sham FMT using PBS, or HFS diet with FMT from the LF mice for 4 weeks (Tab. 2). All animals were singly housed and had access to a wheel for the duration of the study. Animals were sacrificed at 23 weeks of age. Wheel running distance, duration and speed was assessed daily. Body weight and composition and food and water intake were assessed weekly. Femoral neck strength testing was performed to assess maximal strength (N) using published methods<sup>6</sup>. Statistical analyses were performed using a two-way ANOVA (factors = diet, treatment). Tukey's *post-hoc* test was employed when appropriate. Pearson's correlations were used to examine the relationship between femoral neck strength and six study outcomes. Significance was assessed using an  $\alpha$  of 0.05.

**RESULTS:** Total body weight (TBW) and fat mass (FM) at sacrifice were higher in HFS/HFS+ mice, compared to all other groups ( $p<0.001$ ), though % change in TBW and FM from Week 13-17 revealed loss of both TBW and FM in HFS/LF+ and HFS/LF groups, as compared with LF/LF and HFS/HFS+ mice ( $p<0.001$ ). Total caloric intake from Week 13-17 was reduced in HFS/LF+ and HFS/LF mice compared with LF/LF and HFS/HFS+, with HFS/HFS+ consuming greater calories per day than all other groups ( $p<0.018$ ). Wheel running indices reveal an increase (% change from Week 13-17) in duration, distance and speed in HFS/LF+ and HFS/LF mice compared with LF/LF and HFS/HFS+ mice ( $p<0.011$ ). HFS/HFS+ mice showed greater femoral neck strength as compared to HFS/LF and HFS/LF+ mice ( $p<0.003$ ), with no difference compared to LF/LF mice ( $p=0.077$ ). When normalized to total body weight, however, LF/LF mice had the greatest femoral neck strength compared to all other groups ( $p<0.016$ ). Whole femur bone mineral density (BMD, g/cm<sup>2</sup>) was higher in HFS/HFS+ compared to all other groups ( $p<0.023$ ), though when normalized to body weight, LF/LF mice had the highest BMD ( $p<0.029$ ). Significant correlations were found between femoral neck strength and % change in TBW ( $r=0.559$ ,  $p<0.001$ ), % change in FM ( $r=0.538$ ,  $p<0.001$ ), and % change in running distance ( $r=-0.420$ ,  $p=0.008$ ).

**CONCLUSIONS:** A change in diet from HFS to LF led to decreased total body weight, fat mass, and caloric intake and increased running distance, duration and speed, with no apparent additive effect from the presence of "healthy" gut microbes. Femoral neck strength was significantly reduced in these groups, as compared with no change from the HFS diet. This is likely due to the abrupt decrease in caloric intake and increase in exercise, resulting in a negative energy balance. When controlling for body weight, however, control (LF/LF) mice had stronger femoral necks, suggesting that HFS feeding may impair bone strength.

## REFERENCES:

1. Styner M, Pagnotti GM, McGrath C, Wu X, Sen B, Uzer G, Xie Z, Zong X, Styner MA, Rubin CT, Rubin J. Exercise Decreases Marrow Adipose Tissue Through  $\beta$ -Oxidation in Obese Running Mice. *Journal of Bone and Mineral Research*. 2017 Aug;32(8):1692-702.
2. McCabe LR, Irwin R, Tekalur A, Evans C, Schepper JD, Parameswaran N, Ciancio M. Exercise prevents high fat diet-induced bone loss, marrow adiposity and dysbiosis in male mice. *Bone*. 2018 Mar 29.

3. Vellers HL, Letsinger AC, Walker NR, Granados JZ, Lightfoot JT. High fat high sugar diet reduces voluntary wheel running in mice independent of sex hormone involvement. *Frontiers in physiology*. 2017 Aug 25;8:628.

4. Yan J, Charles JF. Gut microbiome and bone: to build, destroy, or both?.*Current osteoporosis reports*. 2017 Aug 1;15(4):376-84.

5. Weaver CM. Diet, gut microbiome, and bone health. *Current osteoporosis reports*. 2015 Apr ;13(2):125-30.

6. Peng Z, Tuukkanen J, Zhang H, Jamsa T, Vaananen HK: The mechanical strength of bone in different rat models of experimental osteoporosis. *Bone* 15:523-532, 1994.

**FUNDING:** This study was funded by the Omar Smith Endowment via Dr. J. Timothy Lightfoot.

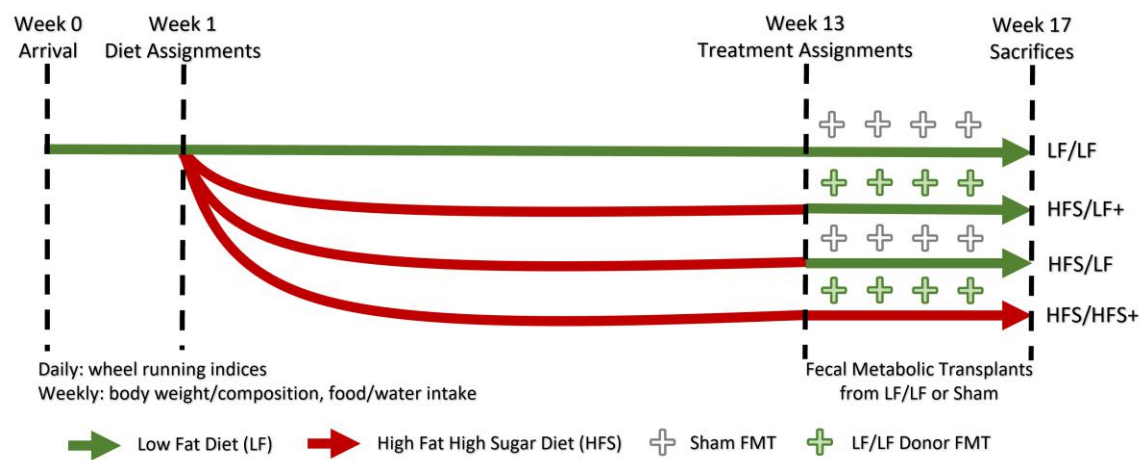


**Figure 1.** Experimental Design Timeline

Macronutrient	Low Fat Diet	High Fat Diet
Carbohydrate	39.5%	35%
Protein	25.2%	20%
Fat	4%	45%
Fiber/Ash	23.3%	0%
Fructose in H <sub>2</sub> O	0%	20%

**Table 1.** Diet composition of experimental diets.

Group ID	Design	Treatment
LF/LF	Low Fat Diet to Low Fat Diet + Sham FMT	Control
HFS/LF+	High Fat High Sugar Diet/Low Fat Diet + FMT	Diet + Microbes
HFS/LF	High Fat High Sugar Diet/Low Fat Diet + Sham FMT	Diet Only
HFS/HFS+	High Fat High Sugar Diet/High Fat High Sugar Diet + FMT	Microbes Only

**Table 2.** Summary of experimental groups.

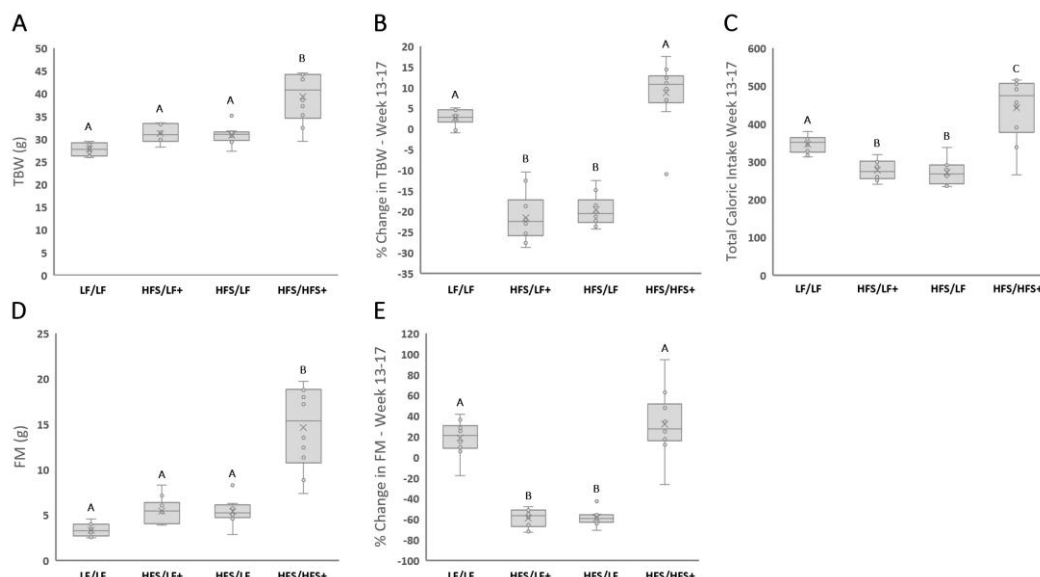


**Figure 2. Body weight, caloric intake and fat mass.** A) Total body weight (TBW, g) at sacrifice. HFS/HFS+ mice had the highest total mass. B) % change in TBW from Week 13-17. HFS/LF+ and HFS/LF mice experienced ~20% loss of total mass. C) Total caloric intake from Week 13-17. HFS/LF+ and HFS/LF mice consumed the fewest calories, while HFS/HFS+ consumed the most. D) Fat mass (FM) at sacrifice. HFS/HFS+ mice had the highest fat mass. E) % change in FM from Week 13-17. HFS/LF+ and HFS/LF mice experiences ~59% reduction in fat mass. Significance assessed using Tukey's *post-hoc* test and  $\alpha$  of 0.05.

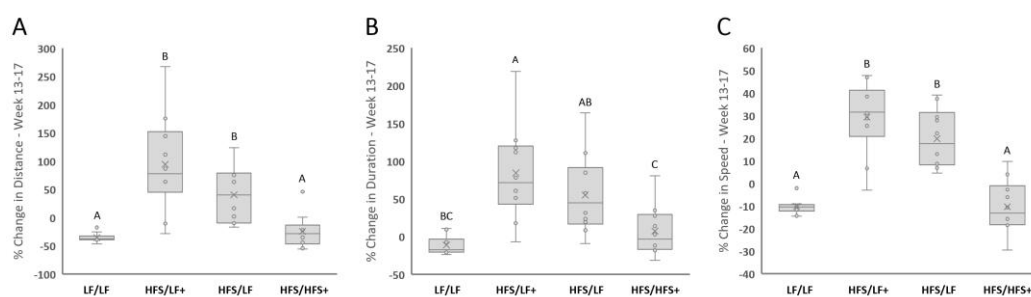


**Figure 3. Wheel running indices.** A) % change in distance from Week 13-17. HFS/LF+ and HFS/LF mice experienced ~95% and ~40% increase in meters run per day, respectively. B) % change in duration from Week 13-17. HFS/LF+ and HFS/LF mice experienced ~84% and ~55% increase in minutes run per day, respectively. C) % change in speed from Week 13-17. HFS/LF+ and HFS/LF mice experienced ~29% and ~19% increase in meters run per minute, respectively. Significance assessed using Tukey's *post-hoc* test and  $\alpha$  of 0.05.

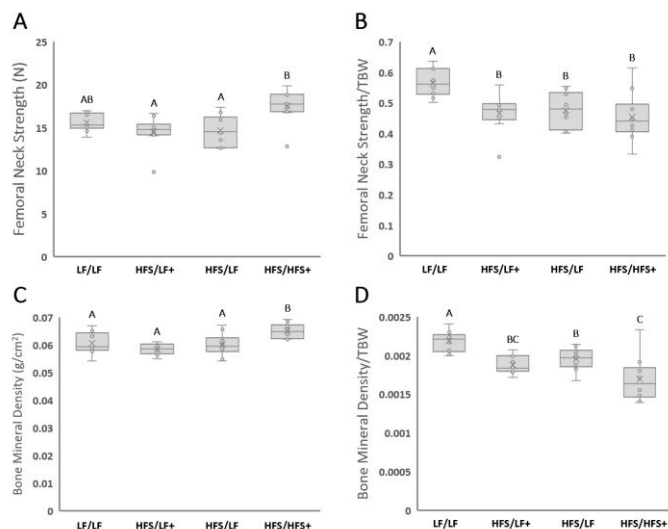


**Figure 4. Femoral neck strength and bone mineral density.** A) Femoral neck strength (N). HFS/HFS+ mice had the greatest absolute strength. B) Femoral neck strength/TBW (N/g). LF/LF mice showed the strongest femoral necks per gram of TBW. C) Whole femur bone mineral density (BMD, g/cm<sup>3</sup>). HFS/HFS+ mice had the greatest BMD. D) Whole femur BMD normalized to TBW. LF/LF mice had the highest BMD per gram of TBW. Significance assessed using Tukey's *post-hoc* test and  $\alpha$  of 0.05.



## Isolation of differentially activated tendon cell populations

Anne E.C. Nichols, PhD<sup>1</sup>, Alayna E. Loiselle, PhD<sup>1</sup>

<sup>1</sup>Center for Musculoskeletal Research, University of Rochester Medical Center, Rochester, NY, USA

**Introduction:** Tendon disorders and injuries are common but there are few therapeutic options available due in part to a lack of understanding of fundamental tendon cell biology. Though tendon cells have traditionally been seen as a homogenous population, we have recently demonstrated that expression of the tendon marker Scleraxis (Scx) and/or the small calcium binding protein S100a4 marks several subpopulations of cells within the murine flexor digitorum longus (FDL) tendon *in vivo*, and that both populations contribute to tendon repair<sup>1</sup>. To date, *in vitro* models of tendon cell behavior have not accounted for this cellular heterogeneity and there are therefore conflicting reports regarding the response of tendon cells to various stimuli. With an increasing appreciation for the heterogeneity of tendon cells, we can now determine how these various populations interact, which populations are present in tendon cell cultures *in vitro*, and whether the isolation method affects cell function or the cell populations present. To begin to address these questions, we first investigated how the two most common isolation methods (explant and collagenase digest) affect cell proliferation, and the expression of tendon markers and markers associated with fibroblast activation. We then utilized genetic lineage tracing methods to identify which *in vivo* tendon cell populations are represented *in vitro*.

**Methods:** Cells from FDL tendons were isolated either by collagenase digest (0.075% collagenase II) or migration from tendon explants. Cells were maintained in Fibroblast Growth Medium-2 (Lonza) and serially passaged upon reaching 70% confluence. At each passage, cells were counted, imaged, and collected for gene expression analysis. To determine the different populations present, tendon cells were isolated from S100a4-Cre; Ai9 and Scx-CreER; Ai9 mice (injected with tamoxifen [100 mg/kg] for three days, five days prior to isolation). In the cells derived from Scx-CreER; Ai9 mice, only cells that expressed Scx prior to isolation are labeled red (Scx-lin+), whereas in the S100a4-Cre; Ai9 mice, any cell that has previously or is currently expressing S100a4 is labeled red (S100a4-lin+). Cultures were imaged every two days and the number of lin+ vs. non-lineage (lin-) cells was quantified.

**Results:** A substantial decrease in proliferation was observed in explant cells vs. collagenase digested cells as indicated by increased doubling time (Fig. 1A). Explanted cells had decreased expression of tendon-related genes and a concomitant upregulation of fibroblast activation genes compared to those isolated by collagenase digest (Fig. 1B). In terms of differential lineage enrichment, explant cultures began as ~50% lin+ and lin- for both Scx and S100a4, and both increased in the proportion of lin+ cells over time. In contrast, the proportion of Scx and S100a4 lin+ and lin- cells isolated via collagenase digest remained consistent over time (Fig. 2). The Scx-lin+ labeling regimen suggests the increase in Scx-lin+ cells seen in explanted cells is due to increased proliferation of these cells relative to the lin- cells, while the increase in S100a4-lin+ cells may be attributed to either increased proliferative capacity of these cells or *de novo* expression of S100a4 in additional cells following isolation. Despite the fact that more Scx-lin+ cells were present in explant culture vs. collagenase digested cultures, explant cells had decreased expression of Scx. Combined with the gene expression data, this suggests that activation of resident tendon cells involves downregulation of Scx.

**Discussion:** Here, we demonstrate that loss of tension and migration through an intact extracellular matrix (explant culture) results in an activated cell phenotype relative to cells from which all matrix cues have been removed (collagenase digest), indicating an important role for cell-matrix cues in regulating tendon cell function. To our knowledge, this is the first study to document increased expression of fibroblast activation markers in tendon cells. While the majority of cells in culture are derived from known resident tendon cells populations (Scx-lin+ and S100a4-lin+), we identified an additional novel population of resident tendon cells (Scx-lin-; S100a4-lin-) whose presence is highly dependent on isolation method. Future studies will determine the specific mechanisms involved in matrix-mediated tendon cell activation, the terminal fate of activated tendon cells both *in vitro* and *in vivo*, as well as the functional relationship between the lineage and non-lineage resident tendon cells identified in this study.

**References:** <sup>1</sup>Best 2019 (FASEB)

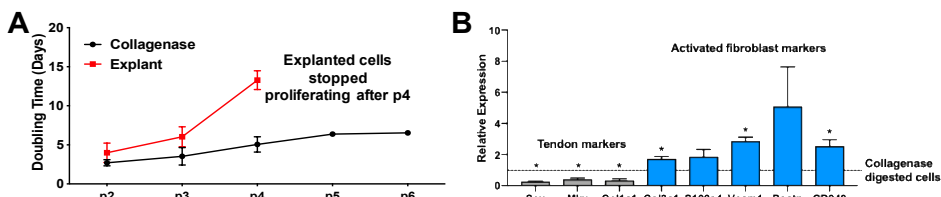


**Figure 1.** Explanted tendon cells were less proliferative (A) and had decreased expression of tendon markers (gray bars) combined with increased expression of fibroblast activation marker genes (blue bars) compared to collagenase digested cells (B). \*p<0.05 compared to collagenase digested cells (n=2).

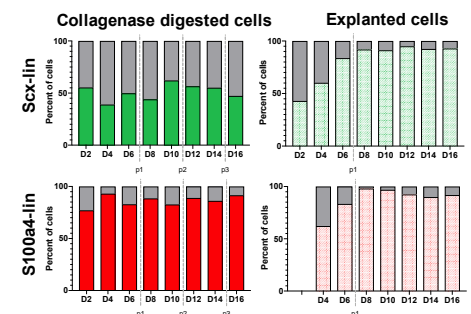


**Figure 2.** Collagenase digested cultures contained both lineage (colored bars) and non-lineage cells (gray bars) in non-varying proportions over time. In contrast, while both Scx-lin+ and S100a4-lin+ cells comprised only ~50% of explanted cells initially, both lineage populations increased to represent >80% of cells present by day 8.



## Advanced Approaches to Bone Biofabrication

Nizeet Aguilar, PhD<sup>1</sup>, David Olivos, PhD<sup>2</sup>, Alexander Brinker<sup>1</sup>, Matthew Prideaux, PhD<sup>3</sup>, Marta Alvarez, PhD<sup>1</sup>, Tien-Min Chu<sup>4,5,6</sup>, Melissa A. Kacena, PhD<sup>1,3</sup>, Diane Wagner, PhD<sup>6</sup>, Ping Li, PhD<sup>7</sup>, Burcin Ekser, MD, PhD<sup>7</sup>, Mark Holland, PhD<sup>8</sup>, Lynda Bonewald, PhD<sup>1,3</sup>, Lester Smith, PhD<sup>8,10</sup>

<sup>1</sup>Department of Orthopaedic Surgery, Indiana University School of Medicine, Indianapolis, IN, USA, <sup>2</sup>Department of Biochemistry and Molecular Biology, Indiana University School of Medicine, Indianapolis, Indiana, USA, <sup>3</sup>Department of Anatomy and Cell Biology, Indiana University School of Medicine, Indianapolis, IN, USA, <sup>4</sup>Weldon School of Biomedical Engineering, Purdue University, West Lafayette, IN, USA, <sup>5</sup>Department of Biomedical and Applied Sciences, Indiana University School of Dentistry, Indianapolis, IN, USA, <sup>6</sup>Department of Mechanical and Energy Engineering, Indiana University Purdue University Indianapolis, Indianapolis, Indiana, USA, <sup>8</sup>Department of Radiology and Imaging Sciences, Indiana University School of Medicine, Indianapolis, Indiana, USA,

Biofabricating bone requires many complex considerations including the bioprinting medium, construct design, bioprinting method, post-bioprinting management, and tissue perfusion. We have developed a versatile tissue biofabrication workflow employing four processes: (i) spheroid microtissue optimization, (ii) a scaffold-free Kenzan 3D bioprinting method, (iii) post-printing optimization, and (iv) the FABRICA Bioreactor Platform. The Kenzan 3D bioprinting method generates tissues by impaling cell-dense microtissue spheroids 450-550  $\mu\text{m}$  in diameter adjacent to one another on a needle array (Kenzan). The spheroids are close enough to fuse together to make a larger tissue construct. Here, we describe how we have utilized each part of the workflow to design, optimize, and biofabricate mature, robust bone-like tissue constructs.

Osteogenic differentiation of spheroids of immortalized mouse bone marrow stromal cells (BMSCs) was performed. BMSCs were seeded in ultra-low attachment (ULA) 96-well plates with 20, 30 or 40K cells to generate self-aggregated spheroids either under normal gravity or centrifugation. Spheroids formed via centrifugation were superior to those formed by gravity, as evidenced by sphericity, smoothness, and double DNA content. The spheroids were cultured in control media (Alpha-Minimum Essential Medium, 10% fetal bovine serum, 1% penicillin-streptomycin glutamate, and 0.001% amphotericin B) or osteogenic differentiation media (control medium supplemented with 50 mg/ml of L-ascorbic acid 2-phosphate and 200 mM  $\beta$ -glycerophosphate disodium salt hydrate) for up to 28 days. A robust osteogenic response to the differentiation medium was observed including higher mRNA expression of alkaline phosphatase, collagen type I, and osteocalcin, as well as greater alkaline phosphatase activity than those cultured in control medium. The optimal spheroid fabrication technique was to aggregate 40K cells under 150 – 300  $\times g$  centrifugation. Optimized BMSC spheroids in 96-well plates were placed into the semi-automated Regenova Bio 3D printer which uses pneumatically pressurized nozzle to lift spheroids from the plate and impale them onto the Kenzan into a pre-designed structure. Workflow improvements included aseptic nozzle installation using a nozzle sheath, flushing spheroids loose from the well floor with a pipette prior to printing, manual nozzle drying between steps, and 7 days of post-printing maturation on the Kenzan for the tissue construct to fuse sufficiently to withstand handling. These improvements resulted in a 4-fold reduction in print times, a 20-fold reduction in the use of bioprinting resources, and more robust constructs.

As access to primary BMSCs can be limiting, cell lines that have previously been shown to produce bone-like matrices were used. IDG-SW3 cells are capable of differentiation from early osteoblasts to late osteocytes and express GFP when DMP1, an early osteocyte marker, is expressed. After 3 weeks of culture off the Kenzan, 3D bioprinted IDG-SW3 tissue constructs exhibited mineral deposition, *Sost/sclerostin* expression, and DMP-GFP expression, indicating osteoblast to osteocyte-like bone differentiation.

The computer-designed FABRICA bioreactor was 3D-printed with biocompatible material and used for a Flow profile study. In this study, five different media were perfused through a 3D-bioprinted construct made from agarose spheroids on a Kenzan and the flow profile was ultrasonically analyzed at increasing volumetric flow rates (VFR). Construct VFR increased with increasing pump VFR. Water and other media increased VFR significantly while human and pig blood showed shallow increases. Ultrasonic visualization of the flow indicates that metered flow rate can be optimized as required by the tissue design.

Future studies will investigate osteogenic outcomes following bioprinted IDG-SW3 tissue construct perfusion in the FABRICA. These conditions will replicate the highly perfused *in vivo* bone environment, resulting in robust constructs that better represent mature bone tissue.

## The Primary Cilium and Osteoclastogenesis

Michael M. Sutton, MS<sup>1</sup>, Christopher R. Jacobs, PhD<sup>1</sup>

<sup>1</sup>Columbia University, New York, NY

**Introduction:** Osteoporosis, presently affecting more than 200 million people worldwide, is a metabolic bone disease characterized by low bone density and deterioration of bone architecture that ultimately increases the risk of fragility fractures. The physical impairment is compounded by the insufficiency of prophylaxis and treatment options devoid of negative side effects<sup>1,2</sup>. As a result, there is a need to discover better therapeutic solutions to address this disease. Our lab and others have established the osteocyte primary cilium – a mechanosensing, antenna-like organelle – as a promising pharmaceutical target to exploit the body's natural anabolic response to physical loading to maintain bone health<sup>4</sup>. However, little is known about the potential impact of targeting the primary cilium in relation to osteoclasts, the bone resorbing cell. In this work, we share results from preliminary examination of the primary cilium specifically within the context of osteoclasts.

**Methods:** We cultured RAW 264.7 cells (an immortal cell line that is a mixture of monocytes/macrophages) in DMEM supplemented with 10% FBS and 1% P/S, and added 30 ng/mL of macrophage colony stimulating factor (m-CSF); this factor drives the equilibrium of the cell mixture towards macrophages, the precursor of osteoclasts. We then seeded these cells onto glass-bottom dishes and performed double immunocytochemistry (Figure 1A). Next, we cultured the cells in  $\alpha$ MEM supplemented with 10% FBS and 1%P/S and added 33 ng/mL of m-CSF and 66 ng/mL of receptor activator of nuclear factor-Kappa B ligand (RANKL); this is the activating molecule of osteoclastogenesis. We seeded these cells onto glass-bottom dishes and, after ten days, performed ICC again (Figure 1B and 1C).

**Results:** After three independent stains of undifferentiated RAW 264.7 cells, we counted a total of 248 cells and noted a 51% cilia incidence, concluding that osteoclast precursors do in fact possess primary cilia, which was previously unknown. These primary cilia appear spatially aligned as protrusions from the cell's centrosome, as expected. In the osteoclast differentiation study, we again did three independent stains. As a result of a low differentiation percentage, only 41 osteoclasts were counted, none of which had clear or distinct primary cilia. Some stains, however, appear as though macrophages in the process of fusing may still express primary cilia.

**Discussion:** In vertebrates, cilia are found on quiescent cells and on proliferating cells in the G1 phase of the cell cycle; in dividing cells, they are resorbed before S phase or during G2<sup>3</sup>. It is not yet clear to what extent the fusion of macrophages during osteoclastogenesis is related to cell division and cilia resorption on the molecular scale. The primary question that now exists is if, and by what mechanism, macrophage primary cilia regulate osteoclast formation and function.

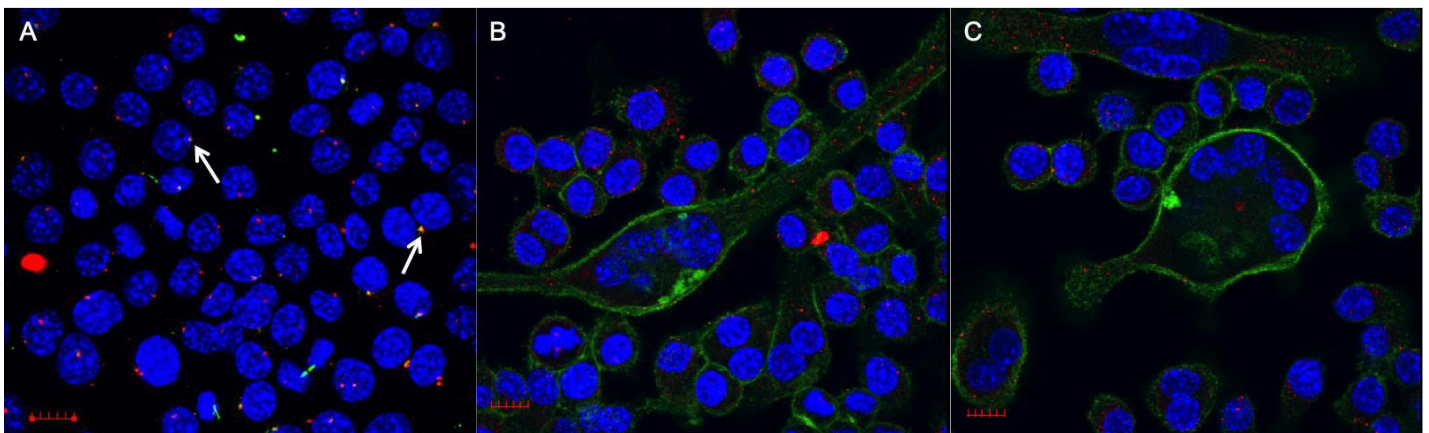


Figure 1: Maximum projection of confocal image z-stack. A) Primary cilia were found on pre-differentiated RAW 264.7 cells. Blue = DAPI (nuclei), green = acetylated alpha-tubulin (primary cilia), and red =  $\gamma$ -tubulin (centrosomes). Arrows indicate centrosome/primary cilia overlay. B,C) Primary cilia were absent on differentiated RAW 264.7 cells. Distinct multinuclear and actin staining demonstrate differentiated osteoclasts. Blue = nuclei, green = actin, and red = primary cilia. Scalebar = 10  $\mu$ m.

# Osteocyte-specific deletion of the auxiliary $\alpha_2\delta_1$ voltage sensitive calcium channel subunit results in impaired skeletal strength and decreases in both lean and fat masses

Christian S. Wright, PhD<sup>1</sup>, Xin Yi, PhD<sup>1</sup>, Artur Schneider<sup>2</sup>, Molly Pederson<sup>3</sup>, Mary C. Farach-Carson, PhD<sup>4</sup>, Alexander G. Robling, PhD<sup>5</sup>, William R. Thompson, DPT, PhD<sup>1,5</sup>

<sup>1</sup>Department of Physical Therapy, School of Health and Rehabilitation Sciences, Indiana University, Indianapolis, IN

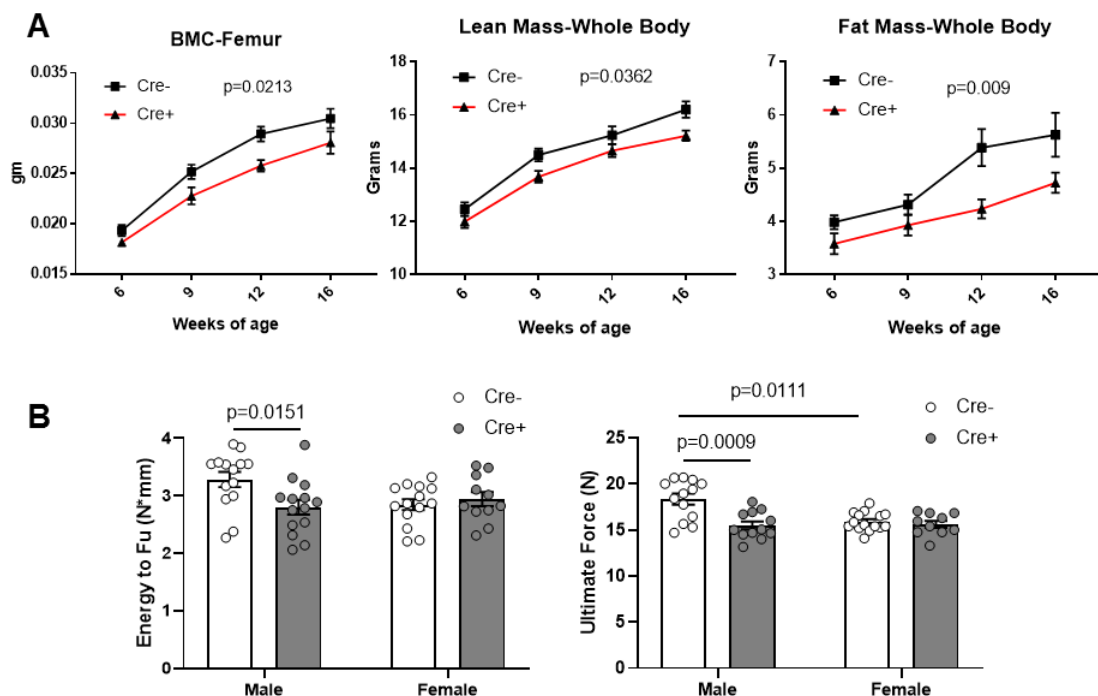
<sup>2</sup>Department of Physiology, College of Osteopathic Medicine, Marian University, Indianapolis, IN

<sup>3</sup>School of Science, Indiana University-Purdue University, Indianapolis, IN

<sup>4</sup>Department of Diagnostic and Biomedical Sciences, School of Dentistry, University of Texas, Houston, TX

<sup>5</sup>Department of Anatomy & Cell Biology, School of Medicine, Indiana University, Indianapolis, IN

Osteocytes are the most abundant and mechanosensitive cells in the skeleton. They are essential for sensing and responding to mechanical forces by controlling the activity of other cells. However, the mechanisms by which osteocytes sense force input and transmit signals to other cells remains unclear. Voltage sensitive calcium channels (VSCCs) regulate anabolic responses to mechanical loading, and inhibition or deletion of these channels impairs bone accrual, mechanosensation, and skeletal integrity. Activity of VSCCs is regulated by auxiliary subunits, which bind the pore-forming  $\alpha_1$  subunit to influence calcium influx. Through its transmembrane domain and large extracellular region, the  $\alpha_2\delta_1$  auxiliary subunit controls the calcium-gating kinetics of the  $\alpha_1$  channel pore, the interaction with and subsequent response to extracellular ligands, and the forward-trafficking of the  $\alpha_1$  channel pore to the cell membrane. Knockdown of  $\alpha_2\delta_1$  in MLO-Y4 osteocytes decreases the cell's ability to respond to membrane stretch, and global deletion of  $\alpha_2\delta_1$  in mice results in osteopenia. Therefore, we hypothesized that osteocyte-specific deletion of  $\alpha_2\delta_1$  would impair skeletal development. Mice (C57BL/6) with LoxP sequences flanking crucial exons of *Cacna2d1*, the gene encoding  $\alpha_2\delta_1$ , were crossed with mice expressing Cre under the control of the *Dmp1* promoter (10 Kb). To assess skeletal phenotype, longitudinal whole body and site-specific DXA and *in vivo*  $\mu$ CT (10 wk old) were assessed. Three-point bending and *ex vivo*  $\mu$ CT were also conducted following sacrifice (20 wk old). Osteocyte-specific deletion of  $\alpha_2\delta_1$  in male mice decreased femoral BMC (p=0.0213) by DXA and impaired cancellous bone at the proximal tibia by  $\mu$ CT, showing decreased trabecular thickness (p=0.0097) and a trend for lower BV/TV (p=0.057) at 10wks. *Cacna2d1*<sup>f/f</sup>, Cre+ male mice also displayed reduced ultimate force (p=0.0009) and energy to failure (p=0.0151) with femora 3-point bending, compared to *Cacna2d1*<sup>f/f</sup>, Cre- controls. In addition to these skeletal outcomes, osteocyte-specific deletion of  $\alpha_2\delta_1$  decreased total body lean (p=0.0362) and fat (p=0.009) masses by DXA. Collectively, the  $\alpha_2\delta_1$  auxiliary subunit is essential for osteocyte's regulation of trabecular structure and femur strength. Furthermore, these data suggest that the  $\alpha_2\delta_1$  auxiliary VSCC subunit controls release of extracellular signals from osteocytes to regulate body composition.



**Osteocyte-specific deletion of the auxiliary  $\alpha_2\delta_1$  voltage sensitive calcium channel subunit results in impaired skeletal strength and decreases in both lean and fat masses.** (A) Longitudinal whole body and site-specific DXA revealed decreased femur BMC and reduced whole body lean and fat masses in osteocyte-specific  $\alpha_2\delta_1$  deleted (Cre+) male mice (N=15). (B) Right femora 3-point bending revealed reduced ultimate force and energy to failure in osteocyte-specific  $\alpha_2\delta_1$  deleted (Cre+) male mice (N=12).

# Older mice attenuate compression-induced intervertebral disc degeneration by suppressing *Serpina1* via Wnt signaling

Marina Zieger, PhD<sup>1</sup>, Christian Mueller, PhD<sup>1</sup>, Nilsson Holguin, PhD<sup>2</sup>

<sup>1</sup>University of Massachusetts, Worcester, MA, <sup>2</sup>IUPUI, Indianapolis, IN

Aging reduces Wnt signaling in the intervertebral disc (IVD) and activating Wnt signaling in IVDs leads to greater aggrecan, but the mediation of aggrecan by Wnt signaling is mild compared to the extensive changes in IVD functionality. This suggests that a more impactful regulatory protein of the extracellular matrix (ECM) is modulated by Wnt signaling. Young-adult (5 mo) and middle-aged (12 mo) mice were subjected to a model of IVD degeneration (tail compression, TC), transcription was analyzed by RNA sequencing (n=3/age) and pathway analysis was performed on Reactome. Adjacent IVD that were not compressed served as controls (n=3/age). Using pathway analysis, aging and TC in 5 mo IVD suppressed pathways related to ECM organization (red, **Fig. 1A**), but were unchanged in compressed IVD of 12 mo mice (grey). Specifically, TC did not affect *Serpina1e* expression in 5 mo IVD, but TC in 12 mo IVD reduced the gene expression of *Serpina1e* by **76-fold** (FDR<0.001). In order to elucidate the role of Wnt signaling, 5 mo *ShhCreErT2/b-Catenin<sup>fl/fl</sup>* (cKO) IVD and *b-Catenin<sup>fl/fl</sup>* (WT) IVD were tail compressed to mimic the response of IVD degeneration in aged IVD that are normally absent of Wnt signaling (n=3/grp). IVD were analyzed by RNA-sequencing and hundreds of genes were regulated. As expected, TC in control mice elevated pathways involved with ECM degradation (red), but deletion of *b-Catenin* elevated ECM production (green), suggesting that inactivated Wnt signaling in aged mice may contribute to the zero-balance regulation of the ECM during compression. Specifically, deletion of *b-Catenin* markedly suppressed the expression of *Serpina1* paralogs by 8-fold (FDR<0.001) compared to the quiescent expression in intact compressed IVD (**Fig. 1B**). *Serpina1* is a multifunctional protein involved in the regulation of elastase and, while ECM-related changes were associated with *Serpina1* changes in middle-aged and cKO mice, its role in the IVD is unknown. Therefore, CRISPR/Cas9-generated KO mice that suppress 5 of the 6 *Serpina1* paralogs expressed in the IVD (*Serpina1a-e*) were aged to 14 mo. Compared to age-matched C57Bl/6 mice (n=3), 14 mo *Serpina1* KO mice (n=7) were protected from annulus fibrosus-specific age-related IVD degeneration (improved degenerative score and 68% more elastin, **Fig. 2**). Together, these data demonstrate that reduced Wnt signaling may limit compression-induced IVD degeneration by reducing *Serpina1* and posit that reducing *Serpina1* in the IVD may serve as a therapeutic approach for IVD degeneration in older individuals.

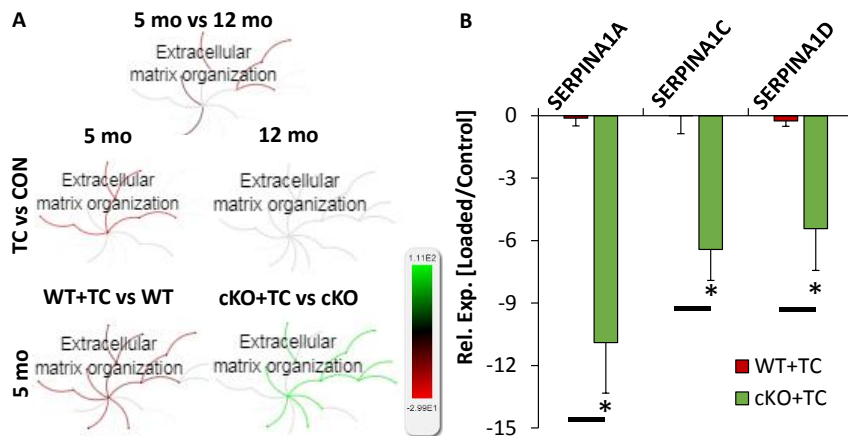


**Figure 1.** (A) Inactivation (red) and activation (green) of pathways related to ECM organization in compressed intervertebral disc of young-adult (5 mo), middle-aged (12 mo) and cKO mice. (B) *Serpina1A*, *C* and *D* are not altered by tail compression (TC) in wildtype (WT) and are reduced 6-10 fold in cKO intervertebral disc. \*: WT vs WT+TC or cKO vs cKO+TC; bar: WT+TC/WT vs cKO+TC/cKO; False Discovery Rate < 0.05.

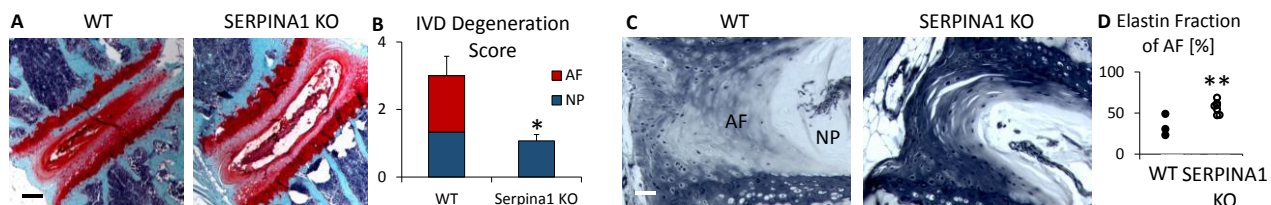


**Figure 2.** (A) Safranin-O stain (red proteoglycan) of 14 mo WT and *Serpina1* KO intervertebral disc. (B) Intervertebral disc degeneration score of the KO intervertebral disc is less than of the WT intervertebral disc. (C) Verhoeff stain (blue: elastin) of the AF. (D) The elastin fraction of the AF of the KO intervertebral disc (open circles) is greater than of the WT (solid circles) intervertebral disc. AF: annulus fibrosus, NP: nucleus pulposus. Scale bar in (A) is 100  $\mu$ m and in (C) is 25  $\mu$ m. \*:  $p<0.05$ ; \*\*:  $p<0.01$ .

## **Distinct muscle-specific ubiquitin ligases regulating bone microarchitecture in their unique ways**

*Vidyani Suryadevara<sup>1</sup> and Monte S. Willis<sup>1,2</sup>*

*<sup>1</sup>Department of Pathology & Laboratory Medicine, <sup>2</sup>Indiana Center for Musculoskeletal Health and Krannert Institute of Cardiology and Division of Cardiology, Department of Internal Medicine, Indiana University School of Medicine, 635 Barnhill Drive, Van Nuys MS 5067, Indianapolis, IN, 46202, USA*

People with osteoporosis have increased risk of fractures and abnormal bone quality due to reduced bone strength. Over the age of 50, one in two women and one in four men are prone to this bone loss. Ubiquitin proteasome system was found to regulate bone loss by modulating osteoblast differentiation and bone formation as well as formation of osteoclasts that contribute to bone resorption. Ubiquitin ligases have been shown to play an important role in bone turnover and metabolism. Muscle Ring Finger (MuRF) are novel ubiquitin ligases, which are muscle specific and have not been much implicated in the bone. MuRF1, MuRF2, MuRF3 are distinct MuRF family proteins with overlapping specificity, they interact with each other and several other substrates. MuRFs have been implicated in several human diseases including heart failure and skeletal muscle atrophy. Muscle-bone interactions are vital not only during development, but also during sarcopenia and osteoporosis. So, this study aims at understanding the role of MuRF in bone loss using MuRF1<sup>+/+</sup>, MuRF1<sup>+/-</sup> & MuRF1<sup>-/-</sup>; MuRF2<sup>+/+</sup>, MuRF2<sup>+/-</sup> & MuRF2<sup>-/-</sup>; and MuRF3<sup>+/+</sup>, MuRF3<sup>+/-</sup> & MuRF3<sup>-/-</sup> mice. All the studies were performed at baseline. The femoras were dissected, cleaned of soft tissue and wrapped in saline soaked gauze and frozen at -20°C. The femoras were assessed with microCT using the SkyScan system to look at the bone microarchitecture in the distal femur metaphysis (1mm) and mid-diaphysis region. Further, three-point bending test was performed to assess the material and structural properties of the bone. The cortical area at the femoral mid-diaphysis region was higher in MuRF1<sup>+/-</sup> mice compared to WT mice, which was further higher in MuRF1<sup>-/-</sup> mice. Also, the cortical thickness was higher in MuRF1<sup>+/-</sup> mice compared to WT mice. However, depletion of MuRF2 and MuRF3 in mice did not have any effect on the cortical parameters, thus highlighting the distinct role on MuRF1. Interestingly, the MuRF2 deficiency seems to alter the structural properties of the bone as seen in increase in toughness in MuRF2<sup>+/-</sup> mice compared to MuRF2<sup>+/+</sup> mice. Thus, ubiquitin ligases seem to be differentially and distinctly regulating the bone microarchitecture and prevents bone loss and seems to be a therapeutic target. Inhibiting MuRF1 and MuRF2 is protective against bone loss and this could be investigated in age-related bone loss, osteoporosis etc.

## IL-4 is protective against murine post-traumatic osteoarthritis

Ericka von Kaeppler<sup>1,2</sup>, Harini Raghu<sup>1,2</sup>, Michelle S. Bloom<sup>1,2</sup>, Qian Wang<sup>1,2</sup>, Heidi H. Wong<sup>1,2</sup>, William H. Robinson<sup>1,2</sup>

<sup>1</sup>Stanford University School of Medicine, Palo Alto, CA, <sup>2</sup>VA Palo Alto Health Care System, Palo Alto, CA

evonk@stanford.edu

**Disclosures:** E. von Kaeppler: None. H. Raghu: None. M.S. Bloom: None. Q. Wang: None. H. Wong: None. W.H. Robinson: 8; Associate editor for Arthritis & Rheumatology.

**INTRODUCTION:** Osteoarthritis (OA), the leading cause of joint failure, is characterized by breakdown articular cartilage and remodeling of the underlying bone in synovial joints. Despite the high prevalence and debilitating effects of OA, no disease-modifying drugs currently exist. Increasing evidence implicates a key role for “low-grade” inflammation in the development of OA, though precise mechanisms remain unclear. A better understanding of contributory inflammatory pathways in degenerative joint disease could transform care for individuals with OA. The cytokine IL-4 has been widely implicated in atopic diseases and has known effects on many cell types found in synovial joints. However, the role of IL-4 in the pathogenesis of OA is poorly defined. Preliminary data showed that IL-4 is downregulated in the synovial membranes of individuals with OA, suggesting that IL-4 is protective against the pathogenesis of OA.

**METHODS:** We tested our hypothesis that IL-4 protects against OA pathogenesis by surgically-inducing osteoarthritis by destabilization of the medial meniscus (DMM) in mice that were globally deficient for either IL-4 (*IL-4<sup>-/-</sup>*) or the signaling mediator STAT6 (*STAT6<sup>-/-</sup>*), had a myeloid-specific deficiency in the IL-4 receptor subunit, IL-4R $\alpha$  (*LysMCre-IL-4R $\alpha$ <sup>-/-</sup>*), or were wildtype (WT). Five months post-surgery, tibio-femoral joints were collected, and Safranin-O stained joint sections were scored according to established metrics for OA severity. To further investigate mechanisms underlying this pathway, two myeloid cell types, macrophages and osteoclasts, were cultured, stimulated *in vitro* and assayed for functional and gene expression changes. Peripheral blood mononuclear cell (PBMC)-derived macrophages were harvested and cultured in the presence of recombinant IL-4. Phagocytic capacity of stimulated macrophages was measured by incubating macrophages with cartilage debris that was covalently labeled with PHrodo-Red dye, a dye that emits fluorescence only after internalization into acidified phago-lysosomes. qPCR was used to characterize gene expression (Tnfa, CD206) in stimulated, cartilage exposed macrophages. Osteoclasts were harvested from bone marrow of WT, *IL-4<sup>-/-</sup>* and *LysMCre-IL-4R $\alpha$ <sup>-/-</sup>* mice and stimulated with recombinant IL-4. Osteoclast differentiation and activation was assayed by measuring tartrate resistant acid phosphatase (TRAP) activity in culture supernatants and by measuring gene expression with qPCR (Nfatc1, Tnfrsf11a, Acp5, Ctsk, Mmp9, Calcr, Car2).

All animal studies were performed under protocols approved by the Stanford Administrative Panel on Laboratory Animal Care (APLAC) and VA Palo Alto Animal Component of Research Protocol (ACORP) committee, and in accordance with the guidelines of the US National Institutes of Health.

**RESULTS:** Following DMM, *IL-4<sup>-/-</sup>*, *STAT6<sup>-/-</sup>*, and *LysMCre-IL-4R $\alpha$ <sup>-/-</sup>* mice (n=10, per group) developed exacerbated cartilage damage, osteophyte formation, and synovitis relative to WT controls (n=10). The semi-quantitative disease severity score was statistically significantly higher in *IL-4<sup>-/-</sup>*, *STAT6<sup>-/-</sup>*, and *LysMCre-IL-4R $\alpha$ <sup>-/-</sup>* mice as compared to WT by two-tailed t-test. *In vitro*, IL-4 stimulated macrophages phagocytosed cartilage debris significantly more than unstimulated macrophages. Additionally, in the presence of cartilage debris, IL-4 stimulated macrophages significantly upregulated the alternative macrophage activation (M2) marker CD206 and significantly downregulated the expression of classical macrophage activation (M1) marker Tnfa. *In vitro*, IL-4 stimulation of WT bone marrow-derived osteoclasts significantly reduced TRAP production and inhibited expression of all markers of osteoclast differentiation (Nfatc1, Tnfrsf11a, Acp5) and activation (Ctsk, Mmp9, Calcr, and Car2). IL-4 stimulation of *LysMCre-IL-4R $\alpha$ <sup>-/-</sup>* bone marrow-derived osteoclasts did not reduce TRAP production, nor inhibit expression of all markers of osteoclast differentiation (Nfatc1, Tnfrsf11a, Acp5) and activation (Ctsk, Mmp9, Calcr, and Car2).

**DISCUSSION:** The exacerbated OA phenotype observed in IL-4-deficient mice supports our hypothesis that IL-4 is protective against OA development. Further, the exacerbated OA phenotype observed in STAT6 deficient mice and in myeloid-specific IL-4R $\alpha$  deficient mice suggests that the IL-4 protective mechanism is mediated through STAT6 signaling in myeloid cell-types. *In vitro*, IL-4 stimulated macrophage M2 polarization and enhanced macrophage phagocytosis of cartilage debris. These data suggested that joint-resident IL-4 might promote an immunomodulatory microenvironment in



which joint-resident macrophages more efficiently clear pro-inflammatory wear-and-tear debris. Additionally, *in vitro*, IL-4 inhibits differentiation and activation of WT bone marrow-derived osteoclasts, but not *LysMCre-IL-4R $\alpha$ <sup>-/-</sup>* bone marrow-derived osteoclasts. These data suggest that the IL-4R $\alpha$  receptor subunit is necessary for osteoclast inhibition by IL-4. These data suggest that IL-4 might promote an anti-osteoclastogenic microenvironment that prevents pathologic activation of subchondral bone osteoclasts in a healthy joint. Taken together, these *in vivo* and *in vitro* results support a role for IL-4 modulation of myeloid cell types in the maintenance of joint health.

**SIGNIFICANCE/CLINICAL RELEVANCE:** (1-2 sentences): Our findings suggest that IL-4 plays a key role in protection against the development of post-traumatic OA, in part, through modulation of myeloid cell types, such as macrophages and osteoclasts. These findings identify a potential novel therapeutic candidate for the treatment of OA.



# Disruption of Notch Signaling targeted to the myeloma bone marrow microenvironment simultaneously inhibits tumor growth and prevents bone loss without inducing gut toxicity

Adam Ferrari, Kevin McAndrews, Jessica Nelson, James Bell, Venkatesan Srinivasan, Frank H. Ebetino, Robert K. Boeckman Jr, G. David Roodman, Teresita Bellido, Jesus Delgado-Calle

Communication between myeloma (MM) cells and cells of the bone marrow via Notch signaling promotes tumor growth/survival and stimulates bone resorption. Systemic inhibition of Notch, using  $\gamma$ -secretase inhibitors (GSIs), decreases MM growth and reduces bone destruction, but the clinical use of GSIs is limited due to dose-limiting severe gut toxicity.

To circumvent GSI side effects, we generated a bone specific Notch inhibitor (BT-GSI) by conjugating GSI-XII to a targeting molecule (BT) with high bone affinity using an acid hydrolyzable linker. *In vitro*, BT-GSI was inactive unless pre-incubated at low pH, and exhibited equal inhibition of Notch target genes in MM cells as unconjugated GSI. *Ex vivo*, BT-GSI decreased Notch expression and reduced MM growth in bone organ cultures that reproduce acidic conditions in the MM-bone microenvironment. *In vivo*, treatment with BT-GSI (5mg/kg/3x/wk, i.p.) for 2 wks decreased Notch signaling in bone more efficiently than unconjugated GSI (10mg/kg/5x/wk, i.p.) in naïve mice. In addition, BT-GSI increased cancellous bone mass (30%) and decreased bone resorption by 40%, without affecting bone formation. In contrast, these parameters remained unchanged by GSI. Next, we examined *in vivo* the impact of BT-GSI on MM growth and bone disease in a preclinical model of established MM. 8-wk-old immunodeficient mice were injected intratibially with  $10^5$  JJN3 human MM (hMM) cells or saline. hMM injected mice exhibited detectable serum levels of the tumor biomarker human K-light chain (40 ng/mL) and visible osteolytic disease (osteolytic area 1.7 mm<sup>2</sup>) 3 wks after hMM inoculation. Then, hMM-injected mice were randomized based on tumor levels to two subgroups to receive either BT-GSI (10mg/kg/3x/wk) or vehicle (DMSO) for 3 wks. Saline-injected mice received vehicle injections. BT-GSI selectively decreased Notch gene expression in bone, but had no effect in the brain or gut. Further, BT-GSI did not increase the expression of Adipsin in the gut, a biomarker of gut toxicity, nor showed evidence of gut toxicity at necropsy. Mice treated with BT-GSI exhibited a 45% decrease in tumor burden (168 vs 254 ng/mL human K-light chain) and 50% less osteolytic area compared to vehicle treated mice bearing hMM (4.4 vs 10.2 mm<sup>2</sup>). Moreover, BT-GSI decreased serum CTX by 30%, but did not affect serum P1NP. Importantly, equimolar administration of the unconjugated BT molecule did not alter MM growth nor prevented bone loss in mice with established MM.

In conclusion, these results show that bone-targeted Notch inhibition reduces MM growth and preserves bone mass in mice with established MM. Because BT-GSI shows bone specific Notch inhibition and lacks gut toxicity, it should circumvent the deleterious side effects that limit GSI use in patients. Thus, BT-GSI is a promising approach to inhibit MM growth and to prevent bone loss in MM patients.

## Using the genetic control of bone mineralization for bone tissue engineering

Steve Falcoz<sup>1,2</sup>, Guillaume Courtemanche<sup>1,3</sup>, Laurent-Pujot-Menjouet<sup>2</sup>, PhD, Jean-Philippe Berteau<sup>1,3</sup>, PhD,

<sup>1</sup> City University of New York, College of Staten Island, USA, <sup>2</sup> Lyon 1 university, France, <sup>3</sup> Université de Technologie Compiègne, France, <sup>4</sup> City University of New York, City College, USA

Bone is a hard soft material that presents a unique combination of stiffness, strength and toughness. While its stiffness and strength mainly come from the gradual hardening a soft collagen matrix by Hydroxyapatite crystals (HA), the toughness is thought to mainly come from sacrificial bindings (Osteocalcin and Osteopontin, OC-OPN complex) between two HA. Both hardening and sacrificial bindings are under the control of the bone Genetic Regulatory Network (GRN) in the nucleus of osteoblasts. Indeed, the GNR activates the production of Tropocollagen (TC) and nucleators and inhibitors of mineralization (BSP, OC, OPN) through the action of transcription factors (RUNX2, OSX, STAB2). Figure 1 provides an overview of this process – from the osteoblast to the creation of sacrificial bindings between two HA. While this process is better and better described, there is still a lack of knowledge on how the GNR can be controlled for building a bone-like material *in vitro*. The goal of our project is to propose a mathematical model of the GRN to guide the hardening a soft matrix *in vitro*. Our hypothesis is to control the mineralization of the soft matrix by acting on the Genetic Regulatory Network (GRN). To do so, we have built a mathematical model using a system of nonlinear differential equations quantifying the number of proteins present in the extracellular matrix of bone according to the stiffness of the mineralized collagen matrix. The interactions between the transcription factors is modelled through Hill function. To validate our model, we have investigated the production of proteins involved in the mineralization by culturing human mesenchymal stem cells on hydrogels with different stiffness's and measured the protein expression.

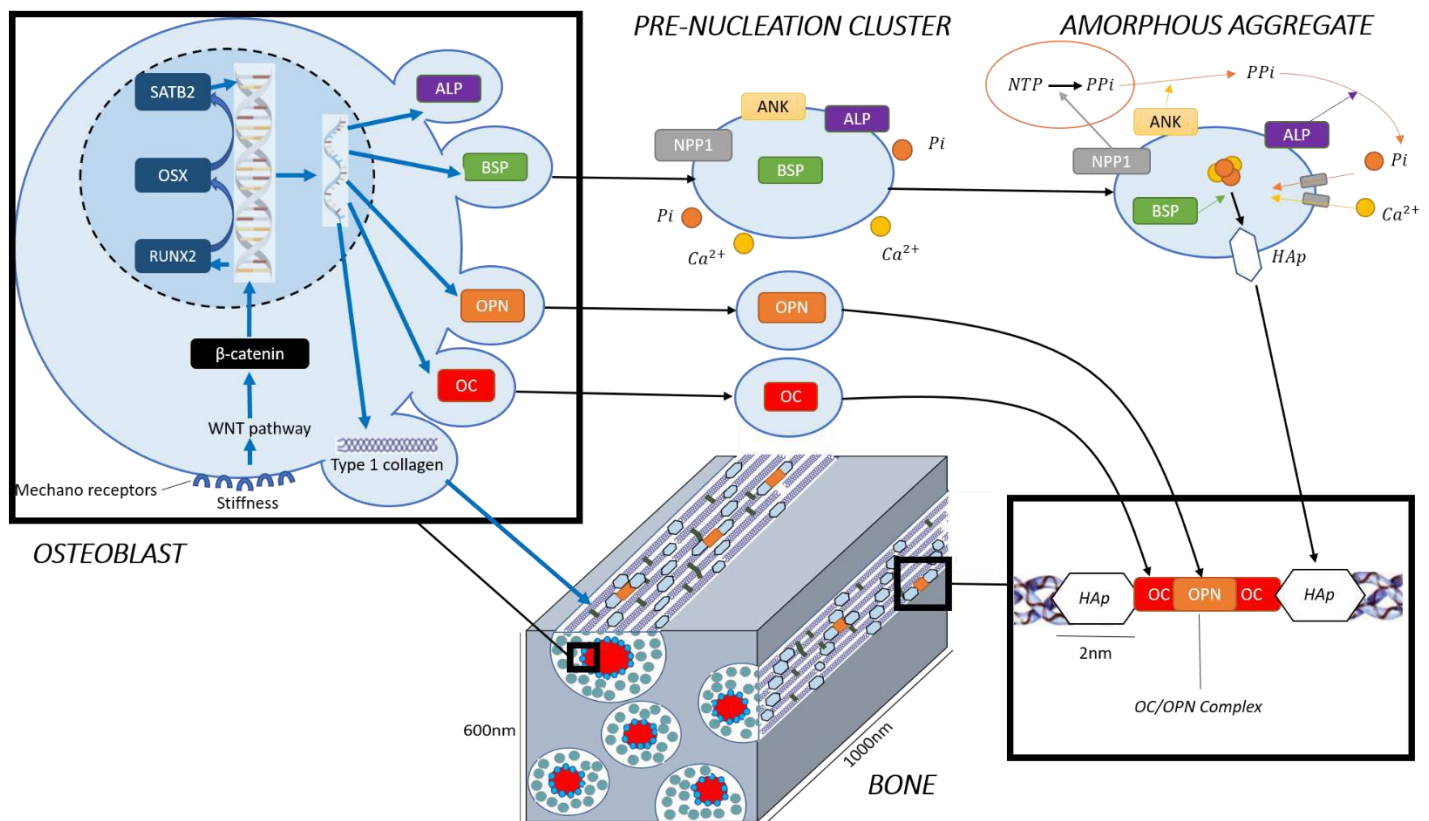


Figure 1: overview of the GNR and the mineralization process – Step 1: Mechano receptors activates the GNR to produce nucleators and inhibitors of bone mineralization. Step 2: Exocytosis of proteins and chemical elements cluster around the matrix vesicle. Step 3 : BSPs nucleate crystals while inhibitors (OC and OPN) create a complex that fits between the crystals to regulate their growth and create sacrificial bindings.

# Disruption of LINC complex in stem cells results in decreased osteogenesis and trabecular architecture

Scott Birks<sup>1</sup>, Stacie Loiate<sup>1</sup>, Destiny Francis<sup>2</sup>, Sarah Manske, PhD<sup>2</sup>, Gunes Uzer, PhD<sup>1</sup>

<sup>1</sup>Boise State University, Boise, ID, <sup>2</sup>University of Calgary, Calgary, AB, Canada

**INTRODUCTION:** Mesenchymal stem cells (MSCs) are multipotent stem cells within bone marrow that support bone modeling at load bearing sites by differentiating into osteoblasts. We recently reported LINC (Linker of Nucleoskeleton and Cytoskeleton) complexes connecting the nucleus to the cytoskeleton play an integral role in MSC response to mechanical challenge by regulating nuclear access of  $\beta$ catenin (1). In this way, depleting LINC complexes results in increased adipogenic bias of MSCs (2). Therefore, we hypothesize that disabling LINC complex function *in vitro* and *in vivo* will negatively impact osteogenesis in MSCs.

**METHODS:** *In vitro*, a dominant negative form of the nesprin KASH domain (DNK) was overexpressed as previously described (2). Osteogenic differentiation was assessed at day 7 by measuring alkaline phosphatase (ALP) mRNA levels via qPCR. For *in vivo* studies, a tamoxifen inducible Cre/Lox mouse model was generated with Cre-mediated disruption of LINC complexes in skeletal MSCs. Briefly, male Tg(Prrx1-cre/ERT2,-EGFP) mice (The Jackson Laboratory) were crossed with female Tg(<sup>HSAfllox</sup>CAG-LacZ/EGFP-KASH2) mice (Didier Hodzic, Washington University School of Medicine in St. Louis) to produce offspring with Cre-mediated EGFP-KASH2 overexpression. Cre expression driven by the Prrx1 promoter was chosen as the Prrx1 gene is shown to be active in bone progenitor cells (3). LINC complex disruption by EGFP-KASH2 overexpression inhibits endogenous nesprin-SUN binding within the nuclear envelope, delocalizing nesprin from the nucleus; thus, disconnecting the nucleus from cytoskeleton (4). Tamoxifen administration began at 7 weeks using +Cre/+LacZ or +Cre/-LacZ male mice and bone endpoints for microCT were collected at 7, 9, and 12 weeks (n=3/group). All procedures approved by Boise State University Institutional Animal Care and Use Committee.

**RESULTS AND DISCUSSION:** As seen in Figure 1, MSCs plated on plastic expressing DNK showed a 61% (p=0.09) decrease in mRNA ALP levels compared to empty plasmid controls. Shown in Table 1, compared to +Cre/-LacZ controls: bone fraction (BV/TV) in +Cre/+LacZ groups was decreased 26% (p=0.1), trabecular separation (Tb. Sp.) was increased by 73% (p=0.09), trabecular number (Tb.N.) was decreased by 35% (p<0.05), and trabecular thickness (Tb.Th.) did not change. Our findings suggest LINC deficiency negatively effects osteogenesis *in vitro* and results in inferior trabecular architecture *in vivo*. We are currently investigating a tamoxifen independent Prrx1-Cre mouse line along with a pre-osteoblastic Osx-Cre strain to study LINC depletion effects on bone growth without the estrogenic effects of tamoxifen (5). Completion of this data will lead to greater understanding of how disrupting LINC-mediated mechanosignaling of bone progenitor cells effects skeletal health *in vivo*.

## REFERENCES:

1. Uzer, G., et al. Sun-mediated mechanical LINC between nucleus and cytoskeleton regulates  $\beta$ catenin nuclear access. Journal of Biomechanics, 2018; 74, 32-40. doi:http://dx.doi.org/10.1016/j.jbiomech.2018.04.013
2. Uzer G, Thompson WR, Sen B, et al. Cell Mechanosensitivity to Extremely Low Magnitude Signals is Enabled by a LINCed Nucleus. Stem cells (Dayton, Ohio). 2015; 33(6):2063-2076. doi:10.1002/stem.2004.
3. Ouyang Z, Chen Z, Ishikawa M, et al. Prx1 and 3.2 kb Col1a1 promoters target distinct bone cell populations in transgenic mice. Bone. October 2013;S8756-3282(13)00426-210.1016/j.bone.2013.10.016. doi:10.1016/j.bone.2013.10.016.
4. Razafsky D, Hodzic D. Temporal and Tissue-Specific Disruption Of LINC Complexes In Vivo. Genesis (New York, NY : 2000). 2014; 52(4):359-365. doi:10.1002/dvg.22755.
5. Zhong ZA, Sun W, Chen H, et al. Optimizing tamoxifen-inducible Cre/lox system to reduce tamoxifen effect on bone turnover in long bones of young mice. Bone. 2015; 81:614-619. doi:10.1016/j.bone.2015.07.034.

	+Cre/+LacZ	+Cre/-LacZ (control)
BV/TV	0.19±0.04	0.25±0.005
Tb. Sp. (mm)	0.29±0.07	0.17±0.016
Tb.N.	3.82±0.8*	5.87±0.4
Tb.Th. (mm)	0.056±0.002	0.056±0.0006

Table 1 Micro-CT bone morphometry measurements for 9-week mice.

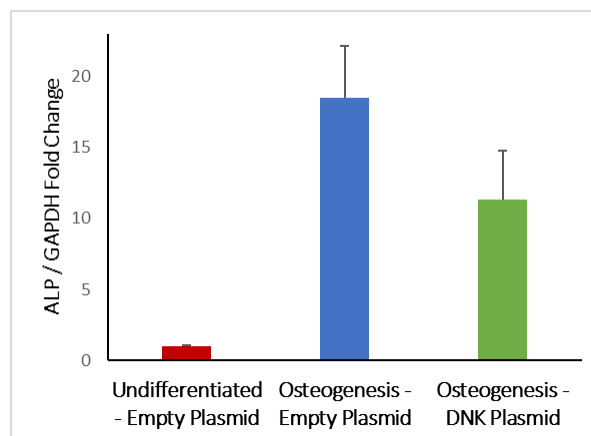


Figure 1 qPCR results probing for alkaline phosphatase expression in undifferentiated MSCs, differentiated MSCs transfected with an empty plasmid, and differentiated MSCs transfected with a DNK plasmid.

# Identification of Multiple Maturational Trajectories: A Longitudinal Assessment of Skeletal Age

Melanie E. Boeyer, MS <sup>1,2</sup>, Emily V. Leary, PhD <sup>1</sup>, Richard J. Sherwood, PhD <sup>1,2</sup> and Dana L. Duren, PhD <sup>1</sup>

Department of Orthopaedic Surgery, University of Missouri, Columbia, MO, <sup>2</sup>Department of Pathology and Anatomical Sciences, University of Missouri, Columbia, MO

Variability in the timing of skeletal growth and development impacts decision making in pediatric clinical practice. However, cross-sectional skeletal maturity assessments rely on the paradigm of linearity (*e.g.*, Greulich and Pyle), which suggests that an ‘average’ maturer will exhibit a 1:1 ratio between chronological and skeletal age throughout childhood and adolescence. The aim of the present study was to characterize changes in the timing and tempo of individual skeletal maturational trajectories and to identify any consistencies that could be characterized as a ‘maturational spurt.’ We leveraged existing data from the Fels Longitudinal Study. The sample included 345 participants, each with approximately 31 consecutive radiographs. Skeletal maturity was assessed using the Fels Hand-Wrist Method. The longitudinal relationship between chronological age and skeletal age, including the presence of a maturational spurt, was assessed independently in each participant using the following three distinct fixed effect models: (1) linear, (2) 4<sup>th</sup> order polynomial, and (3) 5<sup>th</sup> order polynomial. Akaike’s Information Criterion for Finite Sample Sizes (AICc) was used to determine participant-specific model fit; models that exhibited the lowest AICc values were used for subsequent statistical analyses. Maturational milestones (*e.g.*, onset, peak, and cessation) were calculated using the first and second derivative of each participant-specific maturational trajectory. Differences in the chronological age, rate of skeletal maturation (*i.e.*, skeletal age), and duration of time spent between each maturational milestone were calculated and compared among three distinct maturational trajectory types (*e.g.*, childhood spurt only, adolescent spurt only, and both a childhood and adolescent spurt) using a one-way analysis of variance. A non-linear relationship between chronological age and skeletal age is observable in 81% of participants during normal childhood and/or adolescence. A single maturational spurt during adolescence was the most common trajectory type (76% boys; 83% girls), followed by both a childhood and adolescent maturational spurt (15% boys; 13% girls), and a childhood only spurt (9% boys; 4% girls). In both boys and girls, the chronological age of attainment for both onset and peak milestones were significantly earlier in participants who exhibited only an adolescent spurt when compared with those who exhibited both a childhood and adolescent spurt. For example, maturational onset and peak milestones were attained 3.4 and 2.0 years later ( $p < 0.001$ ;  $p < 0.001$ ), respectively, in boys with both a childhood and adolescent maturational spurt when compared with only an adolescent spurt (Table 1). A similar trend was observed in girls ( $p < 0.001$ ;  $p < 0.001$ ), but the magnitude of the differences were larger, on average. We observed no differences in the rate of skeletal maturation among trajectory types, except in the childhood peak milestone for girls ( $p = 0.02$ ). The duration of time spent between maturational milestones was statistically significant, for both boys and girls, between all measurable milestones. This work highlights a critical shift in the skeletal maturational paradigm, particularly in how we interpret variation in the relationship between chronological age and skeletal age during normal growth and development. Because these maturational trajectories are consistent among participants and remarkably similar between boys and girls, rapid changes in skeletal maturation may be predictable given a detailed skeletal maturity assessment in pediatric clinical practice. Additional studies will elucidate specific skeletal phenotypes that drive rapid changes in skeletal maturation for each trajectory type, which will be used to refine future estimates of growth remaining, ultimately enhancing the treatment and management of pediatric patients suffering from growth and/or developmental disorders.

**Table 1.** Maturational Spurt Milestone Estimates by Trajectory Type: mean chronological age (yrs.) of milestone attainment, mean rate (yrs. / yr.) of maturation at milestone attainment, and the standard error (se) of each milestone estimate.

Sex	Trajectory Type	Childhood Peak Age	Onset Age	Adolescent Peak Age	Cessation Age	Childhood Peak Rate	Onset Rate	Peak Rate
Boys	Childhood Only	5.6 (0.22)	---	---	17.6 (0.17)	1.2 (0.04)	---	---
	Adolescent Only	---	6.5 (0.14) **	12.5 (0.22) **	17.5 (0.08)	---	0.8 (0.01)	1.3 (0.02)
	Childhood + Adolescent	5.6 (0.15)	9.9 (0.19) **	14.5 (0.19) **	17.2 (0.16)	1.2 (0.02)	0.9 (0.20)	1.3 (0.19)
Girls	Childhood Only	5.4 (0.18)	---	---	16.7 (0.47)	1.1 (0.18) *	---	---
	Adolescent Only	---	7.0 (0.26) **	11.8 (0.24) **	16.8 (0.11)	---	0.8 (0.02)	1.3 (0.02)
	Childhood + Adolescent	5.6 (0.07)	10.2 (0.20) **	14.6 (0.27) **	16.6 (0.21)	1.3 (0.04) *	0.7 (0.04)	1.3 (0.04)

Note: \* indicates  $p < 0.05$  and \*\* indicates  $p < 0.01$  for maturational milestone estimates between trajectory types within a single sex.

**Optimization of sclerostin and Dkk1 neutralizing antibody ratio to maximize anabolic action in the skeleton.**

Roy Byung-Jun Choi,<sup>1</sup> Alexander G Robling<sup>1</sup>

<sup>1</sup>Department of Anatomy & Cell Biology, Indiana University School of Medicine, Indianapolis, IN

There has been growing interest in identifying molecular targets involved in the Wnt signaling pathway, that could serve as a platform for drug development to treat a variety of skeletal diseases. Among them, sclerostin has been identified as an ideal target for bone degenerative disease, and a neutralizing antibody for sclerostin (Evenity™) has recently been approved for clinical use in Japan to treat patients at high risk of fracture. Sclerostin neutralization is associated with significant osteoanabolic activity. We and others have explored combination therapy to improve the anabolic effects of sclerostin. We found that, whereas antibody-based inhibition of Dkk1 alone has no consistent anabolic effects in the skeleton, Dkk1 antibody is potently anabolic in a Sost knockout background. Further, combined used of sclerostin and Dkk1 antibody (at a 1:1 ratio) has synergistic effects on bone formation that are well beyond individual or additive effects of each therapy. Here, we designed experiments to determine the optimal ratio of sclerostin and Dkk1 antibodies to maximize anabolic action. 8 wk-old female C57BL/6J mice were treated for 5 wks with twice-weekly injection of total antibody at 25 mg/kg. The proportion of Scl-Ab to Dkk1-Ab was varied among groups, but total antibody dose was held constant at 25 mg/kg, such that the groups ranged as indicated in Table 1. Bone density was measured prior to treatment and again after 5 wks of antibody by DXA. After sacrifice,  $\mu$ CT measurements of femur and 5<sup>th</sup> lumbar vertebra were collected. Mechanical testing (3-pt bending) and cortical bone histomorphometry were performed in the femur, using fluorochrome labels injected just prior to the start of antibody treatment and again just before sacrifice. Dkk1-Ab treatment alone was not significantly different from vehicle-treated mice for nearly all of the parameters measured, whereas Scl-Ab alone was, as expected, associated with significant increases (10–50% increase;  $p < 0.05$ ) in DXA-derived properties,  $\mu$ CT measurements in the distal femur and spine, whole bone mechanical properties, and bone formation parameters. The 3:1 mixture of Scl-Ab:Dkk1-Ab exhibited the largest effects on bone properties, and increased trabecular parameters in the femur and spine by ~30% beyond the effect seen in Scl-Ab treatment alone. Cortical properties (e.g., mechanical outcomes, bone formation rates) exhibited less synergy than trabecular properties, but the 3:1 mixture produced the greatest effects for most cortical variables as well. In conclusion, the optimal ratio of sclerostin to Dkk1 neutralizing antibody is roughly 3:1, which produces a significantly greater anabolic effect than sclerostin neutralizing antibody alone, at the same total amount of drug.

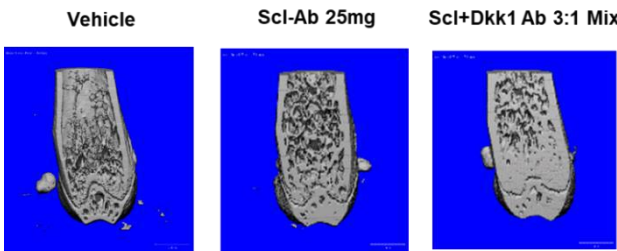
Table 1: Scl-Ab/Dkk1-Ab dose by group

Scl-Ab (mg/kg)	Dkk1- Ab (mg/kg)	Total Ab (mg/kg)	n
25	0	25	6
18.75	6.25	25	7
12.5	12.5	25	7
6.25	18.75	25	7
0	25	25	7
0	0	0	7

**References**

1. Witcher,CP et al., Sclerostin neutralization unleashes the osteoanabolic effects of Dkk1 inhibition. JCI Insight. 2018,3(11):e98673

Figure 1.Trabecular  $\mu$ CT measurements of distal femur



## **Bone-derived Sclerostin has endocrine actions in adipocyte precursors and pancreatic beta-cells.**

Ashley L. Daniel, MS<sup>1</sup>, Adam Ferrari, MS<sup>1</sup>, Jessica H. Nelson, BS<sup>1</sup>, Kevin McAndrew, MS<sup>2</sup>, Meloney Cregor, BS<sup>2</sup>, Ziad Ghazzawi, MD<sup>3</sup>, William Thompson, DPT-PhD<sup>5,6</sup>, Carmela Evans-Molina, MD-PhD<sup>3,4,7</sup>, Teresita Bellido, PhD<sup>2,4,5,7</sup>, Jesus Delgado-Calle, PhD<sup>1,2,5,7</sup>

<sup>1</sup>Department of Medicine, Division of Hematology/Oncology, <sup>2</sup>Department of Anatomy and Cell Biology, <sup>3</sup>Department of Pediatrics, <sup>4</sup>Department of Medicine, Endocrinology, <sup>5</sup>Indiana Center for Musculoskeletal Health, Indiana University School of Medicine, Indianapolis, IN, USA; <sup>6</sup>Department of Physical Therapy, School of Health & Rehabilitation Sciences, Indiana University-Purdue University Indianapolis, Indianapolis, IN, USA, <sup>7</sup>Richard L. Roudebush VA Medical Center, Indianapolis, IN, USA.

Osteocyte (Ot)-derived Sclerostin (Scl) has local actions in bone mediated by Lrp 4/5/6 receptors, inhibiting bone formation and stimulating bone resorption by antagonizing Wnt signaling. Emerging evidence suggests that Scl also exerts functions in distant tissues.

We report here that mice with activated  $\beta$ -catenin in Ots (da $\beta$ catOt) and mice lacking Lrp4 in Ots (Lrp4Ot), two different genetic mouse models that exhibit high serum Scl, display a 2-fold increase in body fat and peripheral white (WAT) and brown (BAT) adipose tissue mass. To determine Scl's contribution to the high fat phenotype, da $\beta$ catOt mice were crossed with SOST knockout mice (da $\beta$ catOt;SOSTKO mice). Deletion of SOST restored to control levels the elevated body-fat mass and WAT mass, but not BAT, of da $\beta$ catOt mice. In contrast, blockade of Scl signaling in bone via genetic deletion of Lrp4 in Ots (da $\beta$ catOt;Lrp4Ot mice) did not alter the high body fat displayed by da $\beta$ catOt mice, demonstrating that Scl effects on adipose tissue were not mediated by Scl actions on Ots. Consistent with direct effects of Scl on adipose tissue, recombinant Scl enhanced by 20% adipogenic differentiation of murine adipocyte precursors (preAd) in vitro, and increased the expression of mitochondrial related genes Pgc1a, Ucp1, and Prdm16 in preAds as well as in ex vivo fat organ cultures established from WAT. Further, Scl augmented mitochondrial respiration in preAds by increasing maximal respiration and spare capacity by 15%, suggesting that Scl promotes adipogenesis in preAds by regulating mitochondrial activity. Both models of high serum Scl, da $\beta$ catOt and LRP4Ot mice, also were hypoglycemic and exhibited impaired glucose tolerance compared to control littermates. Genetic deletion of SOST restored to control values the low blood glucose levels and impaired glucose tolerance of da $\beta$ catOt mice, showing that serum Scl regulates glucose metabolism. Further, Scl fully prevented the increase in insulin mRNA expression induced by Wnt3a in rat pancreatic  $\beta$ -cells and decreased by 45% insulin secretion induced by high-glucose media, demonstrating that Scl acts directly on pancreatic  $\beta$ -cells to impair insulin production.

In concert, these findings demonstrate that Scl exerts endocrine actions in fat tissues and the pancreas to regulate body composition and glucose metabolism, respectively. Further, our results provide new evidence supporting that endocrine actions of Scl mediate the crosstalk between bone and fat and the pancreas

# Pretreatment with Anti-Sclerostin Antibody Protects from Disuse-Induced Bone Loss in the Proximal Tibia of Unloaded Male Rats

Jon P. Elizondo<sup>1</sup>, Jessica E. Brezicha<sup>1</sup>, Scott E. Lenfest<sup>1</sup>, Zach L. Kohn<sup>1</sup>, Susan A. Bloomfield, PhD<sup>1</sup>, Harry A. Hogan, PhD<sup>1</sup>

<sup>1</sup>Texas A&M University, College Station, Texas

Anti-sclerostin antibody treatments enhance bone formation and strength by interfering with osteocyte pro-resorptive signaling.<sup>[1]</sup> The recent FDA approval of this agent is encouraging for NASA, who could use anti-sclerostin antibody to protect astronauts from bone loss on their 2030s Mars mission. Accordingly, this study used the hindlimb unloading (HU) rat model to evaluate the effectiveness of anti-sclerostin antibody as a preventive pretreatment to disuse-induced bone loss.

Prior to any HU, we administered 25 mg/kg of anti-sclerostin antibody (Eli Lilly Corporation, Indianapolis, IN) to 6 mo. old male Sprague Dawley rats once per week for 4 weeks. At the end of the 4 weeks, we assessed the densitometry and geometry of the proximal tibia metaphysis of these animals with *in vivo* pQCT.

We then used the tail traction method of HU to simulate microgravity conditions for 4 weeks. Our methods were an adaptation of the technique originally described by Morey-Holton.<sup>[2]</sup> One group of animals was designated as ambulatory control (CON), while the sclerostin-treated animals (SCL) and an untreated hindlimb unloading control group (HUC) were subjected to HU. After the 4 weeks of HU, we once more performed *in vivo* pQCT scans on our animals.

Following HU, the rats recovered with normal weight-bearing cage activity for 8 weeks. We performed another set of *in vivo* pQCT scans after 4 weeks of recovery and at the end of the 8-week recovery period. We determined statistical significance at  $\alpha=0.05$  with a repeated-measures ANOVA and Tukey post-hoc test.

Immediately after the four-week treatment period (d28), we found elevations in total BMC, total vBMD, and cortical area in the SCL group compared to the untreated control groups. After 4 weeks of hindlimb unloading (d56), HUC animals exhibited reductions in all measures compared to the other two groups. SCL-treated HU rats had higher total vBMD and BMC than did CON animals, and cortical area and thickness in SCL-treated rats were no different from CON. Halfway through recovery (d84), HUC values remained lower than CON and SCL in total BMC and lower than CON in cortical area. No other significant differences were found after the first four weeks of recovery. At the end of 8 weeks' recovery (d112), BMC of the SCL group remained elevated compared to HUC (Fig. 1), but no other significant differences were found for any measure.

Treatment with anti-sclerostin antibody produced positive changes in bone densitometry and geometry in the adult rat proximal tibia. The pre-treatment protected from losses through a subsequent 4-week period of HU. However, the effects of the anti-sclerostin antibody did not seem to persist through a subsequent recovery period, as all three groups somewhat converged during that period. Nevertheless, our data reveal that treatment with anti-sclerostin antibody has potent osteogenic effects that continue after withdrawal and protect from disuse. This drug should thus be a strong candidate therapeutic for long-term spaceflight missions.

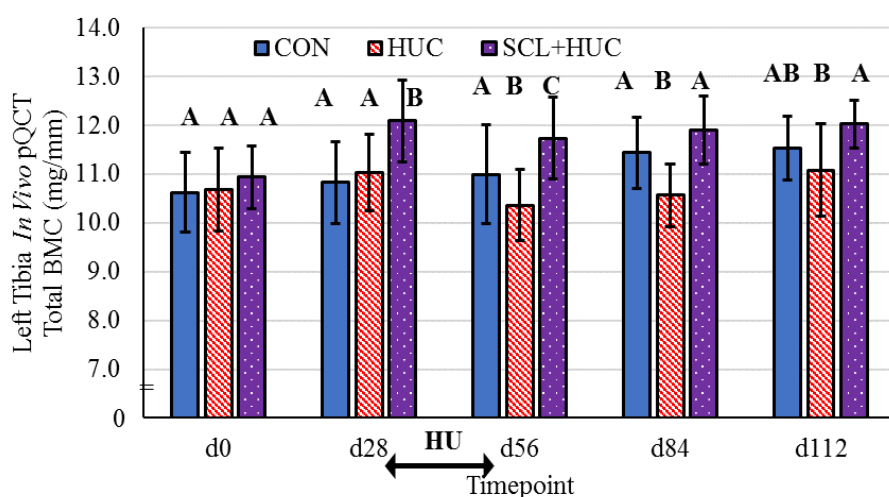


Figure 1. Total BMC at Proximal Tibia; groups not sharing letters at the same timepoint are significantly different

- [1] Spatz JM, Ellman R, Cloutier AM, Louis L, van Vliet M, Suva LJ, Dwyer D, Stolina M, Ke HZ, Bouxsein ML. Sclerostin antibody inhibits skeletal deterioration due to reduced mechanical loading. *Journal of Bone and Mineral Research*. 2013.
- [2] Morey-Holton ER, Globus RK. Hindlimb unloading rodent model: technical aspects. *Journal of applied physiology*. 2002.



## Structural and compositional analysis of bone and its relevance to mechanical properties

Kendall Stauffer<sup>1</sup>, Michael Sieverts<sup>1</sup>, Ian Robinson<sup>2</sup>, Josh Johnson<sup>3</sup>, Caroline Garrett DVM<sup>4</sup>, Pratima Labroo PhD<sup>3</sup>, Nikolai Sopko MD, PhD<sup>1,2,3</sup>

<sup>1</sup> Division of Analytical and Translational Research, Department of Research and Development, PolarityTE, Inc. 1960 S 4250 W Salt Lake City, UT, USA. <sup>2</sup> Division of Cell and Tissue Biology, Department of Research and Development, PolarityTE, Inc. 1960 S 4250 W Salt Lake City, UT, USA. <sup>3</sup> Division of Biomechanical Engineering, Department of Research and Development, PolarityTE, Inc. 1960 S 4250 W Salt Lake City, UT, USA. <sup>4</sup> Department of Veterinary Medicine, PolarityTE, Inc. 1960 S 4250 W Salt Lake City, UT, USA.

Bone mineralization, composition, and mechanical properties are important parameters that affect the integrity of bone. It is essential to understand the relationship between these properties to enable better product design and development and better understand physical properties of native bone and therapeutic adjuvants. The use of micro computed tomography (microCT), mechanical testing, and Raman spectroscopy have been shown to accurately assess the classification and quantification of key characteristics of corticocancellous bone. The purpose of this study was to better understand and describe how these differing biomechanical platforms relate to one another when conducting multimodal elucidation of bone characterization.

Two different bone types, craniofacial and long bone (ulna), were acquired from skeletally mature New Zealand White rabbits. Each type of native bone underwent microCT, mechanical testing, and Raman spectroscopy. Raman spectra were used to extract mineral (hydroxyapatite and carbonate) and matrix components (amides and collagen) for compositional analysis. Mechanical testing (indentation) was performed to determine the modulus, and microCT was used to evaluate bone mineral density (BMD) (mgHA/cc), and bone volume fraction (BVf) (% BV/TV). All data points were compiled and analyzed for reporting trends of interest.

Characterization analysis among alternate bone types show a difference in BMD and BVf between long bone and craniofacial bone. Long bone, in both cases, had a higher BMD and BVf compared to craniofacial bone. This was similar to our observations in Raman spectra-derived phosphate to proline peak ratios and phosphate to carbonate ratios. Both ratios had higher values in long bone compared to craniofacial bone. These findings suggest that there is a difference in hydroxyapatite concentrations between bone types. Mechanical testing via indentation further indicates that both bone types are mechanically strong but long bone had greater mechanical strength as corroborated by BMD and peak ratios.

In conclusion, we have shown that bone mineralization and composition data can be obtained using Raman spectroscopy and microCT, and subsequently correlated with mechanical property analysis. Multimodal examination of each bone type revealed significant differences when compared to each other. The bone characterization technique described herein suggests that BMD, Raman peak ratios, and mechanical indentation testing demonstrate correlative trends of long bone being more minerally dense and structurally stronger when compared to the craniofacial bone. Additionally, these methods and the subsequent data used to characterize bone types may be useful diagnostic tools for medical care providers and orthopaedic-based healthcare organizations.

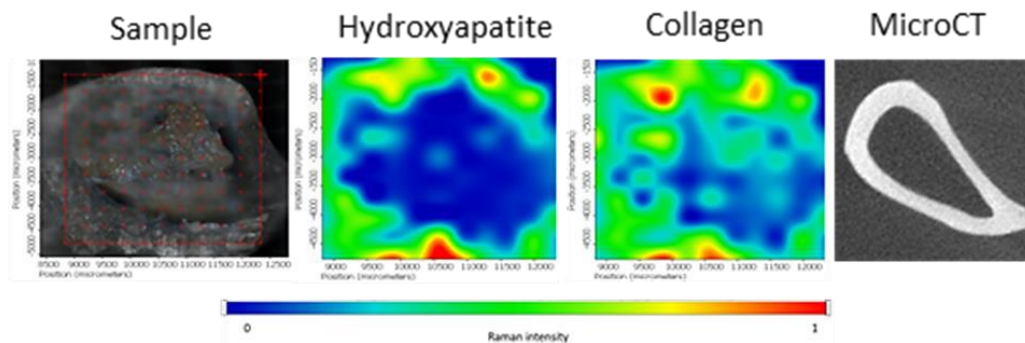


Figure 1. (Left to right) Representative gross images of an osseous cross section, chemigram of hydroxyapatite distribution, chemigram of bone cross section showing collagen distribution, representative axial slice of native long bone.

## A Novel Chondro-Osseous Progenitor Induced During Heterotopic Bone Formation

*Julio Mejia; Elizabeth Salisbury Ph.D.; Zbigniew Gugala M.D., Ph.D.; Elizabeth A Olmsted-Davis Ph.D.; Alan R Davis Ph.D.*

To identify chondrocyte stem cells recruited during in heterotopic bone formation (HBF), lineage tracking studies were done in a glutamate-aspartate transporter (GLAST)- Cre<sup>Ert2</sup>:tdTomato red (TR)<sup>floxSTOPflox</sup> mouse. The results show that approximately 85% of the initial chondrocytes are GLAST-TR<sup>+</sup> cells and 79% of the osteoblasts lining bone. Pulse-chase experiments through delivery of tamoxifen show the majority of cell labeling occurs within 48 hours after delivery of BMP2. Additionally, GLAST-TR<sup>+</sup> cells were identified within HBF at 48 hours and continued to increase until they peaked at day 14 and then decreased at day 21, correlating with the peak of HBF. Analysis of skeletal bone showed the presence of GLAST-TR<sup>+</sup> cells in the epiphyseal region with kinetics of incorporation matching that observed in HBF. GLAST-TR<sup>+</sup> cells were also identified in the circulation where they peaked at day 10, just prior to the peak of GLAST-TR<sup>+</sup> cells at the site of HBF. These circulating GLAST-TR<sup>+</sup> cells also incorporated into fracture callus and were the major cell present in the callus, suggesting that they can function as normal chondrocytes and osteoblasts. GLAST-TR<sup>+</sup> cells isolated by FACS on day 10 were subjected to single-cell RNA seq. Transcriptomes could be clustered into 9 distinct cell types, many of which expressed transcripts associated with osteoblasts and chondrocytes. One cluster appeared to have some overlap with the published neural stem cell transcriptome and was found to be expressing GLAST<sup>(1)</sup>. Further analysis of the data using the Monocle algorithm showed the presence of two distinct terminal populations, which express chondrocyte-associated genes and one that expresses osteoblast-associated genes. These populations all branched from a cluster that expresses both osteoblast and chondrocyte associated genes. The presence of this Sp7<sup>+</sup> Sox9<sup>+</sup> chondro-osseous progenitor (COP) within HBF was confirmed by immunohistochemical analysis. Surprisingly, one additional terminally differentiated cluster uniquely expressed endothelial cell associated transcripts (Pecam, Esam, Epas1, and Flt). Analysis by a differential gene test suggested that several endothelial genes were involved in the branch point from the chondrocyte intermediate. The data suggests that during HBF there are several different populations of chondrocytes, rather than a single phenotype.

# Constitutive Activation of MEK1 in Osteoprogenitors Increases Strength of Mouse Bone Despite Impairing Mineralization

Jeffrey S. Nyman, PhD<sup>1</sup>, R. Clay Bunn, PhD<sup>2</sup>, Phillip Ray, MS<sup>1</sup>, Evangelia Kalaitzoglou, MD<sup>2</sup>, Sasidhar Uppuganti, MS<sup>1</sup>, Kathryn M. Thrailkill, MD<sup>2</sup>, John L. Fowlkes, MD<sup>2</sup>

<sup>1</sup>Vanderbilt University Medical Center, Nashville, TN, USA <sup>2</sup>University of Kentucky Barnstable Brown Diabetes Center, Lexington, KY, USA

**Introduction:** While multiple mouse models have been generated to study diseases that involve the mitogen-activated protein kinase (MAPK) pathway (known as RASopathies) [1], there is currently no translational animal model available to study melorheostosis, a rare genetic disease that presents radiologically as “dripping candle wax” [2]. Prior transgenic mouse models established that the extracellular signal-regulated kinase (ERK)/MAPK pathway promotes osteoblast differentiation and bone mass [3,4] through known transcription factors critical to osteogenesis (RUNX2 and ATF4) [5]. A recent clinical study identified a somatic mutation in the MAPK kinase 1 gene (*MAP2K1*) that causes constitutive activation of MEK1 in osteogenic cells of melorheostotic bones [6]. To understand whether elevated MEK1 signaling has a positive or negative effect on bone, we generated a mouse that postnatally over-expresses a *MAP2K1* mutation resulting in constitutively active MEK1 in cells of the osteoblast lineage.

**Methods:** The *Osx-Cre* transgenic mouse (B6.Cg-Tg(Sp7-tTA,tetO-EGFP/cre)1Amc/J; Jax labs) was crossed with the R26Stop<sup>flox</sup>MEK1DD mouse (C57BL/6-Gt(*ROSA*)26Sor<sup>tm8(Map2k1\*,EGFP)Rsky</sup>/J; Jax labs) producing R26Stop<sup>flox</sup>MEK1DD/*Osx-Cre*<sup>+/-</sup> mice. Cre-negative littermates were the control (Control, n=8). From conception until weaning, dams were fed rodent chow with doxycycline (DOX) to suppress the constitutively active MEK1DD allele. After weaning, pups were fed a regular chow diet without DOX, thereby causing postnatal activation of the mutated allele (MEK1DD-Ob, n=15). Mice were euthanized at 22 weeks, and the left femur was harvested for micro-computed tomography evaluations (6 µm) and three-point bending tests (3 mm/min). The right femur was fixed in ethanol and dehydrated for plastic embedding and histomorphometry of distal femur metaphysis. Pooling the sexes, we used two-tailed t-tests with Welch’s correction or Mann-Whitney test (non-Gaussian distribution) to determine whether a property was significantly different between the genotypes.

**Results:** There was no significant difference in body mass between MEK1DD-Ob and Control mice (p=0.237). In addition, bone formation rate (dynamic histomorphometry) and the number of osteoblasts/osteoclasts (static histomorphometry) did not vary between the genotypes (Table). However, osteoid thickness (O.Th) and mineralization lag time (Mlt) were strikingly higher for MEK1DD-Ob than for Control mice. Corroborating this apparent defect, tissue mineral density of cortical (Ct.TMD) and trabecular bone (Tb.TMD) was significantly lower for the mice with constitutively active MEK1 in osteoblasts than compared to Control. There were 2 additional striking features of the MEK1DD-Ob phenotype: higher metaphyseal bone volume fraction (BV/TV) that extended through the medullary canal and higher cortical porosity (Ct.Po) within the cortex of the mid-shaft. Given the lower Ct.TMD, lower cortical thickness (Ct.Th), higher Ct.Po, and equivalent moment of inertia (*I*<sub>min</sub>), it was surprising to observe that the ultimate stress and ultimate force endured by the femur in bending were significantly higher for MEK1DD-Ob than for control mice. There was no genotype-related difference in bone toughness.

**Discussion:** Melorheostotic bone has been described as dense and rigid, capable of dulling osteotomes when biopsied [6]. This phenotype is counterintuitive because affected bone, compared to unaffected bone of the same patient, is also known to exhibit osteoidosis, elevated vascular-lacunar porosity, reduced degree of mineralization, and reduced tissue-level hardness [2]. The bone phenotype of the MEK1DD-Ob mouse is similar to melorheostotic bone as follows: low TMD, high osteoid thickness, and high strength. A bone-targeted therapy that inhibits the MAPK pathway could treat this rare disease. Conversely, certain aspects of MEK1 signaling pathway could be exploited to increase bone strength in the face of impaired mineralization.

**References:** [1] Hernández-Porras and Guerra. Methods Mol Biol. (2017). [2] Jha et al. J Bone Miner Res. (2019). [3] Ge et al. J Cell Biol. (2007). [4] Matsushita et al. Mol Cell Biol. (2009). [5] Greenblatt, Shim, Glimcher. Annu Rev Cell Dev. (2013). [6] Kang et al. Nat Commun. (2018).

**Acknowledgements:** R56DK055653, R21AR070620, and UK Barnstable Brown Diabetes Center Research Endowment supported this work.

Differences in selected properties between genotypes (mean±SD)					
Property	Units	Control	MEK1DD-Ob	p-value	
BV/TV	%	15.2 ± 6.1	27.5 ± 8.5	0.0008	
Tb.Th	µm	45.1 ± 3.6	49.5 ± 4.7	0.0240	
Tb.TMD	mg·HA/cm <sup>3</sup>	949 ± 18	905 ± 17	<0.0001	
I <sub>min</sub>	mm <sup>4</sup>	0.158 ± 0.029	0.175 ± 0.038	0.241	
Ct.Th	mm	0.167 ± 0.007	0.154 ± 0.009	0.0028	
Ct.TMD	mg·HA/cm <sup>3</sup>	1235 ± 37	1174 ± 16	0.0018	
Ct.Po.N	1/mm	3.17 ± 0.42	4.35 ± 0.62	<0.0001	
Ult force	N	18.7 ± 3.8	25.3 ± 5.1	0.0024	
Ult stress	MPa	157.5 ± 14.4	199.6 ± 34.0	0.0005	
PYD	mm	0.54 ± 0.12	0.47 ± 0.30	0.1901	
Tough.	MJ/m <sup>3</sup>	4.4 ± 0.4	4.9 ± 1.4	0.5579	
N.Ob/B.Pm	100·mm <sup>-1</sup>	33.26 ± 16.16	36.85 ± 31.46	0.8286	
N.Oc/B.Pm	100·mm <sup>-1</sup>	33.66 ± 30.28	22.10 ± 18.60	0.3043	
BFR/BS	mm <sup>3</sup> /cm <sup>2</sup> /y	1.70 ± 0.54	1.54 ± 0.97	0.6602	
OS/BS	%	0.58 ± 0.50	5.70 ± 5.52	0.0002	
O.Th	µm	2.21 ± 0.68	6.32 ± 1.74	<0.0001	
Mlt	Days	0.27 ± 0.20	8.26 ± 6.44	<0.0001	

## ACL femoral enthesis degeneration: a factor to consider in ACL reconstruction

D.M. Patton, C.T. Martin, M. Casden, K.J. Jepsen, J.A. Ashton-Miller, E.M. Wojtys, S.H. Schlecht  
University of Michigan, Ann Arbor, MI, USA

**Introduction:** The incidence rate of a primary ACL graft failure is 6 times higher for younger (< 20 years of age) compared to older individuals<sup>1</sup>. Addressing high revision rates has largely focused on technical errors<sup>2</sup> (i.e., malposition), however, biologic factors account for up to 43% of all graft failures<sup>3</sup>. A major reason for poor surgical outcomes is osteolysis within the graft tunnel resulting in both auto- and allo-graft loosening<sup>4</sup>. Our overarching hypothesis is that tunnel osteolysis is facilitated by the loss of bony structural integrity within the mineralized ACL enthesal structures following native ligament failure. Others have shown that apparent and volumetric bone mineral density (BMD) within the distal femur and proximal tibia decreases following ACL injury<sup>5</sup>. However, clinical BMD is unable to adequately inform on mineralized changes in a small region of interest such as that adjacent to the femoral ACL enthesis, where most native failures occur<sup>6</sup>. Moreover, clinical BMD fails to account for bone morphology and does not differentiate the contributions of cortical and trabecular tissues. Therefore, we tested the hypothesis that injured femoral ACL entheses will show a significant decrease in cortical and trabecular bone mass compared to non-injured controls.

**Methods:** Forty-nine injured (I) patient (Female [F], 13-20 years) femoral ACL enthesis explants were collected during their ACL reconstructive surgery procedure. Ten non-injured (NI) control explants (F, 21-36 years) were collected from donors using the same 'outside-in' surgical procedure as performed on patients. High-resolution (14 $\mu$ m voxel size) scans of the femoral explants were acquired using a nano-CT system (phoenix x-ray, GE, Germany). Images were converted to Hounsfield units and analyzed for cortical and trabecular architecture. For the cortex, volumetric bone mineral density (vBMD), relative bone volume (BV/TV), and porosity were quantified. For the trabecular tissue, vBMD, BV/TV, trabecular thickness (Tb.Th), and trabecular spacing (Tb.Sp) were quantified. Statistics were performed using a two-way analysis of variance to test for age and elapsed time from injury main effects, and age by time-from-injury interactions with a significance of  $p < 0.05$ . Tukey multiple comparisons test were also done to determine the significance of least mean square differences in the presence of important interactions. Prior to analysis, the time-from-injury data was seriated into 4 separate groups (1-7, 8-11, 12-16 and 17+ weeks post-injury).

**Results:** Compared to non-injured femoral explants, the injured explants collectively had significantly less cortical vBMD (NI: 720.3 - 862.5 mg/cc; I: 451.2 - 891.9 mg/cc;  $p < 0.01$ ), BV/TV (NI: 0.659 - 0.867; I: 0.401 - 0.792;  $p < 0.01$ ), and porosity (NI: 0.133 - 0.341; I: 0.209 - 0.600;  $p < 0.01$ ) (Fig 1). Injured patient explants also had significantly less trabecular vBMD ( $p = 0.04$ ) but not trabecular BV/TV ( $p = 0.14$ ), Tb.Th ( $p = 0.36$ ) and Tb.Sp ( $p = 0.66$ ) compared to controls. When assessing main effect differences, cortical vBMD ( $p = 0.01$ ), BV/TV ( $p = 0.05$ ) and porosity ( $p = 0.05$ ) were significantly different from baseline controls across all time from injury groups, but not for age. Age by time-from-injury interaction was only significant for vBMD ( $p = 0.02$ ). For trabecular measures, vBMD, BV/TV and Tb.Th showed no age or time-from-injury main effect differences, but Tb.Sp did show a significant age main effect ( $p < 0.01$ ). Additionally, the age by time-from-injury interaction was only significant for Tb.Th and was specific to the 12-16 week and 17+ week groups.

**Conclusions:** On average, patients with ACL injuries had significantly less cortical and trabecular bone compared to controls. However, some patients maintained bone integrity better than others which may, in part, reflect age and time-from-injury differences. Bone structural integrity at the ACL enthesis may play an important role in ACL graft failure prevalence resulting from tunnel osteolysis. Our results suggest that, at 2 – 3 months post-injury, when the majority of surgical interventions are done, the mineralized enthesal tissue into which a graft is placed may not be in an optimal remodeling state to maximize graft osseointegration with the native mineralized tissue. Further work is needed to assess the cellular integrity of the mineralized enthesal matrices following ACL injury.

**References:** <sup>1</sup>Webster et al. 2014. AJSM; <sup>2</sup>Kamath et al. 2011. AJSM; <sup>3</sup>Dye et al. 1993. AJSM; <sup>4</sup>Wilson et al. 2004. AJSM; <sup>5</sup>van Meer et al. 2014. Osteoarthr Cartilage; <sup>6</sup>Kocher et al. 2002. AAJSM. **Funding:** NIH/NIAMS AR070903 (SHS); AR054821 (EMW, JAAM); AR069260 (KJJ).

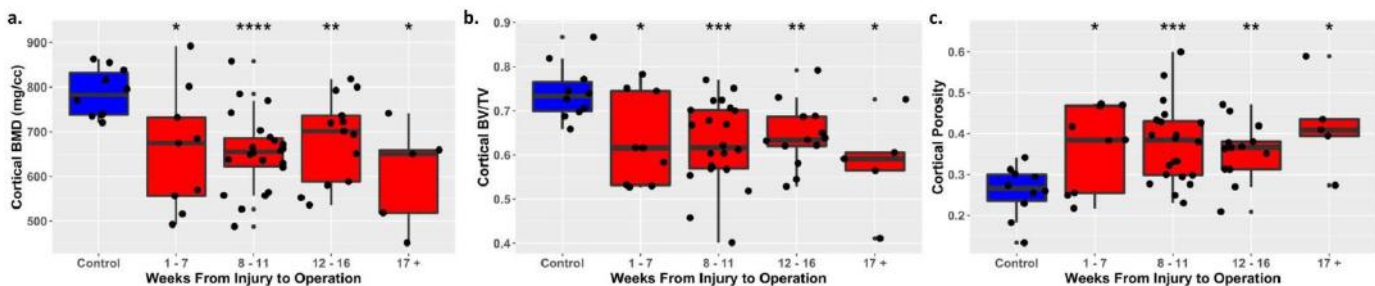


Figure 1: Unpaired t-test between patient and control explants for cortical (a) vBMD, (b) BV/TV, and (c) Porosity (\*  $p < 0.05$ , \*\*  $p < 0.01$ , \*\*\*  $p < 0.001$ , \*\*\*\*  $p < 0.0001$ ).

## Sclerostin antibody rescues hypophosphatemia and increases bone mass in *Hyp* mouse model

Ryan D. Ross, PhD; Kelsey Carpenter, MS - Rush University Medical Center, Chicago, IL USA

X-linked hypophosphatemia (XLH) is the most common form of vitamin-D resistant rickets caused by a loss-of-function mutation in the phosphate regulating gene with homology to endopeptidase located on the X chromosome (PHEX). This mutation leads to elevated fibroblast growth factor 23 (FGF23) levels which subsequently impair phosphate reabsorption in the kidney and inhibit skeletal mineralization. XLH is commonly diagnosed in children who exhibit shortened stature and leg bowing. XLH patients also present with decreased bone mass and are at an increased fracture risk.

Sclerostin, a protein produced primarily in osteocytes, suppresses bone formation by antagonizing Wnt-signaling and is elevated at both the gene level in *Hyp* mice (2,3), the XLH murine homolog, and in the circulation of XLH patients (4). Sclerostin's role in the pathophysiology of XLH has not yet been investigated. We hypothesize that sclerostin is a key regulator of phosphate metabolism and skeletal mineralization and that suppression of sclerostin via sclerostin antibody (Scl-Ab) can improve both metabolic and skeletal pathologies of XLH.

Male hemizygous and female heterozygous *Hyp* mice and wild type littermates were used for this study. Mice were randomly assigned to biweekly subcutaneous injections of either 25 mg/kg Scl-Ab or vehicle (saline) treatment starting at 4-weeks of age until sacrifice at 8 weeks of age. Right femurs were collected for micro-computed tomography ( $\mu$ CT, Scanco  $\mu$ CT50). Cortical area was assessed at the midpoint of the femoral diaphysis, while trabecular bone volume fraction (BV/TV) was assessed at the distal femoral metaphysis, just proximal to the growth plate. Cortical osteoid surface per bone surface (OS/BS) was assessed in histological sections from the distal femur following Goldner's Trichrome staining for unmineralized osteoid. Serum was collected for analysis of circulating phosphate (Biovision) and fibroblast growth factor 23 (FGF23) levels (Immuntopics). Data was compared separately for males and females using a two-way analysis of variance (ANOVA) with genotype and treatment as the independent factors. When main effects were significant post-hoc analysis was performed using an independent student's T-test. A significance threshold of  $p < 0.05$  was set for all primary endpoints.

Scl-Ab treatment increased serum phosphate in treated wild-type and *Hyp* mice of both sexes, with significant treatment effects noted in both males and females (Fig 1a). Scl-Ab treatment significantly suppressed circulating levels of intact FGF23 (Fig 1b). Cortical area and trabecular BV/TV increased with Scl-Ab treatment in both sexes (Fig 2a and 2b, respectively). Scl-Ab treatment significantly reduced the OS/BS in males, with a trend towards significance in the females. The current study demonstrates that short-term treatment of growing *Hyp* mice with Scl-Ab leads to significant improvement in circulating phosphate and bone structure. Surprisingly, there was also a significant reduction in the circulating levels of intact or active FGF23 following Scl-Ab treatment, suggesting that sclerostin influences FGF23 production.

**REFERENCES:** (1) TM Carpenter et al. J Bone Miner Res 2011 26(7): 1381-1388. (2) GJ Atkins et al. J Bone Miner Res 2011 26(7): 1425-1436. (3) LV Zelenchuk et al. Bone 2015 72:23-33. (4) T. Palomo et al. J Clin Endocrinol Metab 2014 99(5):E920-925. **ACKNOWLEDGEMENTS:** Sclerostin antibody provided by Amgen Inc, Thousand Oaks, CA and UCB. Brussels, Belgium.

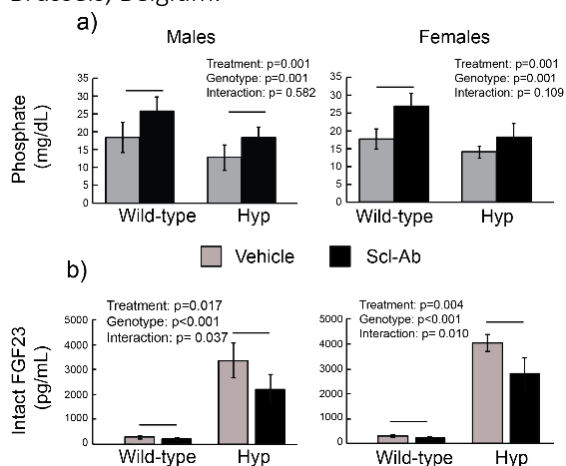


**Figure 1:** Circulating a) phosphate and b) intact FGF23 in male (left) and female (right) mice.

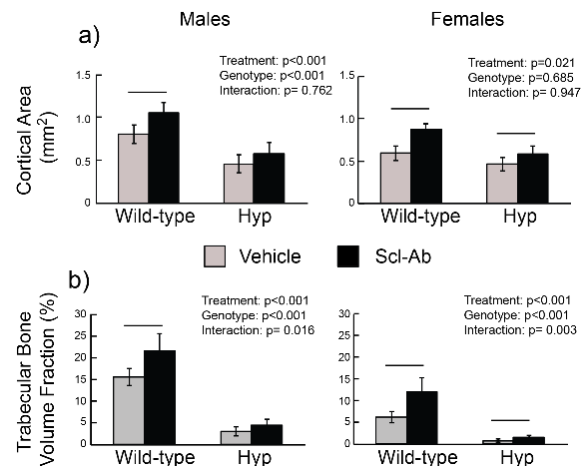


**Figure 2:** a) Cortical area at the femoral mid-diaphysis and b) trabecular BV/TV at the distal femoral metaphysis in male (left) and female (right) mice.

**Vitamin D receptor signaling prevents the adverse actions of glucocorticoid excess in bone, skeletal muscle, and the heart, by interfering with the atrogene pathway.**

Amy Y. Sato, PhD<sup>1</sup>, Meloney Gregor,<sup>1</sup> David L. Halladay,<sup>1</sup> Karyn A. Esser, PhD<sup>2</sup>, Munro Peacock, MD<sup>3</sup>, Monte S. Willis, MD PhD MBA<sup>4</sup>, Teresita M. Bellido, PhD<sup>1,3,4,5</sup>

<sup>1</sup>Department of Anatomy and Cell Biology, Indiana University School of Medicine, Indianapolis, IN, <sup>2</sup>Department of Physiology and Functional Genomics, University of Florida College of Medicine, Gainesville, FL, <sup>3</sup>Division of Endocrinology, Department of Medicine, Indiana University School of Medicine, Indianapolis, IN, <sup>4</sup>Indiana Center for Musculoskeletal Health, University of Indiana School of Medicine, Indianapolis, IN, <sup>5</sup>Richard L. Roudebush Veterans Affairs Medical Center, Indianapolis, IN.

Glucocorticoid (GC) excess has adverse effects in bone and skeletal muscle that lead to increase in fracture risk. GCs upregulate in both tissues the expression of the proteasomal degradation inducers MuRF1, atrogin1, and MUSA1 (atrogenes), thus providing a targetable pathway to prevent GC musculoskeletal actions. We investigated here whether Vitamin D receptor (VDR) activation, which has beneficial effects in bone and may prevent muscle weakness and falls, blocks GC-induced activation of the atrogene pathway and prevents bone and muscle loss. 1,25D<sub>3</sub> (calcitriol) prevented dexamethasone (dex)-induced atrogene expression *ex vivo* in murine bone and muscle organ cultures. *In vivo*, 1,25D<sub>3</sub> or the less hypercalcemic VDR ligand eldecacitol-71 (ED) at 50ng/kg/d 5x/wk prevented the decrease in BMD induced by GC (2.1 mg/kg/d prednisolone pellets, 8 wks, N=10-12) in 4mo C57Bl6 female mice and simultaneously prevented the increase in atrogene expression in bone. Further, 1,25D<sub>3</sub> and ED prevented GC-mediated increase in the bone resorption marker CTX and the decrease in the bone formation markers P1NP and OCN. Both VDR ligands also prevented GC-induced loss of lean body mass, a muscle mass index measured by DEXA, and the decrease in muscle strength, assessed *in vivo* by plantarflexion torque function testing. Further, consistent with clinical evidence, *in vivo* echocardiography demonstrated that GC induced cardiac dysfunction in our mouse model of GC excess. GC-treated mice exhibited decreased left ventricular (LV) anterior and posterior wall thickness at diastole (relaxed) and systole (contracted). In addition, GC increased LV volume at systole, reduced ejection fraction, and decreased fractional shortening, all indexes of inefficient heart contraction. Both VDR ligands prevented LV wall thinning and the dysfunctional heart contraction induced by GC. GC or the VDR ligands did not alter total heart mass, LV mass, or heart rate. Further, GC increased atrogene expression also in the heart *in vivo* and *ex vivo* in murine LV organ cultures. 1,25D<sub>3</sub> prevented GC-induced atrogene expression *ex vivo*, and both 1,25D<sub>3</sub> and ED prevented the increase in MuRF1 induced by GC *in vivo*. These findings demonstrate that atrogene upregulation is a common mechanism underlying the damaging effects of GC excess in bone, skeletal muscle, and heart; and that activation of VDR signaling preserves tissue mass and function by interfering with GC actions on the atrogene pathway in each of these organs.



## Sensate Long Segment Regeneration Scaffolds Can Document Load Changes following Dynamization

John A. Szivek, PhD, David A. Gonzales, BS, Efren Barron Villalobos, BS, David S. Margolis, MD/PhD

Orthopaedic Research Laboratory, College of Medicine, The University of Arizona, Tucson, Arizona, USA

**Introduction:** Rapid bone formation bridges sheep critical sized bone defects when biomimetic scaffolds infiltrated with calcium phosphate ceramic (CPC) particles and adult stem cells are surgically placed into long bone defects. Biomimetic scaffold patterns alone have been noted to induce rapid bone formation compared to scaffolds with similar sized geometric pores after 6 months in a large animal model. More recent adult stem cell-infiltrated scaffolds induced complete critical sized defect bridging in a sheep model after 3 months and remodeled bone in sheep after 6 months. A locked intramedullary rod was used to provide initial support. Using load sensors attached to the scaffolds, load changes in the newly regenerated segments were recorded to assess the effects of dynamization. With measurements at various time points this will become a predictive tool to determine when dynamization and rod removal can be carried out safely. In this study, a sheep model was used to study loading during bone bridging and dynamization at 6 months with sensate scaffolds.

**Methods:** Polybutylene terephthalate (PBT) scaffolds were 3D printed with a Stratasys 1650 FDM using trabecular patterns collected from sheep femoral heads and geometric patterns based on femoral diameters using a SCANCO  $\mu$ CT. A 1000-ohm custom made rosette gauge (EK-06-125BZ-10C/W) was constructed, attached to scaffolds, wired with a cable and water proofed using a published procedure. Cables were wired to NCP/NCS Nano-circular connectors. Gauges on scaffolds assessed stiffness while they were compressed to 294 N at up to 294 N/s in an MTS and stress-strain curves were produced.

Four sheep received 3D printed sensate biomimetic scaffolds infused with CPC particles and infiltrated with endogenous sheep stem cells. During an IACUC approved procedure, a modified humeral rod with 2 locking screws was used to stabilize each scaffold. Multiconductor cables attached to rosettes were led to the back where they were exteriorized. One control sheep received a locked rod but no scaffold. Following initial hard-wired measurements, a 2nd surgery was done to place radio transmitter units. At 6 months rods were dynamized and loads were collected immediately pre-op and post-op.

Activity was monitored with video throughout the study and monthly radiography, as well as blood draws were collected. Post sacrifice  $\mu$ CT scanning and histomorphometry will be used to determine the extent and rate of bone formation.

**Results:** Mechanical testing showed a scaffold stiffness of 2.8 GPa. Surgeries were uneventful and sheep were fully weight bearing within days. Load sensors showed full load bearing by 1 month and sheep continued to be fully weight bearing.

Radiographs prior to dynamization at 6 months showed substantial bone formation in all sheep with scaffolds. In each case the proximal screw was removed through a small incision and there were no complications. Three months after scaffold placement sheep appeared to be pain free and measurements showed significant compression loads (negative) with peaks of about 35 Kg (40% body weight) on the operated limb (Fig. 4a). At 6 months, prior to dynamization, peak loads of 45 Kg (45% body weight) were measured (Fig. 4b). Loads following dynamization did not appear to change substantially (Fig. 4c).

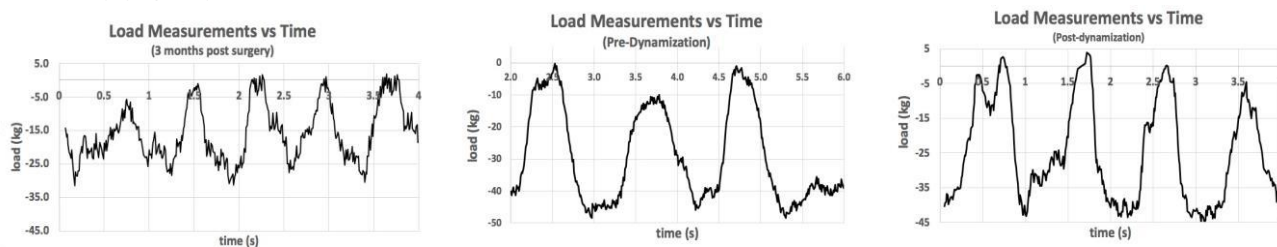


Figure 4: a) 3 months post-op loads showed compression (negative) to peak loads of 40% body weight (BW). Sheep gained weight during next 3 months. Loads (b) pre and (c) post dynamization, from same sheep showed increases though not dramatic ones relative to BW.

**Discussion and Conclusions:** Long segment scaffolds infiltrated with sheep stem cells facilitated rapid bone growth through -out the length of a critical sized defect in a sheep femur over months. This design induces sufficient bone



growth to support physiological loads as early as 3months. After 6 months, better bone ingrowth and bone remodeling were apparent.

Rosette strain gauges calibrated to load and coupled to radio telemetry provided load measurements following scaffold placement, as well as prior to and following dynamization of intramedullary rods. No significant change was noted in measurements immediately following dynamization suggesting that load sharing with the rods, which provided initial stability, was shifting. This suggests that bone remodeling is replacing poor quality bone formed soon after scaffolds were placed with structurally sound cortical bone which will be able to support the sheep once rods are removed.

**Acknowledgements:** The U.S. Army Medical Research Acquisition Activity, 820 Chandler Street, Fort Detrick MD 21702-5014 is the awarding and administering acquisition office. This work was supported by the, Sponsoring Agency: The Assistant Secretary of Defense for Health Affairs endorsed by the Department of Defense, through the Department of Defense, Broad Agency Announcement for Extramural Medical Research under Award No. W81XWH-18-1-0490. Opinions, interpretations, conclusions and recommendations are those of the author and are not necessarily endorsed by the Department of Defense. Student support is provided through an NSF sponsored student support program (L.S.A.M.P./W.A.E.S.O.). In conducting research using animals, the investigator(s) adheres to the laws of the United States and regulations of the Department of Agriculture.

# The Role of AGEs and RAGEs Signaling in Intervertebral Disc Inflammation and Degeneration

Simon Y. Tang<sup>1,2,3</sup>

<sup>1</sup>Washington University in St. Louis, Dept. of Biomedical Engineering, <sup>2</sup>Dept. of Orthopaedic Surgery, <sup>3</sup>Dept. of Mechanical Engineering

**DISCLOSURES:** The authors have nothing to disclose.

**INTRODUCTION:** Lower back pain (LBP), often caused by intervertebral disc (IVD) degeneration, is the leading cause of disability in the US [1]. Understanding the mechanisms IVD degeneration is thus critical for developing therapeutic strategies for treating LBP. Diabetes mellitus is a significant risk factor for IVD degeneration [2,3], and diabetics are susceptible to the accumulation of advanced glycation end-products (AGEs). AGEs diminish the mechanical performance of skeletal tissues including bone and cartilage [4,5]. We have previously shown that AGEs and the upregulation of Receptor for AGEs (RAGE) signaling by High Motility Group Box 1 (HMGB1) increases expression of proteases and inflammatory cytokines, and deteriorates the structure and mechanics of the murine intervertebral disc [6, 7]. Here, we investigate the necessity of RAGE signaling in the AGEs- and HMGB1- mediated degeneration of the intervertebral disc using a global deletion of RAGE in nine-week old mice.

**METHODS:** All animal experiments were done with approval from the Washing University Animal Studies Committee approval. Mice with a global deletion of the RAGE (RAGE KO) [8] along with C57BL/6 WT age and gender matched controls were allowed to age to nine weeks of age (n = 6). The mice were euthanized and 3 lumbar functional spine units (FSU), containing an intact vertebrae-disc-vertebrae structure, from each animal were dissected under aseptic conditions per IACUC approval. The FSU samples were cultured in 2mL of DMEM:F12 supplemented with 20% fetal bovine serum and 1% penicillin-streptomycin. Media was changed every 48 hours. After an initial 48-hour conditioning period, the FSUs from both groups (RAGE KO or WT) are then split further into three groups treated with 100nM of HMGB1 administered once at day 1, 200g/mL of AGEs, or control media throughout the culture period. These samples were then cultured for 21 days. Disc height was measured using a laser micrometer, proteoglycan were measured using biochemical fluorescent assays, and mechanical properties were determined using cyclical dynamic compression [9]. All quantitative analyses were normalized to either the RAGE KO or the WT control groups. Finally, samples were processed for histology and stained with Safranin-O/Fast Green.

## RESULTS:

**A:** Compositional analyses of the IVDs showed that RAGE KO animals significantly blunts the AGEs- and HMGB1- loss of proteoglycans in the IVD ( $p < 0.001$ ;  $p < 0.001$ ). **B:** Likewise, the disc heights in RAGE KO animals for either groups were significantly less than the AGEs- and HMGB1- treated IVDs ( $p < 0.001$ ;  $p < 0.001$ ). **C&D:** Mechanical analyses showed that RAGE KO IVDs had improved stiffness and Tan Delta values at 5% strain levels compared to the WT treated groups ( $p < 0.05$  for all comparisons). **E-G:** Histological analyses show that the RAGE KO IVDs remain structurally intact despite the AGEs- and HMGB-1 treatment.

## DISCUSSION:

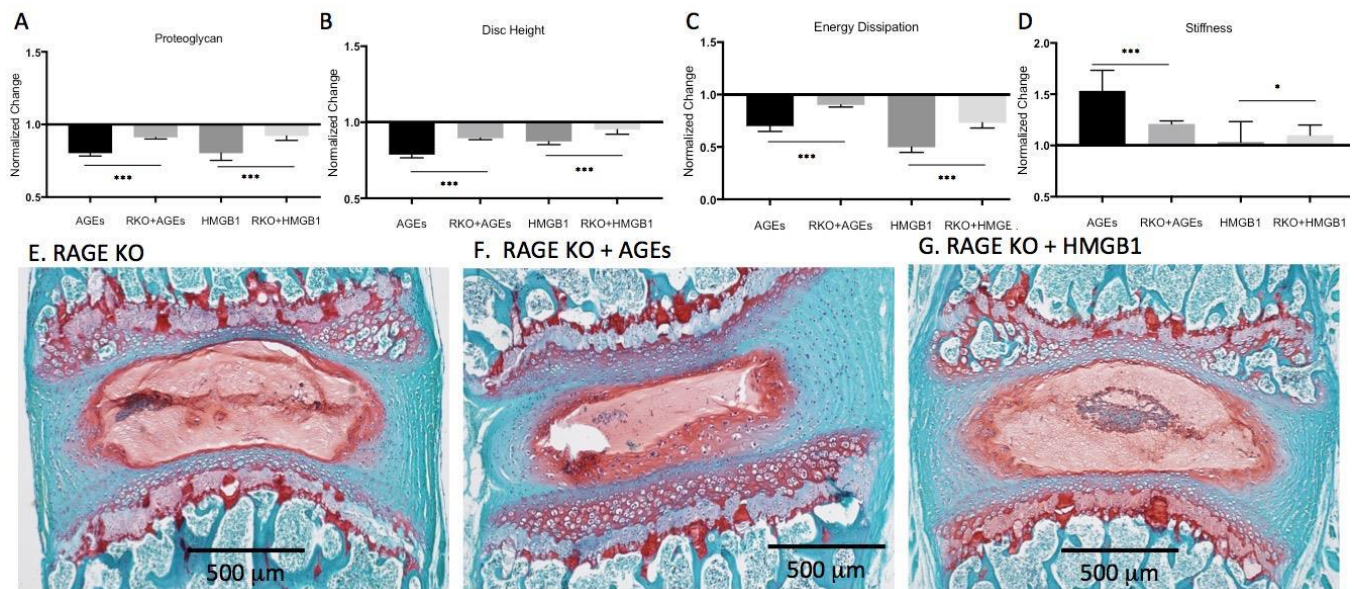
Diabetes increases AGEs accumulation and impairs the mechanical behavior of IVD tissues [10,11]. In this study, the deletion of RAGE appears to have mitigated the adverse effects of AGEs and HMGB1 treatment. We have previously shown that AGEs accumulation and RAGE signaling is elevated in the IVDs of diabetic animals [7]. Furthermore, the AGEs rich environment can stimulate a milieu of inflammatory cytokines including elevated TNF $\alpha$ , NFkB, IL1, as well as depressed TIMPs and increased MMPs that may contribution to inflammation and pain in the IVD. The inhibition of the RAGE pathway may be a viable therapeutic strategy to arrest degeneration and alleviating inflammation relating to pain.

## SIGNIFICANCE:

The deletion of RAGE blunts the AGEs- and HMGB1- mediated degeneration of the IVD and may be a viable therapeutic strategy in diabetes related low back pain and disc degeneration.

**REFERENCES:** [1] Dagenais S et al 2008, [2] Kim RP et al 2001, [3] Ardic F et al 2003, [4] Vlassara H et al 2002, [5] Ahmed N et al 2005 [6] Liu JW et al BMES 2016 [7] Liu JW et al ORS 2017 [8] Liu JW et al 2015 [9] Bierhaus et al 2003. [10] Fields A et al 2015, [11] Illien-Junger S et al 2013.

**ACKNOWLEDGEMENTS:** We would like to acknowledge the Washington University Musculoskeletal Research Center (P30 AR057235), the Washington University Summer Engineering Fellowship, NIH K01 AR069116 and NIH R21AR069804. The authors acknowledge the contributions of Jennifer W Liu in conducting the experiments.



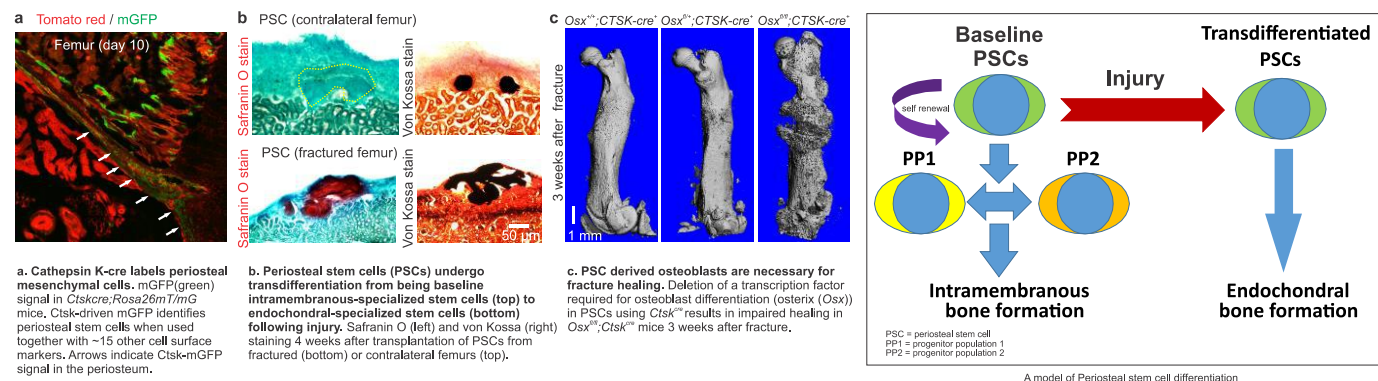
7:00 AM – 8:00 AM	Breakfast	
7:30 AM – 8:00 AM	<b>Regeneron Breakfast Session</b> <b>Cracking the Code of Rare Diseases: Understanding Mechanisms and Developing Therapies</b> Presenter: Aris Economides, PhD	
8:00 AM – 9:00 AM	<b>ASBMR/Harold M. Frost Young Investigator Award Presentations</b> Chair: Teresita Bellido, PhD ( <i>Indiana University</i> ) <b>Identification of a Novel Periosteal Stem Cell Population that Mediates Intramembranous Bone Formation</b> Shawnon Debnath, PhD ( <i>Weill Cornell Medicine, Cornell University</i> ) <b>Single and Combinatorial Gene Therapy Strategies for Treatment of Post-Traumatic and Genetic Forms of Osteoarthritis</b> Matthew Grol, PhD ( <i>Baylor College of Medicine</i> ) <b>Deletion of the Mitochondrial Deacetylase Sirt3 Suppresses Osteoclast Fusion and Increases Bone Mass in Old Mice</b> Ha-Neui Kim, PhD ( <i>University of Arkansas for Medical Sciences</i> )	
9:15 AM - 12:00 PM	<b>Major Methodologies: Material Properties and Tissue Quality - State of the Art</b> Chair: David Burr, PhD ( <i>Indiana University</i> ) <b>Introduction – What are the Physical Attributes of Bone Tissue Properties?</b> David Burr, PhD ( <i>Indiana University</i> ) <b>Measuring Bone's Structure and Mechanical Behavior at Multiple Length Scales</b> Elizabeth Zimmerman, PhD ( <i>Shriners' Hospital for Children</i> ) <b>Measuring Multi-Scale Relationships between Bone Structure, Chemistry and Function and Their Importance to Skeletal Fragility</b> Virginia Ferguson, PhD ( <i>University of Colorado</i> ) <b>Does Loss and Modification of Collagenous and Non-Collagenous Proteins Affect Fracture Risk? Tools, Assays and Disease Models</b> Deepak Vashishth, PhD ( <i>Rensselaer Polytechnic Institute</i> ) <b>Reducing Fracture Risk by Acellular Manipulation of Bone Tissue Properties</b> David Burr, PhD ( <i>Indiana University</i> )	
1:00 PM – 2:30 PM	<b>Career Development Workshop</b> <b>Career Transitions: Planning and Negotiating for Career Advancement</b> Chair: Marjolein van der Meulen, PhD ( <i>Cornell University</i> ) <ul style="list-style-type: none"> <li>• Mentoring: including transition from mentee to mentor</li> <li>• Resources: start up and facilities, budgets, personnel</li> <li>• Personnel: staffing a lab including recruiting graduate students, technicians &amp; staff, postdocs</li> <li>• PI vs team science: maintaining your own projects and collaborating successfully</li> <li>• Transition considerations and concerns: intangibles and other considerations.</li> <li>• Transitions within industry</li> </ul>	
6:00 PM – 8:00 PM	Awards and Recognition Banquet	Lodge Terrace

## Identification of a novel periosteal stem cell population that mediates intramembranous bone formation

Shawon Debnath, PhD<sup>1</sup>, Alisha R. Yallowitz, PhD<sup>1</sup>, Jason Mc. Cormick, MS<sup>2</sup>, Sarfaraz Lalani, MS<sup>1</sup>, Tuo Zhang, PhD<sup>3</sup>, Matthew B. Greenblatt, MD PhD<sup>1</sup>.

<sup>1</sup>Department of Pathology and Laboratory Medicine, <sup>2</sup>Flow Cytometry and <sup>3</sup>Genomics Resources Core Facilities, Weill Cornell Medicine, New York, NY, 10065, USA.

The periosteum is a thin mesenchymal layer present on the outside of bone that makes a unique contribution to bone health<sup>1-2</sup>. However, the identity of the stem cell giving rise to periosteal mesenchyme is still unknown. Using microdissection of the periosteum together a 16-color flow cytometry panel and a Cathepsin K (CTSK)-cre activated reporter, we have identified a novel population of periosteal stem cells (PSCs) in both long bones and calvarial sutures (see attached figure, section a). These PSCs fulfill formal criteria for stemness in terms of displaying clonal multipotency, self-renewal capacity and sitting at the apex of a differentiation hierarchy. Consistent with the lack of marrow recruitment to the periosteal surface, when transferred into the kidney capsule of secondary hosts, PSCs undergo intramembranous bone formation without recruitment of hematopoietic elements (see attached figure, section b, top). PSCs display self-renewal capacity in an *in vitro* mesosphere assay or an *in vivo* serial transplantation assay. Ablation of PSC-derived osteoblasts through CTSK-cre mediated conditional deletion of a gene essential for osteoblast differentiation, osterix (SP7), results in increased cortical bone porosity while preserving endosteal trabecular bone mass. PSCs are also essential for fracture healing as mice with a CTSK-cre mediated osterix deletion show impaired fracture healing (see attached figure, section c). A long-standing paradox in bone biology was how periosteum at baseline undergoes intramembranous ossification but is necessary for endochondral fracture repair<sup>3</sup>. We observed that PSCs after fracture transdifferentiate and acquire expression of CD146 and LEPR, markers of endosteal stem cells normally excluded from PSCs and mediate fracture repair through endochondral pathway (see attached figure, section b, bottom and the model). Transcriptome characterization shows that PSCs bear a distinct transcriptional profile from both their derivatives and from other skeletal stem cells. Lastly, empiric identification of mesenchymal cell types present in bone by single cell RNA sequencing identifies a cellular population with a transcriptional profile consistent with PSCs. Taken together, PSCs are a bona fide stem cell population specialized to meet the physiologic demands of the periosteum and are distinct from other skeletal stem cell types. This finding suggests that bone contains multiple pools of skeletal stem cells that each display distinct functional specialization<sup>4-5</sup> and identifies a cellular basis for intramembranous versus endochondral bone formation.



1. Allen MR, Hock JM, and Burr DB. Periosteum: biology, regulation, and response to osteoporosis therapies. *Bone*. 2004;35(5):1003-12.
2. Ozaki A, Tsunoda M, Kinoshita S, and Saura R. Role of fracture hematoma and periosteum during fracture healing in rats: interaction of fracture hematoma and the periosteum in the initial step of the healing process. *Journal of orthopaedic science : official journal of the Japanese Orthopaedic Association*. 2000;5(1):64-70.
3. Utvag, S. E., Grundnes, O. & Reikeraos, O. Effects of periosteal stripping on healing of segmental fractures in rats. *Journal of orthopaedic trauma*. 1996; 10:279-284.
4. Debnath S, Yallowitz A, McCormick J, Lalani S, Zhang T, Xu R, Liu Y, Yang YS, Eiseman M, Shim JH, Hameed M, Healey JH, Bostrom MP, Landau DA, Greenblatt MB. Discovery of a periosteal stem cell mediating intramembranous bone formation. *Nature*. 2018; 562(7725):133-39.
5. Chan CK, Seo EY, Chen JY, Lo D, McArdle A, Sinha R, Tevlin R, Seita J, Vincent-Tompkins J, Wearda T, et al. Identification and specification of the mouse skeletal stem cell. *Cell*. 2015;160(1-2):285-98.



# Single and Combinatorial Gene Therapy Strategies for Treatment of Post-Traumatic and Genetic Forms of Osteoarthritis

Matthew W. Grol, PhD<sup>1</sup>, Brian Dawson, BS<sup>1</sup>, Racel Cela, BS<sup>1</sup>, Yuqing Chen, MS<sup>1</sup>, Elda Munivez, BS<sup>1</sup>, Ming-Ming Jiang, and Brendan H. Lee, MD, PhD<sup>1</sup>

<sup>1</sup>Department of Molecular and Human Genetics, Baylor College of Medicine, Houston, TX, USA

Osteoarthritis (OA) is a degenerative disease of synovial joints characterized by progressive loss of articular cartilage, subchondral bone remodeling, and intra-articular inflammation with synovitis that leads to the development of chronic pain and motor impairment. While commonly associated with aging and traumatic injury, OA with early-onset also occurs in skeletal dysplasias or as a result of rare dominant mutations in extracellular matrix proteins. A major obstacle limiting the success of therapeutic development is the inherent complexity of OA pathogenesis, which integrates complex alterations

in biomechanical stresses, inflammation, and tissue homeostasis. In addition, efficacy of therapeutics delivered intraarticularly suffer from short half-lives *in vivo* and rapid joint clearance. To address these issues, we are investigating intra-articular gene therapy strategies designed to prevent matrix catabolism, promote joint lubrication and block inflammation in a sustained manner in mouse models of post-traumatic and genetic OA.

To evaluate post-traumatic OA, our lab utilizes destabilization of the medial meniscus (DMM) and cruciate ligament transection (CLT) surgeries in mice to model mild-to-moderate and severe disease, respectively. Combining this with advanced phase-contrast  $\mu$ CT imaging modalities developed by us, we have previously demonstrated that over-expression of proteoglycan 4 (PRG4) – a mucinous glycoprotein implicated in joint lubrication and biomechanics – using helper-dependent adenovirus (HDV) protects mice from OA development following CLT surgery. In addition to alterations in biomechanical stress, OA is associated with upregulation of inflammatory mediators including interleukin-1 (IL-1). IL-1 receptor antagonist (IL-1Ra) is a clinically validated anti-inflammatory cytokine that inhibits IL-1-associated signaling. In this regard, our recent work shows that intra-articular delivery of HDV encoding IL-1Ra (HDV-*Il1ra*) mediates sustained expression and rescues increased thermal hyperalgesia observed following CLT surgery in controls compared to sham mice. Moreover, phase-contrast  $\mu$ CT revealed that a single injection of HDV-*Il1ra* significantly delayed cartilage volume and surface loss compared to surgical controls receiving PBS or HDV-GFP. These results have provided the basis for an application for a phase I clinical trial conducted by Flexion Therapeutics.

Despite these findings, our evidence also suggests that both PRG4 and IL-1Ra gene therapies alone provide relatively short-term protection against pain and cartilage degeneration in these surgical mouse models. In this regard, we recently found that combined delivery of HDV-*Il1ra* and HDV-*Prg4* preserved articular cartilage better than

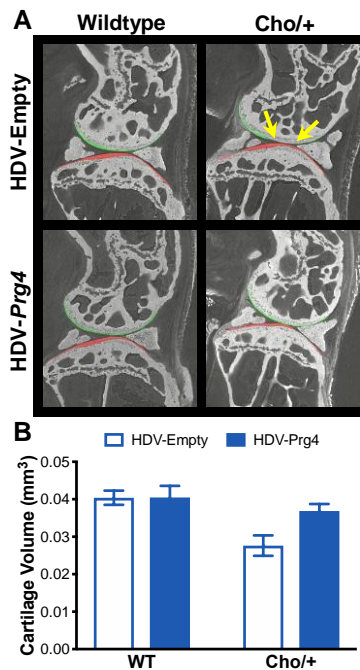


Fig 1. HDV-*Prg4* delays OA progression in *cho/+* mice. A) Representative  $\mu$ CT images with femur cartilage in green and tibia cartilage in red. Yellow arrows indicate damage. B) Femur cartilage volume quantification. Data are means  $\pm$  SEM, n=2-4 mice per group.

either single therapy in both the DMM and CLT surgical models of OA as demonstrated by preservation of cartilage volume and surface. This improved protection was associated with increased expression of pro-anabolic and cartilage matrix genes together with decreased expression of catabolic genes and inflammatory mediators. In addition to improvements in joint tissues, combinatorial IL-1Ra and PRG4 gene therapy prolonged protection against thermal hyperalgesia compared to either monotherapy alone.

Besides trauma, OA of early-onset also occurs in numerous skeletal dysplasias as a result of mutations that affect cartilage extracellular matrix; however, no studies to date have evaluated gene therapy as a means of treating OA arising from a genetic etiology. To address this, we are evaluating our gene therapy strategies in mice heterozygous for the *cho* mutation (a spontaneous single nucleotide deletion in *COLXIA1*), which develop OA beginning at 12-15 months-of-age. In our initial studies, we treated wildtype and *cho/+* mice with HDV-*Prg4* or empty vector (HDV-Empty) at 9 months-of-age and collected at 18 months-of-age to assess for differences in OA pathogenesis as well as pain and motor impairments. Our preliminary data demonstrate that *cho/+* mice exhibit significant reductions in cartilage volume compared to wildtype controls, and that HDV-*Prg4* protects from this loss (Figure 1). In addition, HDV-*Prg4* rescues the increased thermal hyperalgesia observed for *cho/+* mice (Figure 2).

Taken together, our published and preliminary studies demonstrate that single and combinatorial gene therapies targeting inflammation and chondroprotection show promise for treatment of OA arising from differing etiologies.

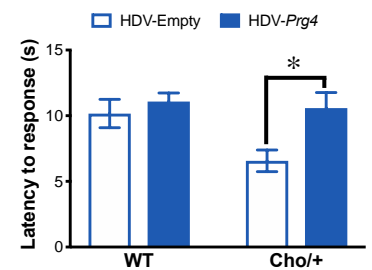


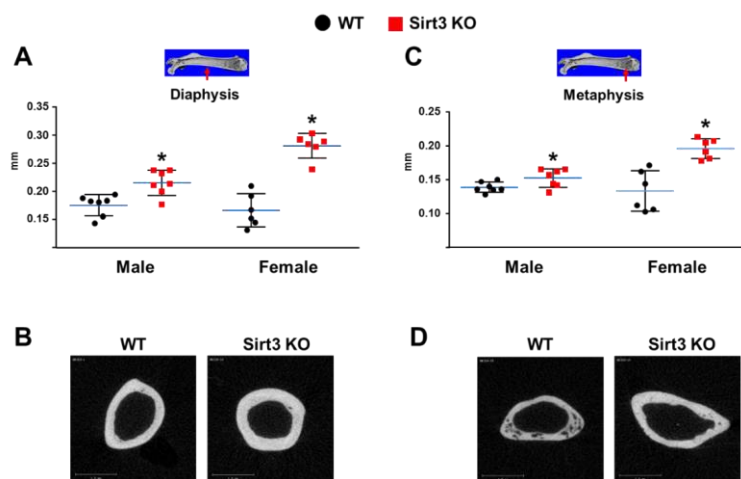
Fig 2. HDV-*Prg4* protects from thermal hyperalgesia in *cho/+* mice. Latency to response to noxious heat in the hot plate assay. Data are means  $\pm$  SEM, n=6-10 mice per group, \* is  $p < 0.05$ .

## Deletion of the mitochondrial deacetylase Sirt3 suppresses osteoclast fusion and increases bone mass in old mice

Ha-Neui Kim

Division of Endocrinology and Metabolism, Center for Osteoporosis and Metabolic Bone Diseases; and the Central Arkansas Veterans Healthcare System, Little Rock, Arkansas

Mammalian Sirtuins (Sirt1-Sirt7) belong to the family of class III histone deacetylase enzymes with NAD<sup>+</sup>-dependent activity and play an important role in inflammation, metabolisms, cancer, neurodegeneration, and aging. Among these, Sirt3 is the primary mitochondrial protein deacetylase involved in regulating mitochondrial function and energy homeostasis. A previous study demonstrated that germline deletion of Sirt3 in mice did not lead to any obvious bone phenotype at 6 months of age. However, its physiological role in bone cells and skeletal homeostasis during aging remains largely unknown. To determine if Sirt3 plays a role in age-associated bone loss, we generated mice with global deletion (KO) of Sirt3 gene and characterized their bone phenotype. Sixteen-month-old male or female Sirt3 KO mice had higher femoral cortical thickness than wild-type littermate controls (WT). This change was due to a decrease in endosteal perimeter at both sides in the diaphysis or metaphysis as determined by micro-CT. Furthermore, the Sirt3 KO mice did not develop age-associated cortical porosity. Cancellous bone volume and BMD were also higher in femur and spine of female, but not male, Sirt3 KO mice. These changes were accompanied by increased trabecular number and thickness, while trabecular spacing was decreased. The high bone mass phenotype was associated with decreased CTx levels in the serum.



To examine the cellular mechanisms responsible for the decrease in bone resorption, we used bone marrow-derived macrophage (BMM) cultures and induced osteoclast formation with RANKL. In the cells from WT mice, Sirt3 mRNA and protein levels were greatly increased during the transition of BMMs to mature osteoclasts in the presence of RANKL. Osteoclast progenitors from Sirt3 KO mice differentiated normally into TRAP-positive osteoclasts albeit with impaired resorptive function due to defective fusion. Most osteoclasts lacking Sirt3 were much smaller than WT osteoclasts. Consistent with this, addition of the Sirt3 inhibitor LC-0296 to osteoclast

progenitor cultures from WT mice was sufficient to replicate the deleterious effects of Sirt3 deletion on osteoclast fusion. Osteoclasts lacking Sirt3 exhibited a striking decrease in expression of mitochondrial markers such as Cox1, Cox3, and CytB as compared to osteoclasts from WT mice. **Taken together, these results indicate that Sirt3 activation in aged mice stimulates bone resorption, most likely by promoting mitochondrial function.**

**Figure:** Left, (A and C) Cortical thickness in femoral diaphysis (A) or metaphysis (C), as indicated by the red arrow, of 16-month-old Sirt3 KO and WT littermates measured by  $\mu$ CT (n = 8-9 animals/group). \*P < 0.05 vs. same gender WT mice using Student's t-test. (B and D) Representative single micro-CT slice of femora from female mice. (B) Diaphysis site. (D) Metaphysis site. Right, Quantification of porosity of the distal half of the femur from 16-month-old Sirt3 KO and WT littermates, as indicated by the red box (n = 8-9 animals/group). P value vs. same gender WT mice using Student's t-test.

### References

1. Sinclair DA, Guarente L. Unlocking the secrets of longevity genes. *Sci Am*. 2006 Mar;294(3):48-51, 54-7.
2. Lombard et al. Mammalian Sir2 homolog SIRT3 regulates global mitochondrial lysine acetylation. *Mol Cell Biol*. 2007 Dec;27(24):8807-14. Epub 2007 Oct 8.



## Measuring bone's structure and mechanical behavior at multiple length-scales

Elizabeth A. Zimmermann, PhD<sup>1,2</sup>

<sup>1</sup>Shriners Hospitals for Children-Canada, Montreal, QC, Canada <sup>2</sup>McGill University, Montreal, QC, Canada

Skeletal fragility can stem from aging, disorders, or disease; however the connecting factor is that the bone's mechanical integrity is somehow compromised. Bone tissue resists fracture through its complex hierarchical structure, which spans from the macroscale bone shape to the secondary osteons at the microstructural level to finally the mineralized collagen fibrils at the nanoscale. As we try to improve diagnostic techniques to assess bone fragility and therapies to improve bone mass and bone quality, we're faced with the following question: what aspects of the bone structure have the biggest impact on skeletal fragility? Fracture occurs when biomechanical loads exceed bone strength. However, as bone is a damage tolerant material that contains cracks, a lower biomechanical load may cause failure if a crack is present. Therefore, to understand the mechanical behavior of bone, we must investigate the tissue's resistance to elasticity and plasticity, which can be measured through strength tests (i.e., three-point bending or tension tests), as well as the tissue's resistance to the initiation and growth of cracks, which can be measured through fracture mechanics tests on samples with a worst case flaw. These experiments have shown that bone fracture resistance is generated at the microstructural scale of the osteons through mechanisms such as crack deflection and uncracked ligament bridging. On the other hand, strength, which is most often measured on a macroscopic sample, is actually generated at small length-scales through plasticity mechanisms that include deformation and sliding of mineralized collagen fibrils as well as sacrificial bonding and void formation at interfaces. Thus, bone's resistance to deformation and fracture involves multiple length-scales within the tissue.

# Measuring multi-scale relationships between bone structure, chemistry and function and their importance to skeletal fragility

Virginia L. Ferguson, PhD<sup>1</sup>

<sup>1</sup>University of Colorado, Boulder, CO

DXA scores are relied on to diagnose osteoporosis, yet only 54% of individuals who suffered hip fractures were classified as having osteoporotic BMD levels<sup>1</sup>. Critically, bone strength and its resistance to fracture are dependent on the amount of bone tissue (i.e., BMD) as well as the quality of the bone material that is present<sup>2-7</sup>. Bone quality is generally defined by a collection of architectural and material properties<sup>8,9</sup>, both of which are largely influenced by bone turnover, occur across multiple length scales, and contribute to structural rigidity<sup>5,7</sup>. However the quality of the bone material itself is equally important<sup>7</sup> and includes mineral and collagen properties, prevalence of non-collagenous proteins, tissue mineralization, cortical porosity, collagen crosslinking, and microdamage<sup>8</sup>. Disruption of any of these constituents may result in bones that are brittle or that cannot adequately sustain physiological loads such as with aging, metabolic and other disease, and with changes in mechanical loading.

Many of the contributors to bone quality also serve as toughening mechanisms<sup>10</sup>. Mineralized collagen fibrils promote strength and ductility, and crack-tip shielding occurs due to extrinsic (e.g., osteonal structures or collagen fibers that bridge emerging cracks) and intrinsic (e.g., the collagen-mineral composite). Heterogeneity of bone structures and material imparts toughness by deflecting of a crack's path, where too little or too great of variance in the material may enable unstable crack growth<sup>10-12</sup> and lead to fracture. Heterogeneity in mineral crystal sizes and orientations, degree of mineralization and the amount of collagen crosslinking also contributes to higher strength and tissue modulus<sup>4,8</sup>.

Finally, bone cells respond to dynamic mechanical and biological cues to form new bone and maintain existing bone, where disruption of these signals leads to poor quality bone material. Fracture risk assessments thus should take into context BMD, bone turnover, and bone material quality measurements<sup>13,14</sup>.

Here we consider how micrometer length scale material changes, both individually and in combination, influence whole bone fragility in models of kidney disease, skeletal disuse, and exercise. By evaluating bone material properties, chemistry, and tissue organization in concert with activities of bone-maintaining cells (e.g., osteocytes), we can bridge across multiple length scales to gain insight into how bone material quality measures can be used to improve our assessment of fracture risk.

In this talk, we will thus consider questions critical to understanding the role of bone material quality in fracture including:

- What is the contribution of spatial variation in bone material to bone toughness<sup>4,8,15</sup>? How does this effect change with aging and disease?
- What is the relative importance of material-level bone quality contributors to intrinsic and extrinsic fracture mechanisms<sup>10-12</sup>, as well as whole bone fracture?
- How do changes within the bone material by osteocytes or of microstructures within bone (e.g., osteocytic osteolysis) affect bone's resistance to failure?

## References:

1. Cummings, S. R., Bates, D. & Black, D. M. Clinical Use of Bone Densitometry. *JAMA* **288**, 1889 (2002).
2. Wang, X., Shen, X., Li, X. & Mauli Agrawal, C. Age-related changes in the collagen network and toughness of bone. *Bone* **31**, 1–7 (2002).
3. Paschalis, E. P., Mendelsohn, R. & Boskey, A. L. Infrared Assessment of Bone Quality: A Review. *Clin. Orthop. Relat. Res.* **469**, 2170–2178 (2011).
4. Seeman, E. & Delmas, P. D. Bone Quality — The Material and Structural Basis of Bone Strength and Fragility. *N. Engl. J. Med.* **354**, 2250–2261 (2006).
5. Hernandez, C. J. & Keaveny, T. M. A biomechanical perspective on bone quality. *Bone* **39**, 1173–1181 (2006).
6. Bouxsein, M. L. Bone quality: where do we go from here? *Osteoporos. Int.* **14**, 118–127 (2003).
7. van der Meulen, M. C. ., Jepsen, K. . & Mikić, B. Understanding bone strength: size isn't everything. *Bone* **29**, 101–104 (2001).
8. Boskey, A. L. & Imbert, L. Bone quality changes associated with aging and disease: a review. *Ann. N. Y. Acad. Sci.*

1410, 93–106 (2017).

9. Donnelly, E. Methods for Assessing Bone Quality: A Review. *Clin. Orthop. Relat. Res.* **469**, 2128–2138 (2011).
10. Zimmermann, E. A. & Ritchie, R. O. Bone as a Structural Material. *Adv. Healthc. Mater.* **4**, 1287–1304 (2015).
11. Heveran, C. M. *et al.* Chronic kidney disease and aging differentially diminish bone material and microarchitecture in C57Bl/6 mice. *Bone* **127**, 91–103 (2019).
12. Ural, A. & Vashishth, D. Hierarchical perspective of bone toughness – from molecules to fracture. *Int. Mater. Rev.* **59**, 245–263 (2014).
13. Gourion-Arsiquaud, S. *et al.* Use of FTIR Spectroscopic Imaging to Identify Parameters Associated With Fragility Fracture. *J. Bone Miner. Res.* **24**, 1565–1571 (2009).
14. Gordon, C. L., Lang, T. F., Augat, P. & Genant, H. K. Image-Based Assessment of Spinal Trabecular Bone Structure from High-Resolution CT Images. *Osteoporos. Int.* **8**, 317–325 (1998).
15. Tai, K., Dao, M., Suresh, S., Palazoglu, A. & Ortiz, C. Nanoscale heterogeneity promotes energy dissipation in bone. (2007).

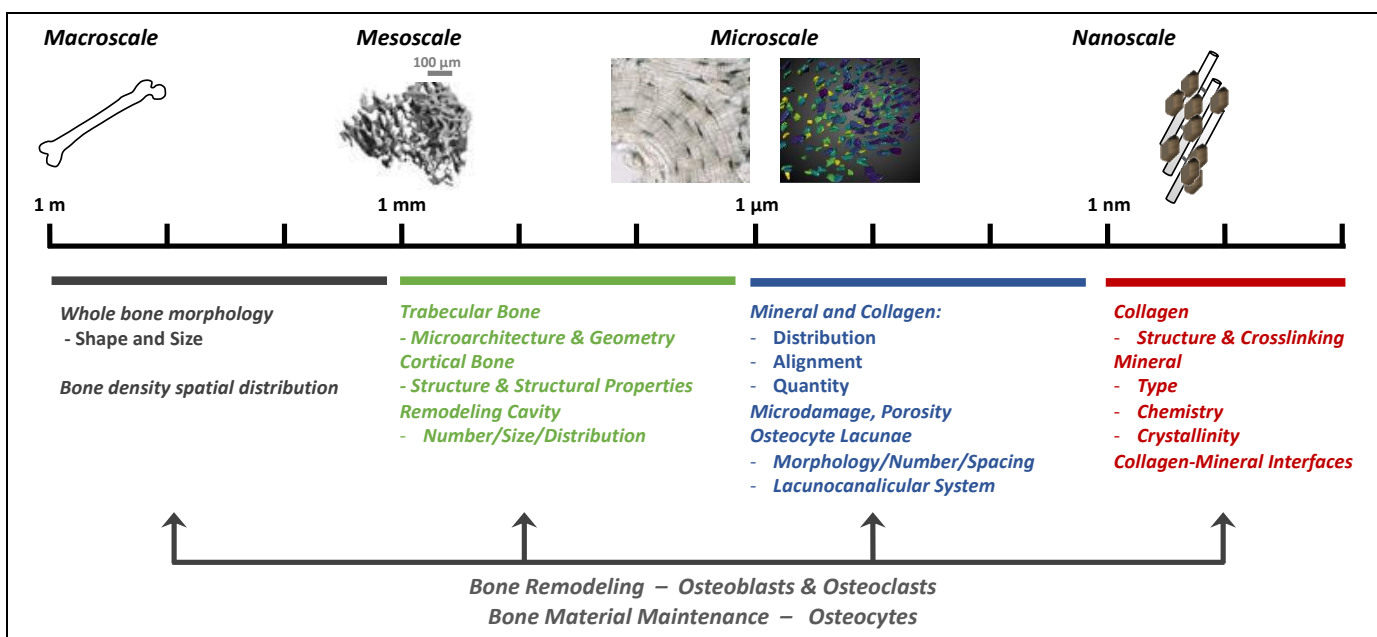


**Figure.** Bone strength and toughness depend on bone mineral density (BMD) and a range of metrics that describe bone structural and material quality. All of these measures are controlled by bone modeling and remodeling, via osteoblasts and osteoclasts, as well as osteocyte-directed maintenance of local bone material. Aspects of bone material quality are shown on a scale depicting hierarchical structure of bone according to approximate length scales of analysis.

*Note: length scales were selected to match mechanical and compositional assessment techniques of bone quality as described by Eve Donnelly in <sup>9</sup>.*

## **Does Loss and Modification of Collagenous and Non-Collagenous Proteins Affect Fracture Risk? Tools, Assays and Disease Models**

*Deepak Vashishth, PhD, Rensselaer Polytechnic Institute*

Bone mineral density or BMD is not a reliable predictor of fracture risk. Thus, other factors including the organic bone matrix components and their interactions may be of crucial to the understanding of fragility fractures. In addition to collagen, non-collagenous proteins (NCPs) play a significant role in the structural organization of bone and influence its mechanical properties. However, their contribution to fracture remains undefined. NCPs regulate the matrix assembly and both collagen and NCPs undergo different post-translational modifications during aging, disease, and anti-osteoporosis treatments. These undesired changes may increase fracture risk. Thus, it is important to take into account the organic portion of bone to understand the complex changes in bone that occur at macro-, micro-, and nanoscale levels, and to determine what parameters contribute to the decreased bone quality of osteoporotic tissue. Such new information will enable the development of new diagnostic tools and more effective therapies.

Acknowledgements: NIH grants AG20618 and AR49635

**Reducing Fracture Risk by Acellular Manipulation of Bone Tissue Properties**David B. Burr, PhD, Indiana  
Center for Musculoskeletal Health, Indiana University School of Medicine

Indianapolis, IN

Selective Estrogen Receptor Modulators (SERMs) decrease bone resorption and increase bone mineral density. These effects are thought to be initiated by the interaction of SERMs with the estrogen receptor followed by a tissue selective transcriptional regulation. A flagship molecule of that class is raloxifene (RAL), which mimics the protective effect of estrogen on the skeletal system without triggering the estrogen antagonistic effects on the breast and endometrium of the uterus. Many clinical studies have validated the effectiveness of RAL in reducing the risk of vertebral fractures in postmenopausal osteoporosis patients by significantly slowing bone turnover, preventing bone loss and maintaining the structural integrity of cancellous bone.

The ability of RAL to reduce fracture risk is far greater than would be predicted based solely on its effect on bone mineral density (BMD), which is very modest (~2%). Yet it reduces the relative risk of vertebral fracture by roughly the same degree as the bisphosphonates – about 40-55% in the first year. Preclinical studies have documented that raloxifene leads to improved mechanical properties (most notably material-level toughness) of bone despite little/no change in BMD (Figure 1). This mechanical property enhancing

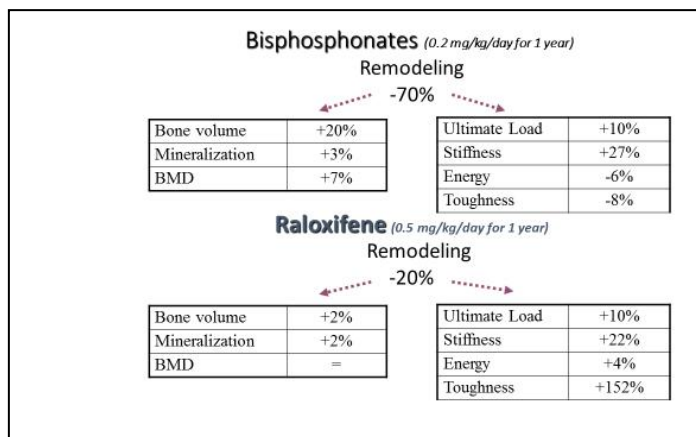


*Figure 1. One year of treatment with a bisphosphonate (alendronate) in a canine model increases vertebral bone volume and BMD much more than one year of treatment with raloxifene. However, at the end of the year, strength and stiffness are nearly the same, and bone toughness is significantly increased rather than decreased with raloxifene*

effect of RAL is cell-independent and does not require living cells to have an effect. Using AFM, ultra-short echo time (UTE) MRI, and short and wide angle X-ray scattering (SAXs, WAXs) we determined that

RAL increases the bound water fraction within the bone matrix, which alters strain transfer between collagen and hydroxyapatite (HAP) (Figure 2). This occurs because RAL is bound to a groove in the

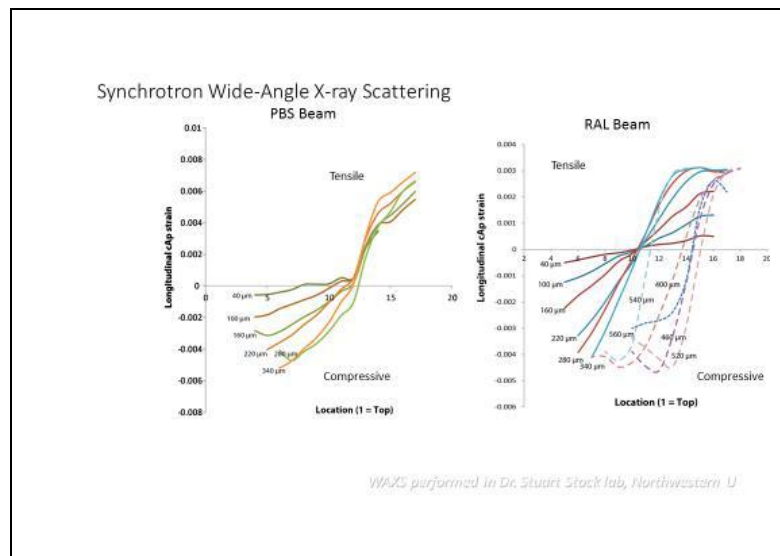
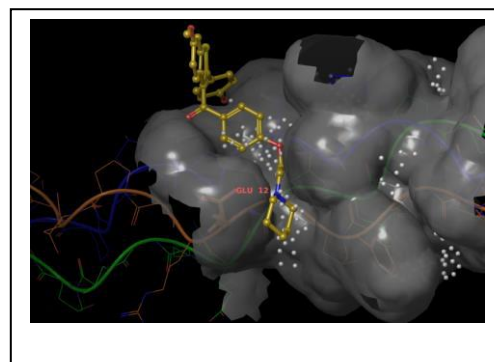


*Figure 2. These are graphs of the hydroxyapatite (HAP) strain over the thickness of the beam under different displacement. The magnitudes of the compressive longitudinal strains at the top surface (lower position numbers) are comparable. The tensile longitudinal strains at the bottom of the beams (higher position numbers) are much larger (doubled) in the PBS beam and plateau in RAL but not in PBS. Beams in PBS fracture shortly after the yield load is reached. RAL-treated beams continue to deform (substantially more displacement) and the HAP longitudinal strains become compressive over almost the whole thickness.*

collagen fibril that alters the distribution of water in the matrix (Figure 3). This structure is hydrophobic and pushes water away from other areas of the collagen molecule, which causes the formation of local regions of hyper- and hypo-hydration that affect the mechanical behavior of the bone. This improves bone's ductility and reduces bone fragility without manipulation of cell activity.

*Figure 3. Site map analysis of the raloxifene molecule or its analogues on the collagen surface indicates a groove with sufficient space to accommodate RAL*



This direct effect on mineral-matrix interactions suggests that off-target effects of RAL on bone toughness may have clinical relevance that cannot be detected through monitoring of BMD alone, but require some measure of mechanical properties at the material level or alternative imaging methods such as MRI. This also may suggest a new approach to the treatment of osteoporosis that is biophysical and cell-independent.

7:00 AM – 8:00 AM	Breakfast
7:30 AM – 8:00 AM	<b>Ultragenyx Breakfast Session</b> <b>Understanding Bone Remodeling in XLH: Insight into Restoring Phosphate Homeostasis</b> <i>Presenter: Javier San Martin. MD</i>
8:00 AM – 9:00 AM	<b>ASBMR/Harold M. Frost Young Investigator Award Presentations</b> Chair: Alexander Robling, PhD ( <i>Indiana University</i> ) <b>Serum Bone-Derived Extracellular Vesicles are Associated with Bone Loss with Antiretroviral Therapy in Adults with HIV</b> Erika Marques de Menezes, PhD ( <i>University of California - San Francisco</i> ) <b>Innervation Controls Epiphyseal Stem Cell Niche Performance</b> Phillip Newton, PhD ( <i>Karolinska Institute</i> ) <b>Intra-articular Ablation of Periostin Attenuates Post-traumatic Osteoarthritis in Mice via Canonical Wnt and NFkB Pathways</b> Muhammad Farooq Rai, PhD ( <i>Washington University in St. Louis School of Medicine</i> )
9:15 AM - 12:00 PM	<b>Epigenetics and Musculoskeletal Disease</b> Chair: Regis J. O'Keefe, MD, PhD ( <i>Washington University</i> ) <b>Brief Overview of Epigenetics</b> Regis J. O'Keefe, MD, PhD ( <i>Washington University</i> ) <b>Histone Deacetylase 3 in Cartilage Development and Osteoarthritis</b> Jennifer Westendorf, PhD ( <i>Mayo Clinic</i> ) <b>Defining DNMT3b and Downstream Targets in the Pathogenesis of Osteoarthritis</b> Regis J. O'Keefe, MD, PhD ( <i>Washington University</i> ) <b>Genome-wide DNA Methylation Changes in Mice under Simulated Microgravity Conditions</b> Mario Fraga ( <i>University of Oviedo</i> )
1:00 PM – 2:30 PM	<b>Career Development Workshop</b> <b>Bringing Discoveries to Market: Navigating the FDA</b> Chair: Jose Moreno, PhD ( <i>FDA</i> ) The workshop will provide the audience with an overview of the various mechanisms available to obtain FDA feedback regarding the potential regulatory pathway ahead for any products resulting from their research efforts. This information is of special interest for researches applying to the Small Business Innovation Research (SBIR) and Small Business Technology Transfer (STTR) funding programs, where such regulatory information can have a larger impact in the funding process. Attendees will gain key knowledge regarding the current regulatory pathways for device, drug, biological and combination products, and the mechanisms available to present the results of their research efforts to FDA.

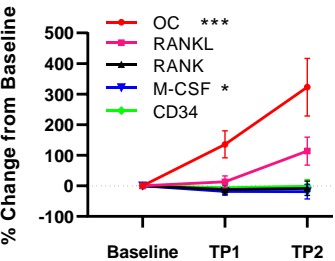


7:30 PM - 9:30 PM	<b>Rare Diseases of Phosphate Handling and Tissue Mineralization: Too Much or Too Little</b> Chair: Javier San Martin ( <i>Ultragenyx, Inc.</i> )
	<b>Introduction to Phosphate Metabolism</b> Javier San Martin ( <i>Ultragenyx, Inc.</i> )
	<b>From Therapeutics Target Identification to Drug Development, with an Anti-FGF23 Antibody, Burosumab</b> Javier San Martin ( <i>Ultragenyx, Inc.</i> )
	<b>Targeting a Unique Pathophysiology for Improved Outcomes in X-linked Hypophosphatemia</b> Thomas Carpenter, MD ( <i>Yale University</i> )
	<b>Pathogenic Mechanisms and Therapeutic Targets for Multiple Osteochondroma, a Pediatric Musculoskeletal Disorder</b> Maurizio Pacifici, PhD ( <i>Children's Hospital of Philadelphia</i> )

Abstract

**Introduction:** Bone mineral density (BMD) decreases after initiating antiretroviral therapy (ART).<sup>1</sup> Since bone loss is consistently observed across different ART regimens, one theory is that the inflammatory state associated with immunologic reactivation and the repopulation of T cells after the initiation of ART leads to an imbalance in bone remodeling favoring osteoclastogenesis and bone resorption.<sup>2,3</sup> However, the mechanism underlying these effects is not fully characterized. Extracellular vesicles (EVs) are now recognized as a mechanism for intercellular communication in the bone remodeling microenvironment and serum EVs may reflect the state of cells in the bone under healthy and pathologic conditions.<sup>4,5</sup> We aimed to clarify whether serum EV phenotypes changed after ART initiation and determined whether an early change in EVs expressing bone markers correlated with changes in BMD by DXA at 12 months. **Methods:** Using advanced flow cytometry techniques, EVs were measured from blinded serum from 15 adults with HIV at baseline (B), and 1, 3, 6 and 12 months after ART initiation. Not all samples were available at each time point so we averaged early (TP1, 1-3 months) and late (TP2, 6-12 months) time points. EVs were stained for markers that are related to bone metabolism (osteocalcin (OC), RANK, RANKL) or cell of origin (M-CSF, CD34) and reported as EVs/ $\mu$ L. Serum OC (ng/mL), serum procollagen type I N-terminal propeptide (P1NP) (ng/mL), and serum C-terminal telopeptide (CTX) (ng/mL), parathyroid hormone (PTH) (pg/mL), and the inflammatory markers IL-6 (pg/mL) and TNF- $\alpha$  (pg/mL) were measured at similar time points. **Results:** A significant decrease in BMD was observed from baseline to 12 months at the lumbar spine ( $-2.6\pm1.9\%$ ), femoral neck ( $-3.7\pm3.6\%$ ) and total hip ( $-4.3\pm2.9\%$ ). Levels of OC+EVs, serum OC, serum P1NP, and serum CTX were significantly higher at early and late time points (TP1, TP2) compared to baseline (**Fig. 1A, B**). Change in serum OC, P1NP, CTx, PTH and IL-6 from baseline to TP1 or TP2 did not correlate with change in BMD. Serum TNF- $\alpha$  change from baseline to TP1 was associated with 12-month change in lumbar spine BMD ( $r=0.67$ ,  $p=0.01$ ). However, change in total hip BMD at 12 months negatively correlated with change from baseline to TP1 in EVs expressing OC, RANKL, RANK, and CD34 (**Fig. C**). **Conclusion:** Our observations suggest that early changes in bone-derived EVs were associated with total hip bone loss 12 months after ART initiation. These correlations were not observed for classic soluble bone turnover markers. These data suggest that bone-derived EVs may have value as novel serum biomarkers of bone remodeling.

Fig. 1A



B

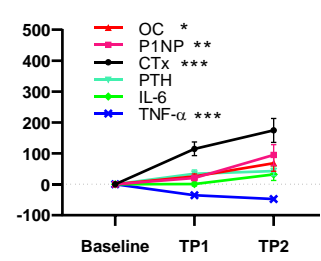


Figure 1. Bone EV markers after ART initiation.

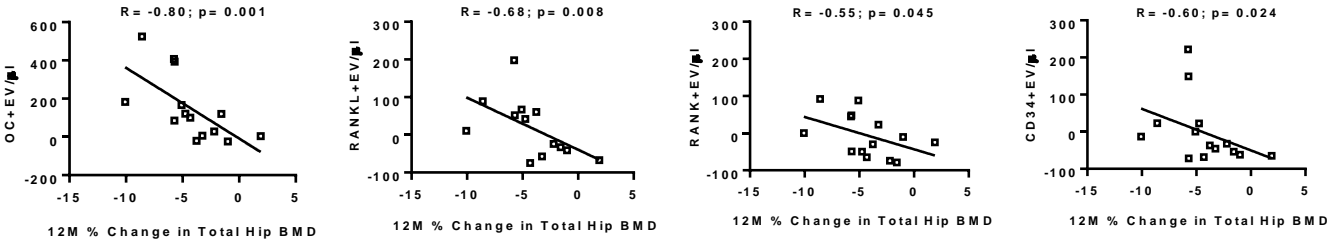
A) EV levels relative to baseline at 1-3 months (TP1) or 6-12 months (TP2) after ART initiation. Increases in OC+ EVs and the decrease in M-CSF+ EVs were significant.

B) Serum markers showed significant elevations in OC, P1NP, and CTx and decrease in TNF- $\alpha$ .

C) Early changes (within 3 months) in levels of bone-derived EVs are associated with the magnitude of change in total hip at 12 months.

\* $p<0.05$ , \*\* $p<0.01$ , \*\*\* $p<0.001$

Fig. C



References

1. Brown TT, Qaqish RB. Antiretroviral therapy and the prevalence of osteopenia and osteoporosis: a meta-analytic review. *AIDS*. 2006;20(17):2165–2174.
2. Vikulina T, Fan X, Yamaguchi M, et al. Alterations in the immuno-skeletal interface drive bone destruction in HIV-1 transgenic rats. *Proceedings of the National Academy of Sciences*. 2010;107(31):13848–13853.
3. Ofotokun I, McIntosh E, Weitzmann MN. HIV: Inflammation and Bone. *Current HIV/AIDS Reports*. 2012;9(1):16–25.
4. Ohayshiki JH, Umezu T, Ohayshiki K. Extracellular vesicle-mediated cell–cell communication in haematological neoplasms. *Philosophical Transactions of the Royal Society B: Biological Sciences*. 2018;373(1737):20160484.
5. Li D, Liu J, Guo B, et al. Osteoclast-derived exosomal miR-214-3p inhibits osteoblastic bone formation. *Nature Communications*. 2016;7:10872.

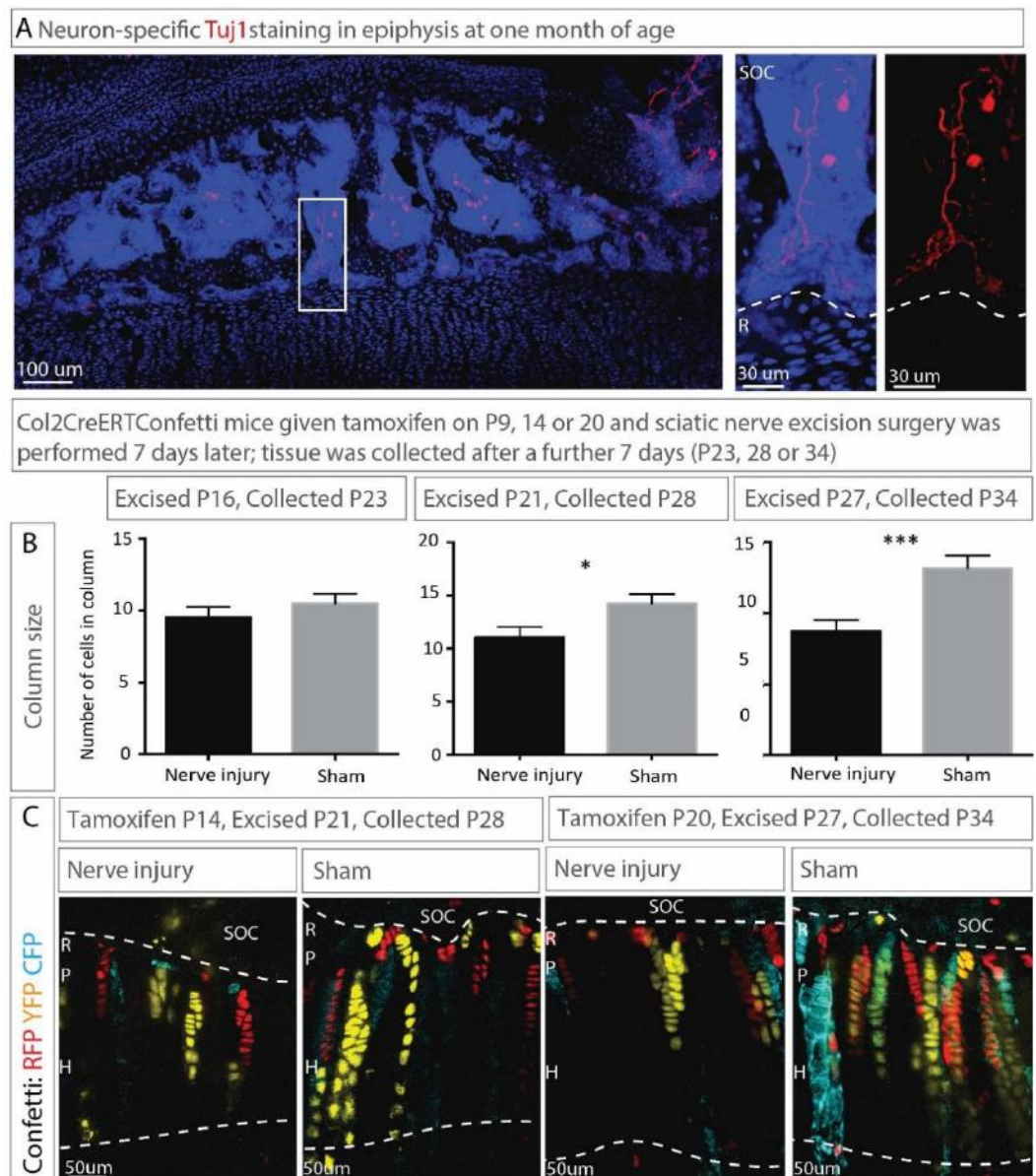
## Innervation controls epiphyseal stem cell niche performance

Phillip T. Newton, PhD<sup>1,2</sup>, Lei Li<sup>1</sup>, Maria Hovorakova<sup>3</sup>, Lars Sävendahl, MD, PhD<sup>1,2</sup>, Andrei S Chagin, PhD<sup>1,4</sup>

<sup>1</sup>Department of Physiology and Pharmacology, Karolinska Institutet, Stockholm, Sweden, <sup>2</sup>Department of Women's and Children's Health, Karolinska Institutet and Pediatric Endocrinology Unit, Karolinska University Hospital, Stockholm, Sweden,

<sup>3</sup>Department of Developmental Biology, Institute of Experimental Medicine, Czech Academy of Sciences, 14220 Prague, Czech Republic, <sup>4</sup>Institute for Regenerative Medicine, Sechenov First Moscow State Medical University, Moscow, Russian Federation

During postnatal long-bone growth, blood vessels invade the cartilage and form secondary ossification centers (SOC) within the epiphyses. SOC growth and maturation consumes epiphyseal chondrocytes, and substantially changes the microenvironment surrounding the remaining resting zone cells. We recently showed that SOC maturation in mice at 3-4 weeks of age causes the remaining resting zone chondrocytes to completely change their identity and acquire stem cell properties, forming the epiphyseal stem cell niche in the growth plate <sup>1,2</sup>. However, it remains unclear exactly how the SOC is capable of influencing the epiphyseal niche. A classical regulator of previously described stem cell niches are peripheral nerves and their nerve-derived factors, such as Sonic hedgehog (Shh) <sup>3</sup>. Using immunofluorescent staining in one-month old mice, we determined that peripheral nerves inside the SOC approach the resting zone cells to within 20  $\mu\text{m}$  (Fig. A). To test the function of these nerves upon the epiphyseal niche we conducted sciatic nerve ablation (at postnatal days (P) 16, 21 or 27) in combination with clonal genetic tracing using the Col2CreERTConfetti mouse model <sup>1</sup>. Denervation at P21 and P27, but not P16, significantly reduced clonal expansion of chondrocytes when compared with the contralateral sham-operated controls (Fig. B, C Bar = mean  $\pm$  SEM, \*  $p \leq 0.05$ , \*\*\*  $p \leq 0.001$ ,  $n \geq 3$ ), without affecting SOC size (data not shown). These data suggest nerves do not influence epiphyseal niche formation, but can influence its activity. Using Shh-GFP reporter mice we determined that nerves are not a source of Shh in the SOC (data not shown). Altogether, these data suggest that the peripheral nerves regulate postnatal longitudinal growth by influencing epiphyseal niche performance.



1. Newton, P. T. *et al.* A radical switch in clonality reveals a stem cell niche in the epiphyseal growth plate. *Nature* **567**, 234–238 (2019).
2. Wuelling, M. & Vortkamp, A. A newly discovered stem cell that keeps bones growing. *Nature* **567**, 178 (2019).
3. Brownell, I., Guevara, E., Bai, C. B., Loomis, C. A. & Joyner, A. L. Nerve-derived sonic hedgehog defines a niche for hair follicle stem cells capable of becoming epidermal stem cells. *Cell Stem Cell* **8**, 552–565 (2011).



# Intra-articular Ablation of Periostin Attenuates Post-traumatic Osteoarthritis in Mice via Canonical Wnt and NFkB Pathways

Xin Duan, PhD<sup>1</sup>, Lei Cai, PhD<sup>1</sup>, Christine Pham MD<sup>1</sup>, Samuel A. Wickline, MD<sup>2</sup>, Ryan M. Nunley, MD<sup>1</sup>, Robert H. Brophy MD<sup>1</sup>, Muhammad Farooq Rai, PhD<sup>1</sup> <sup>1</sup>Washington University, St. Louis, MO, <sup>2</sup>University of South Florida, Tampa, FL, United States

**Introduction:** Osteoarthritis (OA) is characterized by progressive loss of cartilage from the articulating surface as well as subchondral bone sclerosis [1]. Although the etiology of the disease still remains unknown, many studies have shown that changes in chondrocytes and extracellular matrix contribute to the degeneration of articular cartilage[2]. Periostin (Postn), also called osteoblast-specific factor 2 or fasciclin-1-like protein, is a matricellular secretory protein, which is highly expressed in human and mouse OA cartilage [3, 4]. Postn has been shown to contribute to tissue repair, although it also activates NF- $\kappa$ B signaling and promotes degradation of cartilage matrix via induction of matrix degrading enzymes [3, 4]. Postn also promotes Wnt/ $\beta$ -catenin [5], which plays key role in bone and joint pathology [6]. The precise role(s) and mechanism(s) of Postn in post-traumatic OA are not fully understood. Here, we investigated the effect of Postn on OA progression in a mouse model of post-traumatic OA to test the hypothesis that suppression of Postn is chondroprotective.

**Methods:** Destabilization of the medial meniscus (DMM) was performed on the right knees of 10-week old male C57BL/6J mice (n = 8 per group) to induce post-traumatic OA. The left knees served as controls. Each mouse received one of the following treatment options: HBSS, scrambled siRNA or Postn siRNA. We used a novel peptidic nanoparticle [7] complexed to Postn or scrambled siRNA (15  $\mu$ l, 0.1  $\mu$ g) for intra-articular delivery immediately after surgery. The treatment was then repeated every two weeks for up to 8 weeks. Mice were sacrificed 8 weeks after DMM. Bone changes were evaluated by micro-CT. Cartilage degeneration was gauged by histology using the OARSI scoring system for all four compartments of the knee. Immunostaining was performed for Postn, MMP-13, Wnt/ $\beta$ -catenin and NFkB. siRNA-mediated Postn ablation was also explored in IL-1 $\beta$ -stimulated human primary chondrocytes using peptide-siRNA nanoparticles.

**Results:** DMM surgery induced OA in mice as evidenced by cartilage fibrillation and subchondral bone sclerosis and increased BV/TV and volumetric bone mineral density. OA severity was significantly diminished by intra-articular injection of Postn siRNA. We observed that the Postn-siRNA group had significantly less severe OA (mean OARSI score = 10.94  $\pm$  1.86) than both the HBSS control (21.80  $\pm$  2.28) and scrambled siRNA (24.63  $\pm$  1.00) groups (**Fig. 1**). Micro-CT data further showed significantly lower BV/TV and volumetric bone mineral density of the medial tibia in the Postn siRNA treated knees

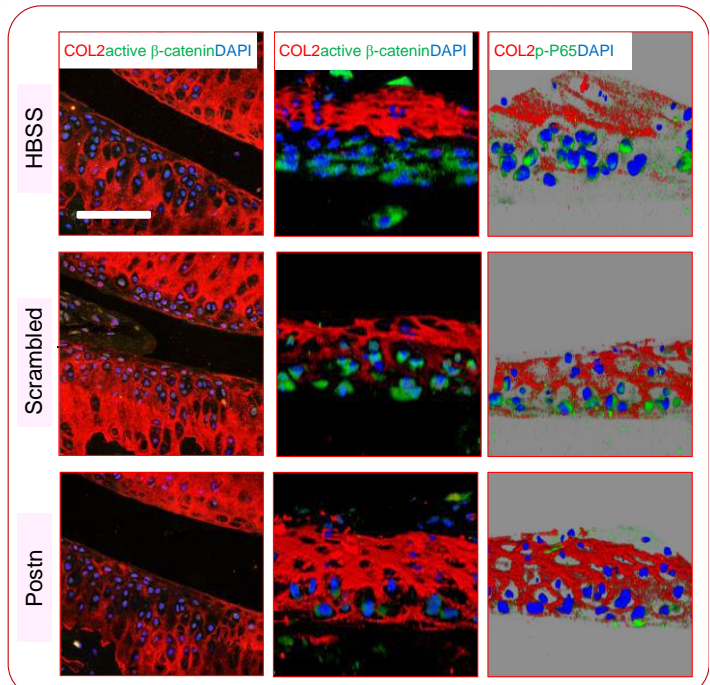


compared to both control and scrambled treated knees. Expression of Postn, as demonstrated by immunostaining, was markedly reduced in the cartilage of the Postn siRNA group. Expression of MMP-13 protein was also markedly decreased in the Postn siRNA group in both cartilage and synovium. Postn silencing also inhibited canonical Wnt/ $\beta$ -catenin and NFkB signaling in DMM knees (**Fig. 2**). We further confirmed that in human chondrocytes Postn knockdown abrogated Wnt/ $\beta$ -catenin- and NFkB-dependent catabolic markers.

**Conclusions:** Intra-articular ablation of Postn mitigated post-traumatic OA progression by preserving cartilage matrix and reducing subchondral bone sclerosis. The protective effect on cartilage and bone appears to be mediated via inhibition of canonical Wnt/ $\beta$ -catenin and NFkB signaling. The potential of Postn inhibition to delay/prevent post-traumatic OA merits further investigation in large pre-clinical and clinical models.

**References:** 1. Chen et al. Bone Res 2017; 5:16044. 2. Maldonado et al. Biomed Res Int 2013; 2013:284873. 3. Chinzei et al. Osteo Carti 2018; 26:588. 4. Attur et al. FASEB J 2015; 29:4107. 5. Zhang et al. Sci Rep. 2017; 7:41634. 6. Zhou et al. Curr Rheumatol Rep. 2017; 19:53. 7. Yan et al PNAS. 2016; 113:E6199.

**Fig. 2**



## Histone deacetylase 3 in bone development and skeletal disorders

*Jennifer J. Westendorf, PhD. Mayo Clinic, Rochester, MN*

Histone deacetylases (Hdac) are enzymes that remove acetyl groups from lysine residues on histones and other proteins. Hdac inhibitors are FDA-approved epigenetic-based therapies for some cancers and neurological disorders; however, their use is limited because they block multiple Hdacs and produce side effects. We previously showed that Hdac inhibitors cause bone loss in vivo. To better understand how Hdacs contribute to endochondral ossification, we conditionally deleted Hdac3 pre- and postnatally in Col2a1-expressing chondrocytes. Hdac3 was required for viability during embryogenesis. Postnatal deletion of Hdac3 delayed secondary ossification center formation and slowed growth plate chondrocyte maturation. Other skeletal phenotypes of the mice included increased cortical bone density, increased marrow adiposity, thicker articular cartilage at 8 but not 4 weeks of age, and increased osteoclast activity. To understand these phenotypes, RNA sequencing and ChIP sequencing were performed. Hdac3-deficient chondrocytes expressed more cytokine and matrix-degrading genes (Il-6, Mmp3) and fewer genes related to extracellular matrix production, bone development and ossification (Acan, Col2a1). H3K27 acetylation was higher within and near induced genes but was not altered in downregulated genes. Increased cytokine signaling promoted autocrine activation of Jak-Stat signaling, suppressed chondrocyte maturation, and induced paracrine activation of osteoclasts and bone resorption. Blockade of Il-6–Jak–Stat signaling and bromodomain extra terminal proteins, which recognize acetylated lysines and promote transcriptional elongation, significantly reduced Il-6 and Mmp13 expression in Hdac3-deficient chondrocytes, as well as secondary osteoclast activation. Ruxolitinib, a Jak inhibitor, reduced osteoclast activity in Hdac3 CKO mice. Thus, Hdac3 controls the temporal and spatial expression of tissue-remodeling genes in chondrocytes via epigenetic mechanisms to ensure proper endochondral ossification.

## Defining DNMT3b and Downstream Targets in the Pathogenesis of Osteoarthritis

Jie Shen, PhD, Cuicui Wang PhD, Jun Ying, MD, and Regis J. O'Keefe, MD, PhD

We have demonstrated that the development of OA is associated with reduced expression of the DNA methyltransferase enzyme, Dnmt3b, in articular chondrocytes. Gene deletion of Dnmt3b resulted in catabolism and progression of osteoarthritis (OA) in murine articular cartilage through a mechanism involving increased mitochondrial respiration. We have identified two targets downstream of Dnmt3b, TGF- $\beta$ /BMP signaling and 4-aminobutyric acid transferase (Abat). Both TGF- $\beta$ /BMP signaling and Abat alter cellular energy metabolism. Abat is an enzyme that metabolizes gamma-aminobutyric acid to succinate, a key intermediate in the tricarboxylic acid cycle, and thus directly influences cell energy metabolism and mitochondrial respiration. We show that Dnmt3b binds to the *Abat* promoter, increases methylation of a conserved CpG sequence just upstream of the transcriptional start site, and inhibits *Abat* expression. *Dnmt3b* deletion in articular chondrocytes results in reduced methylation of the CpG sequence in the *Abat* promoter that subsequently increases expression of *Abat*. Increased Abat expression in chondrocytes leads to enhanced mitochondrial respiration, and elevated expression of catabolic genes. Over-expression of Abat in murine knee joints via lentiviral injection results in accelerated cartilage degradation following surgical induction of OA. In contrast, lentiviral-based knock down of Abat attenuates the expression of IL-1 $\beta$ -induced catabolic genes in primary murine articular chondrocytes *in vitro*, and also protects against murine articular cartilage degradation *in vivo*. Strikingly, treatment with the FDA approved small molecule Abat inhibitor, Vigabatrin, completely prevents the development of injury-induced OA in mice. In summary, these studies establish Abat as an important new target for therapies to prevent OA.

## Genome-wide DNA Methylation Changes in Mice Under Simulated Microgravity Conditions

*Raúl F. Pérez, Juan Ramón Tejedor, Agustín F. Fernández, Mario F. Fraga*

*Nanomaterials and Nanotechnology Research Center (CINN-CSIC), Universidad de Oviedo, Principado de Asturias, Spain.*

*Instituto Universitario de Oncología del Principado de Asturias (IUOPA), Hospital Universitario Central de Asturias (HUCA), Universidad de Oviedo, Principado de Asturias, Spain.*

*Fundación para la Investigación Biosanitaria de Asturias (FINBA), Instituto de Investigación Sanitaria del Principado de Asturias (ISPA), Principado de Asturias, Spain.*

Epigenetic marks such as DNA methylation regulate gene expression through the biochemical modification of the chromatin landscape, in central processes such as development, aging or cancer. These mechanisms play an important role in the assimilation of environmental stimuli and execution of responses by the genomic function. Thus, extrinsic factors such as xenobiotics, diet or stress have been extensively associated to the alteration of epigenetic pathways. In this setting, a profound environmental alteration like the experiencing of zero-gravity conditions in space is known to produce severe alterations in bone physiology. In consequence, epigenetic marks constitute clear candidates for the regulation of mechanisms which orchestrate these stimuli-induced changes. The murine tail suspension model has been widely used to study mechanical alterations in bone biology and could serve as a proxy of the weightlessness experienced during space travel. Therefore, we have performed a genome-wide analysis of the DNA methylation changes associated to tail suspension by the use of Reduced Representation Bisulfite Sequencing (RRBS). We have found extensive DNA methylation changes across the genome, predominantly loss of methylation enriched at CpG-sparse locations. The alterations were found at different gene locations including genes related to bone physiology, pointing towards a relationship between epigenetic mechanisms and the biological response to the tail-suspension stimulus, suggesting that a zero-gravity environment in space could also be associated to DNA methylation changes.



## From Therapeutics Target Identification to Drug Development: XLH, FGF23, and Burosumab

Javier San Martin, MD<sup>1</sup>

<sup>1</sup>Ultragenyx Pharmaceutical Inc, Novato, CA, USA

X-linked hypophosphatemia (XLH) was first described as vitamin D resistant rickets in 1937, and characterized by high phosphate excretion and rickets.<sup>(1)</sup> More than 50 years later, using a positional cloning approach, researchers linked this phosphate wasting disorder to loss-of-function mutations in *PHEX* (phosphate-regulating gene with homology to endopeptidase on the X chromosome).<sup>(2)</sup> *PHEX* encodes a member of the M13 family of endopeptidases, and is predominantly expressed in osteoblasts, osteocytes, and teeth.<sup>(3)</sup> Less than a decade later, researchers found patients with XLH had elevated levels of fibroblast growth factor 23 (FGF23),<sup>(4)</sup> a secreted protein hormone implicated in a similar phosphate wasting disorder called autosomal dominant hypophosphatemic rickets.<sup>(5)</sup> In the renal tubule of the kidney, active FGF23 binds a protein cofactor called Klotho on its c-terminus and a receptor called FGFR1 on its n-terminus, leading to downstream inhibition of Na-Pi co-transport and 1 $\alpha$ -hydroxylase activity in the renal proximal tubule cell;<sup>(6)</sup> this inhibition results in decreased serum phosphorus, TmP/GFR, and 1,25-dihydroxyvitamin D (1,25(OH)<sub>2</sub>D). The mechanism by which *PHEX* leads to inhibition of FGF23 is still unknown. In the *PHEX*-deficient hypophosphatemic mouse model, Hyp, an injection of murine anti-FGF23 antibody restored phosphate homeostasis as demonstrated by increased serum phosphorus and 1,25(OH)<sub>2</sub>D, increased expression of the Na-Pi co-transporters and 1 $\alpha$ -hydroxylase, and decreased expression of 24-hydroxylase in the kidney.<sup>(7)</sup>

Understanding the underlying pathophysiology of XLH, excess FGF23, led to the development of burosumab – a fully human, monoclonal antibody that binds and inhibits FGF23 activity. Antibody therapy has been historically well-tolerated and effective for therapeutic targets that are in circulation or exposed on cellular surfaces. Additionally, the long-lasting pharmacokinetics of antibody therapy allows for less frequent dosing. In a partnership between Kyowa Hakko Kirin and Ultragenyx Pharmaceutical Inc., the safety and efficacy of burosumab was established in a clinical program consisting of 12 studies in children and adults with XLH. Prior to this partnership there were no controlled clinical trials in subjects with XLH and no regulatory guidance on interventional trials for XLH. Retrospective and non-interventional research, such as patient interviews and chart reviews, helped set the stage for determining clinically meaningful endpoints for this rare disease. Across the clinical program, data were collected on pharmacodynamic, radiographic, histological, and physical outcomes.<sup>(8-12)</sup> Early clinical trials focused on dose regimen, preliminary efficacy, and therapeutic range. Late stage clinical trials demonstrated the clinical benefit beyond restoring phosphate homeostasis. Also in late stage trials, careful consideration went into deciding how to design studies with appropriate comparator arms, given the lack of standardization and data with use of oral phosphate salts and vitamin D metabolites in patients with XLH. The clinical program also informed the safety profile. This favorable benefit:risk profile led to regulatory approval of burosumab for the treatment of XLH in the United States and Europe in 2018 (conditions of approval vary). While this program was able to evaluate the biochemical and clinical features of the disease, future research will be necessary to understand and address additional clinical features of XLH such as dental health, enthesopathy, and early osteoarthritis.

## References

1. Albright F et al. *Am J Dis Child*. 1937;54:529-47.
2. Francis F et al. *Nat Genet*. 1995;11(2):130.
3. Beck L et al. *J Clin Invest*. 1997;99(6):1200-9.
4. Yamazaki et al. *J Clin Endocrinol Metab*. 2002 Nov;87(11):4957-60.
5. Bianchini J et al. *Birth Defects Orig Artic Ser*. 1971;7:287-94.
6. Levine BS et al. *Clin J Am Soc Nephrol*. 2009;4(11):1866-77.
7. Aono Y et al. *J Bone Miner Res*. 2009;24(11):1879-88.
8. Whyte MP et al. *Lancet Diabetes Endocrinol*. 2019;7(3):189-99.
9. Imel EA et al. *Lancet*. Epub 2019/05/21.
10. Portale AA et al. *Calcif Tissue Int*. 2019;1-14.
11. Carpenter TO et al. *N Engl J Med*. 2018;378(21):1987-98.
12. Insogna KL et al. *J Bone Miner Res*. 2018;33(8):1383–93.

## Targeting a Unique Pathophysiology for Improved Outcomes in X-Linked Hypophosphatemia

Thomas O. Carpenter, MD

Yale University School of Medicine, New Haven, CT

X-Linked Hypophosphatemia (XLH) is caused by loss-of-function mutations in *PHEX*, and is the prototype disorder of excess activity of the phosphatonin, FGF23. In addition to childhood manifestations of rickets, skeletal deformities and short stature, the disorder has significant morbidity in adulthood, including bone pain, weakness, mineralizing enthesopathy, fractures/pseudofractures, poor dentition and hearing loss.

As excessive renal phosphate loss and altered vitamin D metabolism are cardinal features in XLH, conventional therapy has consisted of frequent doses of oral phosphate with co-administration of 1,25 dihydroxyvitamin D. The treatment is cumbersome, requires frequent monitoring, and often leaves patients with incomplete correction of deformity. With the identification of FGF23 as the primary mediator of the renal phosphate wasting, therapies directed to this unique pathophysiology have been developed. Two Phase 2 clinical trials in children using the humanized monoclonal antibody (burosumab) to inhibit FGF23 activity as a novel therapeutic approach for XLH have shown improvements in biochemical, radiographic, and patient-reported outcomes after 40 weeks in 5-12 year olds, and in 1-4 year olds with XLH, despite prior conventional therapy. A recent Phase 3 randomized head-to-head trial of burosumab vs calcitriol/phosphate has documented more rapid correction of radiographic and biochemical abnormalities than conventional therapy. Finally, a phase 3 study in adults with XLH showed improved biochemical and patient-related outcomes with burosumab therapy as compared to a placebo-treated group, as well as a striking increase in the healing of the prevalent fractures and pseudofractures evident at baseline.

XLH is a lifelong disorder with significant morbidities in adulthood. Both children and adults affected with XLH would likely benefit from a more effective and better-tolerated therapy than conventional measures. Administration of burosumab improved clinically important outcomes in growing children, and in affected adults biochemical, radiographic, and patient-reported outcomes all improved. Inhibition of FGF23 activity using an anti-FGF23 inhibitory antibody appears to be safe and effective for improving outcomes in this lifelong condition.

## Fibrodysplasia Ossificans Progressiva and Multiple Osteochondroma: Two distinct pediatric disorders, one drug treatment for both

Maurizio Pacifici, PhD<sup>1</sup>

<sup>1</sup>Children's Hospital of Philadelphia, Philadelphia, PA, USA

Fibrodysplasia Ossificans Progressiva (FOP) and Multiple Osteochondroma (MO) are distinct, rare and often severe pediatric conditions that are caused by mutations in different genes: *ACVR1* and *EXT1/EXT2*, respectively. *ACVR1* encodes the bone morphogenetic protein (BMP) receptor ALK2, while *EXT1* and *EXT2* encode Golgi glycosyltransferases responsible for heparan sulfate (HS) synthesis. FOP involves the formation of heterotopic endochondral bone starting at young age that accumulates throughout the body over time at the expense of muscles and connective tissues. MO (also known as Hereditary Multiple Exostoses or HME) involves the formation of benign cartilaginous/bony tumors within the perichondrium flanking the growth plates. In both FOP and MO, such ectopic tissue masses eventually hamper normal skeletal growth and function, causing skeletal deformations, chronic pain, reduced joint mobility and ankyloses, and progressive loss of life quality. Studies in mouse models showed that the gain-of-function *ACVR1* mutations in FOP result in excessive canonical BMP signaling and provoke formation of heterotopic bone. Studies in my lab showed that similarly, the loss-of-function *EXT1* or *EXT2* mutations cause ectopic canonical BMP signaling within perichondrium and induce formation of osteochondromas. Because of such shared pathogenesis, FOP and MO could plausibly be amenable to a similar drug treatment. We had previously identified the retinoic acid receptor (RAR) gamma agonist Palovarotene as a powerful drug treatment for FOP in mouse models and found it to effectively antagonize canonical BMP signaling. More recently, we demonstrated that targeting such signaling pathway also represents a very effective treatment for MO in mouse models. These and other studies have provided the basis and rationale for two ongoing clinical trials to test Palovarotene as a therapeutic for both FOP and MO patients. Thus, one drug appears to offer a first ever remedy for two very distinct pediatric disorders. I

7:00 AM – 8:00 AM	Breakfast & Registration
7:50 AM – 8:00 AM	<b>ORS Membership Presentation</b> <i>Presenter: Christopher Hernandez, PhD</i>
8:00 AM - 9:00 AM	<b>ASBMR/Harold M. Frost Young Investigator Award Presentations</b> <i>Chair: Teresita Bellido, PhD (Indiana University)</i>
	<b>Vitamin D Receptor Signaling Prevents the Adverse Actions of Glucocorticoid Excess in Bone, Skeletal Muscle, and the Heart, by Interfering with the Atrogene Pathway</b> <i>Amy Sato, PhD (Indiana University School of Medicine)</i>
	<b>Could Many Non-Contact Anterior Cruciate Ligament Injuries be a Result of Fatigue-Damage Accumulation?</b> <i>Stephan Schlecht, PhD (University of Michigan)</i>
	<b>Osteocalcin Deficiency Rescues Glucose Metabolism in a Model of Severe Osteogenesis Imperfecta</b> <i>Josephine Tauer, PhD (McGill University)</i>
	<b>Stimulation of Piezo1 by Mechanical Signals Promotes Bone Anabolism</b> <i>Jinhu Xiong, PhD (University of Arkansas for Medical Sciences)</i>
9:15 AM - 12:00 PM	<b>Musculoskeletal Regenerative Medicine Meets the Clinic</b> <i>Chair: Lisa Larkin, PhD (University of Michigan)</i>
	<b>Bridge Enhanced ACL Repair: From Concept to Clinical Trial</b> <i>Braden Fleming, PhD (Rhode Island Hospital/Warren Alpert Medical School of Brown University)</i>
	<b>Rotator Cuff Healing: Gaps in Knowledge, Progress and Opportunities</b> <i>Kathleen Derwin, PhD (Cleveland Clinic)</i>
	<b>A Tissue Engineering Approach to Repair Volumetric Muscle Loss</b> <i>Lisa Larkin, PhD (University of Michigan)</i>
12:30 PM – 5:00 PM	<b>Guided Hikes</b>
	<b>Pioneer Cabin</b> <i>(rigorous, 8 miles round-trip, led by David Burr)</i>
	<b>TBD Location</b> <i>(shorter and easy, led by Sue Bloomfield)</i>
	Attendees meet at the back door of the Sun Valley Resort Inn at 12:30 PM
7:30 PM - 9:30 PM	<b>Targeting Musculoskeletal Tissues</b> <i>Chair: Brendan Boyce, MD (University of Rochester Medical Center)</i>
	<b>Introduction to Targeting Strategies</b> <i>Brendan Boyce, MD (University of Rochester Medical Center)</i>
	<b>Targeting Chloroquine and Hydroxychloroquine to Bone to Increase Bone Mass</b> <i>Brendan Boyce, MD (University of Rochester Medical Center)</i>
	<b>Genome Engineering of New Stem Cell Therapies for Arthritis</b> <i>Farshid Guilak, PhD (Washington University)</i>
	<b>Bone-targeting Bortezomib in Pre-clinical Myeloma Studies</b> <i>Lianping Xing, PhD (University of Rochester Medical Center)</i>

## Vitamin D receptor signaling prevents the adverse actions of glucocorticoid excess in bone, skeletal muscle, and the heart, by interfering with the atrogene pathway.

Amy Y. Sato, PhD<sup>1</sup>, Meloney Gregor,<sup>1</sup> David L. Halladay,<sup>1</sup> Karyn A. Esser, PhD<sup>2</sup>, Munro Peacock, MD<sup>3</sup>, Monte S. Willis, MD PhD MBA<sup>4</sup>, Teresita M. Bellido, PhD<sup>1,3,4,5</sup>

<sup>1</sup>Department of Anatomy and Cell Biology, Indiana University School of Medicine, Indianapolis, IN, <sup>2</sup>Department of Physiology and Functional Genomics, University of Florida College of Medicine, Gainesville, FL, <sup>3</sup>Division of Endocrinology, Department of Medicine, Indiana University School of Medicine, Indianapolis, IN, <sup>4</sup>Indiana Center for Musculoskeletal Health, University of Indiana School of Medicine, Indianapolis, IN, <sup>5</sup>Richard L. Roudebush Veterans Affairs Medical Center, Indianapolis, IN.

Glucocorticoid (GC) excess has adverse effects in bone and skeletal muscle that lead to increase in fracture risk. GCs upregulate in both tissues the expression of the proteasomal degradation inducers MuRF1, atrogin1, and MUSA1 (atrogenes), thus providing a targetable pathway to prevent GC musculoskeletal actions. We investigated here whether Vitamin D receptor (VDR) activation, which has beneficial effects in bone and may prevent muscle weakness and falls, blocks GC-induced activation of the atrogene pathway and prevents bone and muscle loss. 1,25D<sub>3</sub> (calcitriol) prevented dexamethasone (dex)-induced atrogene expression *ex vivo* in murine bone and muscle organ cultures. *In vivo*, 1,25D<sub>3</sub> or the less hypercalcemic VDR ligand eldecacitol-71 (ED) at 50ng/kg/d 5x/wk prevented the decrease in BMD induced by GC (2.1 mg/kg/d prednisolone pellets, 8 wks, N=10-12) in 4mo C57Bl6 female mice and simultaneously prevented the increase in atrogene expression in bone. Further, 1,25D<sub>3</sub> and ED prevented GC-mediated increase in the bone resorption marker CTX and the decrease in the bone formation markers P1NP and OCN. Both VDR ligands also prevented GC-induced loss of lean body mass, a muscle mass index measured by DEXA, and the decrease in muscle strength, assessed *in vivo* by plantarflexion torque function testing. Further, consistent with clinical evidence, *in vivo* echocardiography demonstrated that GC induced cardiac dysfunction in our mouse model of GC excess. GC-treated mice exhibited decreased left ventricular (LV) anterior and posterior wall thickness at diastole (relaxed) and systole (contracted). In addition, GC increased LV volume at systole, reduced ejection fraction, and decreased fractional shortening, all indexes of inefficient heart contraction. Both VDR ligands prevented LV wall thinning and the dysfunctional heart contraction induced by GC. GC or the VDR ligands did not alter total heart mass, LV mass, or heart rate. Further, GC increased atrogene expression also in the heart *in vivo* and *ex vivo* in murine LV organ cultures. 1,25D<sub>3</sub> prevented GC-induced atrogene expression *ex vivo*, and both 1,25D<sub>3</sub> and ED prevented the increase in MuRF1 induced by GC *in vivo*. These findings demonstrate that atrogene upregulation is a common mechanism underlying the damaging effects of GC excess in bone, skeletal muscle, and heart; and that activation of VDR signaling preserves tissue mass and function by interfering with GC actions on the atrogene pathway in each of these organs.

# Could many non-contact anterior cruciate ligament injuries be a result of fatigue-damage accumulation?

Stephen H. Schlecht, PhD<sup>1</sup>, Jinhee Kim, MS<sup>2</sup>, Junjie Chen, PhD<sup>3</sup>, So Young Baek, ME<sup>1</sup>, James A. Ashton-Miller, PhD<sup>1</sup>, Mark M. Banaszak Holl, PhD<sup>2</sup>, Edward M. Wojtys, MD<sup>1</sup>

<sup>1</sup>University of Michigan, Ann Arbor, MI, USA, <sup>2</sup>Monash University, Clayton, Victoria, AUS, <sup>3</sup>GlaxoSmithKline, King of Prussia, PA, USA

**Introduction:** The prevailing dogma is that a majority of non-contact ACL failures result from an abrupt shift in ACL load during an awkward movement<sup>1</sup>. This perspective is largely derived from injury video analyses<sup>2</sup> that suggest many ACL injuries result from excessive knee abduction during landing, pivoting, and cutting maneuvers<sup>3</sup>. While this can transpire, it does not explain many non-contact injuries that occur during routine athletic maneuvers. We hypothesize that non-contact ACL failures may result from accumulated tissue fatigue damage resulting from repetitive sub-maximal loading and that this damage signature correlates with that of failed ACLs removed from patients during ACL reconstruction.

**Methods:** With IRB approval, 12 pairs of knees were acquired from donors between 21-64 years of age from the University of Michigan Medical School and Gift of Life Michigan. Knees from 7 donors were fatigue tested with their contralateral used as an internal control. Knees of 5 donors were used for asymmetry analyses. Knees were dissected while preserving the capsule and trans-knee muscle tendons. Knees were tested at 4x body weight using a custom apparatus that simulates a repeated single-leg pivot landing, allowing for impulsive knee compression and flexion, internal tibial torque, and trans-knee muscle force loads<sup>4</sup>. Cyclic loading was performed for 100 loading trials or until the ACL failed. Femoral ACL entheses were then removed from both knees of each donor using an 'outside-in' surgical procedure. Femoral ACL explants were also collected from 5 patients undergoing ACL reconstructive surgery. Patients ranged from 16-44 years of age. Multi-scalar analyses of fatigue-induced damage were conducted on donor and patient cryosectioned tissue (20µm thick) and included atomic force microscopy-infrared (AFM-IR), fluorescent imaging of a collagen hybridizing peptide (CHP) that binds to disrupted tropocollagen and second harmonic imaging microscopy (SHIM). Damage signatures of donor and patient tissue were compared using a two-tailed paired t-test to test for significant differences ( $p < 0.05$ ).

**Results:** AFM-IR revealed a 1740cm<sup>-1</sup> spectral band in tested and patient tissue, but not in controls (Fig 3A). This is a chemical signature of a disrupted collagen backbone structure. Spectroscopic assignment of this band was confirmed using a CHP fluorescent probe to detect unraveled collagen triple helices. Tested and patient

tissue showed more CHP fluorescent intensity than controls ( $p = 0.02$ ). AFM revealed a thinner tissue surface topography ( $p < 0.001$ ) and 45% greater mean void density ( $p = 0.08$ ) in tested and patient tissue compared to controls (Fig 3B). Thinner surface topography is a result collagen triple helix unraveling. Voids were 30-100nm in size and consistent with ACL fibril width. Tested and patient tissue also showed a lower SHIM signal intensity ( $p < 0.001$ ) than that of controls, indicating collagen crystallinity breakage regions consistent with ACL fibril width (10-100µm) (Fig 3C).

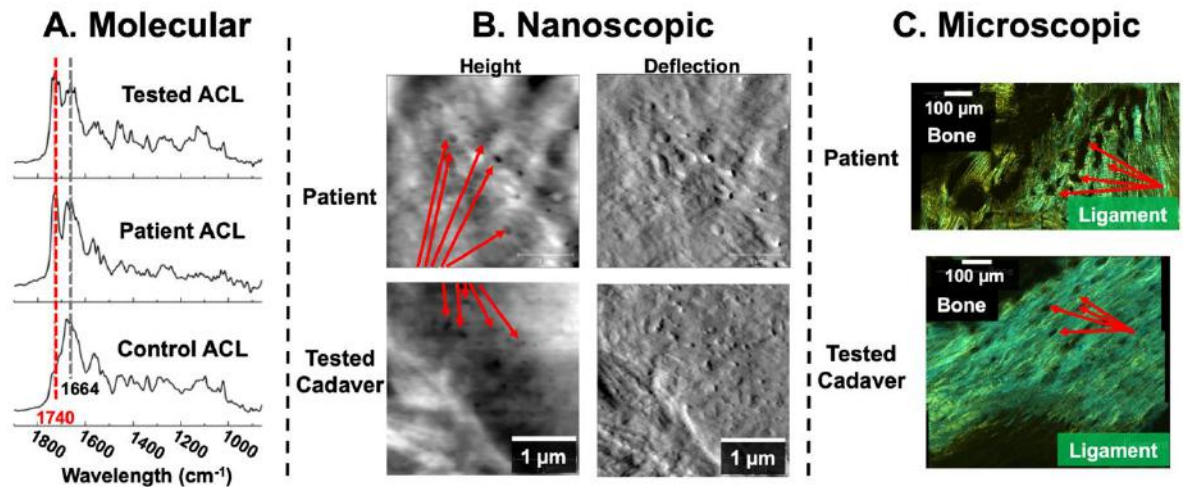


**Figure 1.** Hierarchical collagen damage comparison. A) Distinct 1740cm<sup>-1</sup> band (red dashed line) in tested knees and patients indicating disrupted tropocollagen. Only the Amide I 1664cm<sup>-1</sup> band (black dashed line) is prominent in controls. B) Distinct voids (arrows) in tested knees and patients comparable to the size of collagen fibrils (30-100nm). C) Collagen fiber sized (10-100µm) fluorescent signal loss (arrows) in tested knees and patients (i.e., collagen crystallinity breakage).

**Discussion:** This *in vivo* experiment generated multi-scalar tissue damage signatures also present in patients that suffered an *in vivo* ACL tear. Thus, ACL injuries in these patients may be a result of material fatigue damage within collagen fibrils and fibers that accumulated at a rate beyond their physiological repair capacity. Moreover, our *in vitro* and *in vivo* findings suggest that hierarchical structural changes within the ACL femoral enthesis may at least in part be responsible for a reduction in structural integrity of the ACL occurring as a result of repetitive athletic maneuvers.

**Significance:** At least some, if not many, non-contact ACL injuries may be more attributable to tissue overuse as damage accumulates and propagates at a faster rate than can be repaired, than to a single overload event caused by an unusually large ACL strain via an awkward movement. This hypothesis is currently being confirmed *in vivo* using a murine model<sup>5</sup>.

**References:** <sup>1</sup>Hewett et al. 2005. Am J Sports Med; <sup>2</sup>Boden et al. 2009. Am J Sports Med; <sup>3</sup>Quatman et al. 2011. J Orthop Res; <sup>4</sup>Wojtys et al. 2016. J Orthop Res; <sup>5</sup>Schlecht et al. 2019. J Orthop Res. **Funding:** NIH/NIAMS AR070903 (SS); AR054821 (EW, JAM); AR069620 (JAM, SS)

# Osteocalcin deficiency rescues glucose metabolism in a model of severe Osteogenesis imperfecta.

Josephine T. Tauer, PhD<sup>1</sup>, Svetlana V. Komarova, PhD<sup>1</sup>

<sup>1</sup> Shriners Hospital for Children and Faculty of Dentistry, McGill University, Montreal, Quebec H4A 0A9, Canada

**Objective:** Osteocalcin, an osteoblast-derived hormone, is among the most abundant proteins in bone and is involved in the regulation of whole-body metabolism, muscle adaptation, reproduction, and cognition. High bone turnover and low bone mass are clinical hallmarks of Osteogenesis Imperfecta (OI), a bone disease mainly caused by mutations in the collagen type I gene. Recently, we have shown that growing mice with a severe form of OI, *Col1a1*<sup>Jrt/+</sup> mice, displayed significantly elevated serum levels of undercarboxylated osteocalcin (GLU13) as well as an altered glucose/insulin metabolism and energy expenditure (Figure 1) (Boraschi-Diaz et al., J Endocrinol. 2017: 234(3)). Additionally, *Col1a1*<sup>Jrt/+</sup> mice fed on a high-fat diet were protected against diet induced obesity but not insulin resistance (Tauer et al, JBMR 2018:32(Suppl1)). To further confirm the role of uOCN, we crossed *Col1a1*<sup>Jrt/+</sup> mice (OI) with mice lacking one or both osteocalcin genes (*OCN*<sup>+/-</sup>, *OCN*<sup>-/-</sup>) to generate OI/*OCN* mice.

**Methods:** Wild-type (WT/WT) and OI/*OCN* mice were phenotypically characterized and random glucose measurements, as well as glucose tolerance tests, were performed

**Results:** Fertile *OCN*<sup>+/-</sup> and *Col1a1*<sup>Jrt/+</sup> mice were used to create the first generation of OI/*OCN* mice. Within the first generation, about 27% of born mice were WT/*OCN*<sup>+/-</sup>, 24% OI/WT, 26% OI/*OCN*<sup>+/-</sup>, and 22% WT/WT. One percent of mice were found dead. For further breeding, OI/*OCN*<sup>+/-</sup> mice were

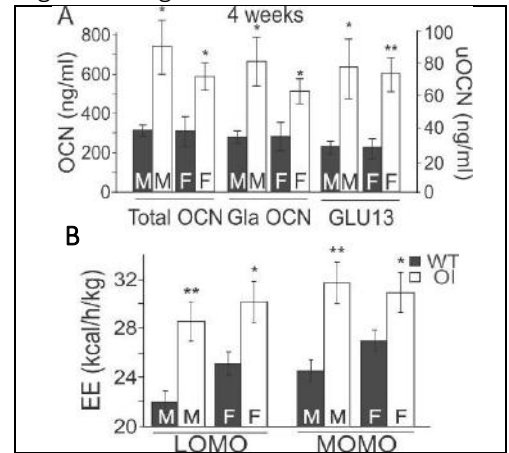


**Figure 1. Circulating OCN levels in OI (A) and energy expenditure (EE) (B) in 4-week old mice<sup>1</sup>.** (A) Total, carboxylated (Gla), and undercarboxylated (GLU13) OCN. (B) . Averaged measures during low mobility (LOMO) and moderate mobility (MOMO) periods for VO2. Data are means±SE, n = 3-4 \*p<0.05; \*\*p<0.01

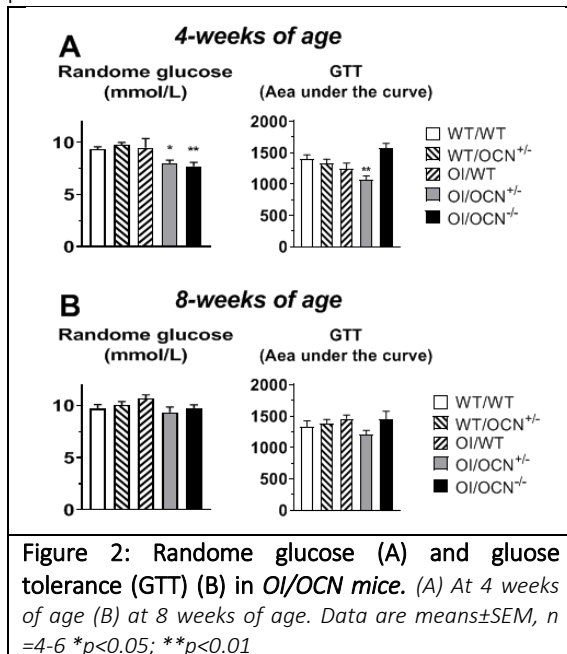


**Figure 2: Random glucose (A) and glucose tolerance (GTT) (B) in OI/*OCN* mice.** (A) At 4 weeks of age (B) at 8 weeks of age. Data are means±SEM, n =4-6 \*p<0.05; \*\*p<0.01

used and gave birth to pups with a genetic distribution of about 18% OI/*OCN*<sup>+/-</sup>, 15% WT/*OCN*<sup>+/-</sup>, 18% OI/*OCN*<sup>-/-</sup>, and 3% WT/*OCN*<sup>-/-</sup> or OI/WT. Twelve percent of mice in the second generation were found dead. Compared to WT/WT, 4-week old mice harboring the genotype OI/WT, OI/*OCN*<sup>+/-</sup>, and OI/*OCN*<sup>-/-</sup> were smaller in size and up to 30% lower in body mass. Weight difference reduced to about 15% difference at 8-weeks of age. At 4 weeks of age, OI/*OCN*<sup>+/-</sup> and OI/*OCN*<sup>-/-</sup> mice exhibited lower random glucose levels than WT/WT littermates, but only OI/*OCN*<sup>+/-</sup> mice revealed improved glucose tolerance while OI/*OCN*<sup>-/-</sup> mice did not differ from WT/WT littermates. However, at 8-weeks of age, no significant differences in random glucose or glucose tolerance were found in OI/*OCN*<sup>+/-</sup> or OI/*OCN*<sup>-/-</sup> mice compared to WT/WT.

**Conclusion:** Genetic inactivation of one or both osteocalcin genes in *Col1a1*<sup>Jrt/+</sup> mice did not affect body mass. However, knockout of both osteocalcin genes restored glucose tolerance to WT levels in *Col1a1*<sup>Jrt/+</sup> mice, strongly supporting the causative role of osteocalcin driving alteration in glucose/insulin metabolism in OI mice.



## Stimulation of Piezo1 by mechanical signals promotes bone anabolism

Xuehua Li, MD, PdD<sup>1,2</sup>, Intawat Nookaew, PhD<sup>1,4</sup>, Erin Mannen, PhD<sup>1,2</sup>, Matthew J. Silva, PhD<sup>5</sup>, Maria Almeida, PhD<sup>1,2,3</sup>, and Jinhu Xiong, PhD<sup>1,2</sup>

<sup>1</sup>Center for Musculoskeletal Disease Research, <sup>2</sup>Department of Orthopaedic Surgery, <sup>3</sup>Division of Endocrinology, and

<sup>4</sup>Department of Biomedical Informatics, University of Arkansas for Medical Sciences, Little Rock, AR, USA. <sup>5</sup>Department of Orthopaedic Surgery, Washington University, St Louis, MO, USA.

Mechanical stimuli increase bone mass by stimulating the activity and production of bone forming osteoblasts. In contrast, loss of mechanical signals decreases bone mass by reducing bone formation and stimulating production of bone resorbing osteoclasts. Osteocytes, which are cells buried in the bone matrix and derived from osteoblasts, are able to sense changes in mechanical load and orchestrate bone resorption and formation. A variety of cell surface proteins and structures, including integrins, focal adhesions, and primary cilia, have been proposed to sense mechanical signals in bone cells. In addition, several lines of evidence suggest that calcium channels are involved in the sensing of mechanical signals by osteocytes. However, a definitive role for a specific calcium channel in the response of the skeleton to mechanical loading has not been demonstrated.

To identify calcium channels that respond to mechanical signals in osteocytes, we compared gene expression profiles of the osteocytic cell line MLO-Y4 under static and fluid flow conditions by RNA-seq. Piezo1 was the most abundant calcium channel transcript among the 78 different calcium channel mRNAs detected in MLO-Y4 cells. In addition, *Piezo1* expression was highly up-regulated by fluid flow in MLO-Y4 cells. Moreover, knock-down of *Piezo1* in MLO-Y4 cells significantly blunted the increase in intracellular calcium induced by fluid-flow as well as fluid-flow stimulation of *Ptgs2* and *OPG*, two well-known targets of fluid shear stress in osteocytes. These results demonstrate that Piezo1 contributes to the response of MLO-Y4 cells to fluid shear stress.

To determine the role of Piezo1 in osteocytes in vivo, we deleted *Piezo1* using a *Dmp1-Cre* transgene. Mice lacking the *Piezo1* gene in *Dmp1-Cre* targeted cells, hereafter referred to as CKO mice, exhibited normal body weight but lower bone mineral density at 5, 8, and 12 weeks of age compared to littermate controls. Micro-CT analysis revealed that cortical thickness was lower in CKO mice compared with controls at 12 weeks of age. Periosteal and endocortical circumferences were also decreased in the femur of CKO mice. In contrast to the changes in bone width, the length of the femurs was not different between genotypes. Analysis of cancellous bone in the femur and vertebra revealed that BV/TV was decreased in CKO mice. Biomechanical testing by 3-point bending showed that the femurs from CKO mice had reduced stiffness and ultimate force. Bone formation rate and osteoblast number were decreased, and osteoclast number was increased, in cancellous bone of CKO mice. Consistent with these cellular changes, gene expression analysis revealed that *Wnt1*, a stimulator of bone formation, was downregulated, whereas *RANKL* expression was increased, in CKO mice.

To determine whether Piezo1 in osteocytes is required for the skeletal response to increased mechanical loading, we performed compressive loading on tibia of 16-week-old CKO and control mice. Two weeks of loading increased periosteal bone formation in control mice, whereas the load-stimulated bone formation was significantly blunted in CKO mice. These results demonstrate that Piezo1 plays an essential role in the response of the skeleton to mechanical loads.

Finally, we determined whether activation of Piezo1 is sufficient to mimic the effects of mechanical stimulation in osteocytes and bone. Treatment of MLO-Y4 cells with Yoda1, a small molecule agonist of Piezo1, increased expression of *Ptgs2* and *OPG*, similar to the effect of fluid flow on these cells. Importantly, silencing of *Piezo1* completely prevented these increases induced by Yoda1. Yoda1 also promoted expression of *Ptgs2*, *OPG*, and *Wnt1*, and decreased *Sost* in cortical bone organ cultures from C57BL/6J mice. To determine whether Yoda1 is able to increase bone mass in vivo, we administered Yoda1 to 4-month-old female WT C57BL/6J mice for 2 weeks. Yoda1 increased cortical thickness and cancellous bone mass in the distal femur. Yoda1 also increased cortical thickness in the vertebra. However, we did not detect changes in cancellous bone volume in vertebrae. Consistent with the effect on bone mass, the serum levels of osteocalcin, a bone formation marker, were increased in Yoda1-treated mice. These results demonstrate that activation of Piezo1 by Yoda1 mimics the effects of fluid shear stress on osteocytes and increases bone mass in mice.

In conclusion, our results demonstrate that Piezo1 is essential for the skeletal response to changes in mechanical load and identify a novel target for anabolic bone therapy.

## **Bridge Enhanced ACL Repair: From Concept to Clinical Trial**

*Braden C. Fleming, PhD<sup>1</sup>, Martha M. Murray, MD<sup>2</sup>*

*<sup>1</sup>Warren Alpert Medical School of Brown University, Providence, RI, USA; <sup>2</sup>Boston Children's Hospital, Boston, MA, USA*

Abstract Body (Calibri Light 11)

Anterior cruciate ligament (ACL) rupture is a common injury, particularly in the young and active population. It produces a severe functional deficit in most patients and increases the patient's risk for pre-mature osteoarthritis. Historically, primary suture repair of the ACL, in which the torn ligament was sutured back together, was plagued with a high failure rate, and was abandoned in the 1980s. ACL reconstruction surgery, where a graft of tendon is implanted to replace the torn ligament, then became the standard of care. While ACL reconstruction has proven to be excellent operation for restoring knee stability, complications such as muscle weakness, graft failure and premature osteoarthritis persist. Thus, new methods for treating this injury are being explored. We focused our efforts on stimulating the injured ACL to heal using a tissue engineering strategy. We determined that the ACL's inability to heal was due to a failure of the intra-articular ligament to form a provisional scaffold, which is required to promote healing. Thus, a bioactive extracellular matrix scaffold was developed to bridge the wound site to facilitate healing. The procedure, which is based on this scaffold, is called Bridge-Enhanced ACL Repair (BEAR). This presentation will highlight the translation of this technology from the bench to the bedside. It will detail the clinical importance of ACL injuries, the reason why primary suture repair was unsuccessful, the development of the bio-active scaffold, the pre-clinical studies performed to demonstrate that the BEAR procedure was safe and effective, the FDA approval process, and the two-year results from the first-in-human study. Additional clinical trials are now underway, and if all goes well, the scaffold could get FDA approval for the treatment of ACL injuries in the future.

## Rotator Cuff Healing: gaps in knowledge, progress and opportunities

Kathleen A. Derwin, PhD

Cleveland Clinic, Cleveland, OH

Rotator cuff tears affect at least 30% of people by age 70 and are a common cause of debilitating pain, reduced function, and weakness in the shoulder (1, 2). Over 250,000 rotator cuff repairs are performed annually in the United States (3), at an estimated \$3 billion in medical costs (4). Despite improvements in the understanding of the disease process and advances in surgical treatment, healing after rotator cuff repair remains a significant clinical challenge. The reported rates of unsuccessful repair range from 20% to 70% depending on patient age, tear size and chronicity, muscle atrophy and degeneration, tendon quality, repair technique, and postoperative rehabilitation (5-7). **Hence, there is a need for strategies to augment the repair by mechanically reinforcing it while biologically enhancing the intrinsic healing potential of the tendon.**

Over the last decade, tissue engineering strategies, including the use of scaffolds, platelet-rich plasma (PRP), specific growth factors, and cell therapy, have been investigated for improving the healing of rotator cuff repairs and/or inducing the regeneration of functional tissues (8, 9). These strategies are conceptually attractive and supported by basic science investigation, but only limited clinical evidence supports their efficacy in improving healing rates and patient functional outcomes (8, 9). It is possible that these products may be effective only in particular patient populations and/or surgical indications. Their efficacy may be dependent on the manner in which they are formulated or delivered. This talk will review the current literature on tissue engineering approaches to improve rotator cuff healing in human subjects. A specific example of our groups' work to design a scaffold for rotator cuff repair, including the role and limitations of laboratory and animal models in the development, will be also be presented.

More fundamentally, many patients with a failed repair report less pain and higher functional scores after surgery (10-12), whereas patients believed to have an intact repair sometimes demonstrate degenerative muscle changes and persistent shoulder weakness (13-20). We postulate that these inconsistent and often paradoxical findings are due to weak relationships between traditional *imaging* measures of structural repair integrity and clinical outcomes. Lack of a precise understanding and an accurate means to measure tendon healing also limit our ability to effectively assess treatment and rehabilitation strategies aimed to improve healing and outcomes. **Hence there is a need for more granular imaging methods to measure tendon healing in human subjects.**

To that end, this talk will also review our groups' work to expand the current definition of rotator cuff healing by quantifying tendon retraction and identifying 'failure with continuity' following repair surgery (21). Progress to measure tendon retraction using CT analysis of implanted radio-opaque markers in a prospective cohort of 125 rotator cuff repair patients and investigate its relationship to repair integrity by traditional MRI and clinical outcomes at 6, 12 and 24 months will be reported. We expect to show associations between tendon retraction and clinical outcomes, and assess the degree to which tendon retraction (failure with continuity) might explain the inconsistent relationships observed between tendon healing and clinical outcomes. These novel measurement methods might then allow improved assessment of treatment strategies aimed to enhance surgical healing and clinical outcomes following rotator cuff repair.

## References

1. Reilly P, Macleod I, Macfarlane R, Windley J, Emery RJ. Dead men and radiologists don't lie: a review of cadaveric and radiological studies of rotator cuff tear prevalence. *Annals of the Royal College of Surgeons of England*. 2006;88(2):116-21. Epub 2006/03/23. doi: 10.1308/003588406X94968. PubMed PMID: 16551396; PMCID: 1964063.
2. Tashjian RZ. Epidemiology, natural history, and indications for treatment of rotator cuff tears. *Clin Sports Med*. 2012;31(4):589-604. Epub 2012/10/09. doi: 10.1016/j.csm.2012.07.001. PubMed PMID: 23040548.
3. Colvin AC, Egorova N, Harrison AK, Moskowitz A, Flatow EL. National trends in rotator cuff repair. *J Bone Joint Surg Am*. 2012;94(3):227-33. Epub 2012/02/03. doi: 10.2106/JBJS.J.00739. PubMed PMID: 22298054; PMCID: 3262185.
4. Vitale MA, Vitale MG, Zivin JG, Braman JP, Bigliani LU, Flatow EL. Rotator cuff repair: an analysis of utility scores and cost-effectiveness. *J Shoulder Elbow Surg*. 2007;16(2):181-7. Epub 2007/04/03. doi: 10.1016/j.jse.2006.06.013. PubMed PMID: 17399623.
5. Tashjian RZ, Hollins AM, Kim HM, Teefey SA, Middleton WD, Steger-May K, Galatz LM, Yamaguchi K. Factors affecting healing rates after arthroscopic double-row rotator cuff repair. *Am J Sports Med*. 2010;38(12):2435-42. Epub 2010/10/30. doi: 10.1177/0363546510382835. PubMed PMID: 21030564.

6. Toussaint B, Schnaser E, Bosley J, Lefebvre Y, Gobeze R. Early structural and functional outcomes for arthroscopic double-row transosseous-equivalent rotator cuff repair. *Am J Sports Med.* 2011;39(6):1217-25. Epub 2011/03/24. doi: 10.1177/0363546510397725. PubMed PMID: 21427446.
7. Koh KH, Kang KC, Lim TK, Shon MS, Yoo JC. Prospective randomized clinical trial of single- versus double-row suture anchor repair in 2- to 4-cm rotator cuff tears: clinical and magnetic resonance imaging results. *Arthroscopy.* 2011;27(4):453-62. Epub 2011/03/30. doi: 10.1016/j.arthro.2010.11.059. PubMed PMID: 21444007.
8. Charles MD, Christian DR, Cole BJ. The Role of Biologic Therapy in Rotator Cuff Tears and Repairs. *Current reviews in musculoskeletal medicine.* 2018;11(1):150-61. Epub 2018/02/08. doi: 10.1007/s12178-018-9469-0. PubMed PMID: 29411322; PMCID: PMC5825350.
9. Amini MH, Ricchetti E, Iannotti J, Derwin K. Rotator cuff repair: challenges and solutions. *Orthop Res Rev.* 2015;7:57-69.
10. Galatz LM, Griggs S, Cameron BD, Iannotti JP. Prospective longitudinal analysis of postoperative shoulder function : a ten-year follow-up study of full-thickness rotator cuff tears. *J Bone Joint Surg Am.* 2001;83-A(7):1052-6. Epub 2001/07/14. PubMed PMID: 11451975.
11. Posada A, Uribe JW, Hechtman KS, Tjin ATEW, Zvijac JE. Mini-deltoid splitting rotator cuff repair: do results deteriorate with time? *Arthroscopy.* 2000;16(2):137-41. Epub 2000/03/08. PubMed PMID: 10705323.
12. Zandi H, Coghlan JA, Bell SN. Mini-incision rotator cuff repair: a longitudinal assessment with no deterioration of result up to nine years. *J Shoulder Elbow Surg.* 2006;15(2):135-9. Epub 2006/03/07. doi: 10.1016/j.jse.2005.06.008. PubMed PMID: 16517354.
13. Goutallier D, Postel JM, Bernageau J, Lavau L, Voisin MC. Fatty muscle degeneration in cuff ruptures. Pre- and postoperative evaluation by CT scan. *Clin Orthop Relat Res.* 1994;304(304):78-83. Epub 1994/07/01. PubMed PMID: 8020238.
14. Thomazeau H, Boukobza E, Morcet N, Chaperon J, Langlais F. Prediction of rotator cuff repair results by magnetic resonance imaging. *Clin Orthop Relat Res.* 1997(344):275-83. Epub 1997/12/31. PubMed PMID: 9372778.
15. Prickett WD, Teefey SA, Galatz LM, Calfee RP, Middleton WD, Yamaguchi K. Accuracy of ultrasound imaging of the rotator cuff in shoulders that are painful postoperatively. *Journal of Bone and Joint Surgery-American Volume.* 2003;85A(6):1084-9. PubMed PMID: ISI:000183208900016.
16. Kyrola K, Niemitukia L, Jaroma H, Vaatainen U. Long-term MRI findings in operated rotator cuff tear. *Acta Radiol.* 2004;45(5):526-33. Epub 2004/11/02. PubMed PMID: 15515515.
17. Fuchs B, Gilbert MK, Hodler J, Gerber C. Clinical and structural results of open repair of an isolated one-tendon tear of the rotator cuff. *J Bone Joint Surg Am.* 2006;88(2):309-16. Epub 2006/02/03. doi: 10.2106/JBJS.E.00117. PubMed PMID: 16452742.
18. Gladstone JN, Bishop JY, Lo IK, Flatow EL. Fatty infiltration and atrophy of the rotator cuff do not improve after rotator cuff repair and correlate with poor functional outcome. *Am J Sports Med.* 2007;35(5):719-28.
19. Liem D, Lichtenberg S, Magosch P, Habermeyer P. Magnetic resonance imaging of arthroscopic supraspinatus tendon repair. *J Bone Joint Surg Am.* 2007;89(8):1770-6.
20. Sugaya H, Maeda K, Matsuki K, Moriishi J. Repair integrity and functional outcome after arthroscopic double-row rotator cuff repair. A prospective outcome study. *J Bone Joint Surg Am.* 2007;89(5):953-60. Epub 2007/05/03. doi: 10.2106/JBJS.F.00512. PubMed PMID: 17473131.
21. McCarron JA, Derwin KA, Bey MJ, Polster JM, Schils JP, Ricchetti ET, Iannotti JP. Failure with continuity in rotator cuff repair "healing". *Am J Sports Med.* 2013;41(1):134-41. Epub 2012/09/29. doi: 10.1177/0363546512459477. PubMed PMID: 23019253.

## **A Tissue Engineering Approach to Repair Volumetric Muscle Loss**

*Lisa Larkin, Ph.D.*

*Professor*

*Molecular & Integrative Physiology*

*Biomedical Engineering*

*University of Michigan*

*Biomedical Science Research Building (BSRB)*

*109 Zina Pitcher Place*

*Room #2025*

*48109-2200*

*Phone: 734-936-8181*

The inherent regenerative capacity of skeletal muscle is overwhelmed in the case of volumetric muscle loss (VML). VML is defined as a muscle volume loss of 30% or more that results in a sustained impairment of function and is often accompanied by peripheral nerve injuries. Current surgical treatments are limited by tissue availability and donor site morbidity. In an effort to combat these limitations, our lab has developed scaffold-free tissue-engineered skeletal muscle units (SMUs) for the treatment of VML. To address the nerve injuries that often accompany VML, our lab has also developed an engineered neural conduit (ENC) composed primarily of collagen to bridge gaps between native nerve and the injury site. This talk will present our latest data on the efficacy of our SMUs and ENCs in restoring muscle function in a clinically relevant large animal model: sheep receiving a 30% VML injury in a load-bearing hindlimb, specifically the peroneus tertius (PT) muscle, following a 3- and 6-month recovery period. This study constitutes a significant step towards development of a VML treatment that restores both muscle mass and force production on a scale that is clinically relevant to humans.

## Targeting Chloroquine and Hydroxychloroquine to Bone to Increase Bone Mass

Zhenqiang Yao<sup>1</sup>, Akram Ayoub<sup>1</sup>, Venkat Srinivasan<sup>1</sup>, Frank H. Ebetino<sup>1,2</sup>, Robert K. Boeckman Jr<sup>1</sup>, Lianping Xing<sup>1</sup>, Brendan F. Boyce<sup>1</sup>, <sup>1</sup>University of Rochester Medical Center, Rochester, NY, USA; <sup>2</sup>BioVinc, Pasadena, CA, USA

**Introduction.** All medications can have adverse effects on non-target tissues. These can be mild and short-lived, such as nausea, acute-phase reaction, rash or headache, or they can be serious, such as coronary thrombosis, stroke, peripheral neuropathy or blindness. These adverse effects typically limit the amount of drug that can be administered. When drugs are used to treat life-threatening diseases, such as cancer or crippling inflammatory conditions, severe adverse effects can be acceptable, but they can still restrict the dose regimens and render treatment less effective. Thus, targeting drugs to specific tissues with linker compounds that have high affinity for such tissues is an attractive strategy. For example, ARIAD Pharmaceuticals developed small molecule inhibitors of Src tyrosine kinase in the 1990s and linked them to bisphosphonate (BP) moieties with no intrinsic anti-osteoclastic activity to target them to bone to treat osteoporosis and metastatic bone disease. This approach was based on prior studies showing that Src expression is required in osteoclasts for effective bone resorption, but it failed because of unanticipated serious side effects in non-human primates in pre-clinical toxicology studies. Since these initial studies, we and others have used related approaches. We reported previously that CQ inhibits osteoclast (OC) formation in vitro and in vivo in mice. More recently, we linked chloroquine (CQ) and hydroxychloroquine (HCQ) (FDA-approved drugs for inflammatory bone diseases) to a BP to enhance their efficacy by delivering higher effective doses to bone, to create a depot release mechanism, and to limit their ocular and other side effects. We have tested these new conjugates in animal models of RA and osteoporosis.

**Methods.** We linked CQ and HCQ to a BP (Figure 1) using a protocol that we developed in-house. We utilized a carbamate-linking group that was designed to be stable in the bloodstream, but labile on bone surfaces, such that the CQ or HCQ would be released over several days at the bone surface in a depot-like fashion, subsequent to delivery to bone.

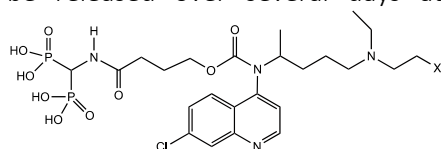


Figure 1. x= Chloroquine or Hydroxychloroquine.

Here, we compared the efficacy of bone-targeted CQ (BT-CQ) and BT-HCQ with CQ and HCQ in standard in vitro OC formation and resorption assays. These included immersing bone slices in CQ, HCQ, BT-CQ and BT-HCQ overnight and then washing the slices in PBS before adding bone marrow macrophages and treating the cells with M-CSF and RANKL to induce OC formation. We also tested the effects of BT-CQ and BT-HCQ in vivo in mouse models of rheumatoid arthritis, ovariectomy- (Ovx) and age-related osteoporosis to determine if they inhibit joint inflammation and bone resorption.

**Results.** 1  $\mu$ M BTCQ inhibited OC and resorption pit formation as effectively as 3  $\mu$ M CQ. After overnight incubation with 0, 10, 30 and 100  $\mu$ M BTCQ or CQ, the bone slices were transferred to wells in new plates to assess OC formation from mouse bone marrow cells. We found that the bone slices incubated with 10, 30 and 100  $\mu$ M BTCQ had a dose-dependent, significantly reduced resorption pit area compared to those incubated with similar doses of CQ. A form of BT-CQ designed such that the linker was not cleavable had no significant effect on resorption pit formation. Furthermore, BT-CQ inhibited RANKL-induced TRAF3 degradation more effectively than CQ. We treated WT mice with BT-CQ or CQ (2, 15 or 50 mg/kg) for 10 days and gave PTH injections (10ug, 3 times per day) during the last 3 days. PTH increased OC formation in tibial sections (361 $\pm$ 74/mm<sup>2</sup> vs. 97 $\pm$ 26/mm<sup>2</sup> in vehicle-treated controls). Only high dose (50 mg/kg; not 15 and 2 mg/kg) CQ inhibited PTH-induced OC formation (189 $\pm$ 55, 312 $\pm$ 84 and 367 $\pm$ 75 OCs/mm<sup>2</sup>, respectively), while BTCQ (as low as 2 mg/kg) effectively prevented PTH-induced OC formation (125 $\pm$ 52/mm<sup>2</sup>). Similarly, BT-HCQ inhibited osteoclast formation and bone resorption in vitro and prevented PTH-induced osteoclast formation in mice in vivo more effectively than HCQ. Interestingly, BT-HCQ pre-treated mesenchymal progenitor cells have enhanced ALP+ OB differentiation. 0.00625 mM/kg BT-HCQ and BT-CQ, but not parent HCQ and CQ, prevented OVX-induced bone loss in mice. Furthermore, BT-HCQ and BT-CQ reversed established bone loss induced by OVX in mice. However, treatment of TNF-transgenic mice with CQ, HCQ, BT-CQ or BT-HCQ did not inhibit joint inflammation, osteoclast formation or bone resorption.

**Conclusion.** BT-HCQ and BT-CQ could be promising agents to treat osteoporosis by targeting delivery of HCQ or CQ to bone and slowly releasing it.

## Genome Engineering of New Stem Cell Therapies for Arthritis

Farshid Guilak, PhD

Department of Orthopaedic Surgery, Washington University and Shriners Hospitals for Children, St. Louis MO USA

Stem cells provide tremendous promise for the development of new therapeutic approaches for musculoskeletal conditions. In addition to their multipotency, certain types of stem cells exhibit immunomodulatory effects that can mitigate inflammation and enhance tissue repair. However, the translation of stem cell therapies to clinical practice has proven difficult due to challenges in intra- and inter-donor variability, engraftment, variability in recipient microenvironment and patient indications, and limited therapeutic biological activity. In this regard, the success of stem cell-based therapies may benefit from cellular engineering approaches to enhance factors such as purification, homing and cell survival, trophic effects, or immunomodulatory signaling. By combining recent advances in CRISPR-Cas9 gene editing, synthetic biology, and tissue engineering, the potential exists to create new classes of “designer” cells that have prescribed cell-surface molecules and receptors, as well as synthetic gene circuits that provide for autoregulated drug delivery or enhanced tissue repair. Here we describe some of the first applications in stem cell engineering to allow for controlled attenuation of their detrimental responses to inflammatory cytokines [e.g., interleukin-1 (IL-1), tumor necrosis factor (TNF)]. For example, murine iPSCs have been engineered to harbor a functional deletion of the interleukin-1 receptor I (*Il1r1*). These cells were capable of synthesizing a cartilaginous matrix that was protected against IL-1-mediated inflammation or tissue degradation, as measured by a decreased expression of pro-inflammatory genes and a reduced loss of proteoglycan content. In other studies, dead Cas9 (dCas9)-KRAB was used for epigenome editing at loci encoding cytokine receptors *IL1R1* and tumor necrosis factor receptor 1 (*TNFR1*) to inactivate these receptors. This approach showed the ability to inhibit downstream activation of NF- $\kappa$ B and to increase stem cell survival, without changes in the gene sequence. Coupling dCas9 with a transactivation domain such as VP64 has been used for highly targeted gene activation providing alternative approaches for conferring anti-inflammatory properties to stem cells or activation of specific transcription factors for inducing stem cell differentiation.

The CRISPR-Cas9 provides a system for targeted gene editing that can allow for epigenetically stable, robust transgene expression for applications in which the use of viral vectors may not be desired. For example, we have used this approach to engineer iPSCs that contain artificial gene circuits that are cytokine-activated and feedback-controlled to regulate the expression of biologic therapies. Such “smart” stem cells were used to engineer articular cartilage capable of inducible and transient anti-inflammatory responses to inflammatory cytokines (Fig. 1). Specifically, using CRISPR gene editing, targeted gene addition of IL1-Ra or soluble TNF receptor (sTNFR1) cDNA downstream of the *Ccl2* promoter was used to produce “smart” iPSCs that initiated a dynamic negative feedback loop upon stimulation with IL-1 or TNF. These iPSCs were engineered to form implantable self-regulating tissue constructs and have shown promising efficacy in early studies in a model of inflammatory arthritis. “Designer” stem cells have the potential to overcome challenges with long-term therapeutic delivery of biologic drugs, as well as limitations involved in cell homing and engraftment. The development of self-regulating or exogenously controlled systems for transgene expression may allow for a new generation of stem cells that can not only be used to engineer tissue replacements, but simultaneously may serve as an inducible and tunable depot for localized delivery of biologic drugs. Furthermore, the field of synthetic biology has made significant advances in the creation of biologic components with precise and controlled responses to stimuli. Application of this toolkit of gene switches, classifiers, and synthetic transcription systems to stem cell therapies for orthopaedic problems may allow for more specific control of the delivery of therapeutic transgenes.

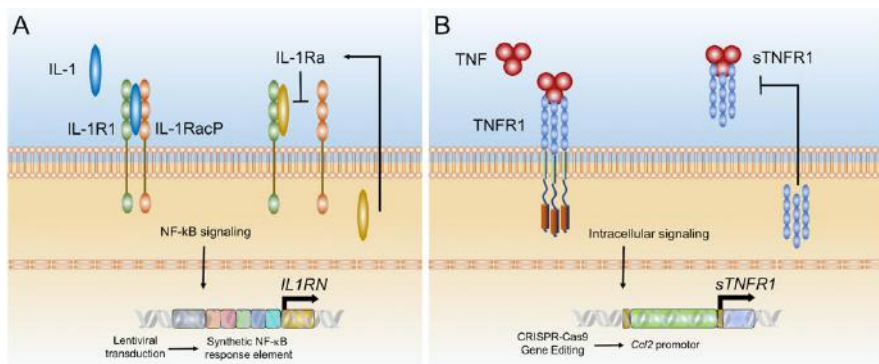


**Fig. 1. Synthetic gene circuits for self-regulating biologic drug delivery systems.** A. Synthetic promoter containing multiple NF- $\kappa$ B recognition motifs upstream of *IL1RN* (gene for IL-1Ra) to create an inducible promoter that is activated by inflammation. B. CRISPR-Cas9 gene editing was used to insert (*sTNFR1*) in the *Ccl2* locus. Activation of the endogenous *Ccl2* promoter by TNF results in dynamic expression of *sTNFR1*, which then inhibits TNF, creating a self-regulating system.



## Bone-Targeting Bortezomib in Pre-Clinical Myeloma Studies

Jianguo Tao<sup>1</sup>, Venkat Srinivasan<sup>1</sup>, Yingchun Zhao<sup>2</sup>, Hengwei Zhang<sup>1</sup>, Peter Villalta<sup>2</sup>, Brendan F. Boyce<sup>1</sup>, Frank H. Ebetino<sup>1,2</sup>, Robert K. Boeckman Jr<sup>1</sup>, Lianping Xing<sup>1</sup>

<sup>1</sup>University of Rochester, Rochester, NY; <sup>2</sup>University of Minnesota, Minneapolis, <sup>3</sup>BioVinc, Pasadena, CA, USA

**Introduction.** Bortezomib (Btz) is a FDA approved proteasome inhibitor to treat multiple myeloma (MM). However, the development of Btz resistance (BR) and neurological adverse effects limit its use. We synthesized a bone-targeted form of Btz by conjugating it to a bisphosphonate (BP) with no anti-resorptive activity. We hypothesize that BP-Btz will more effectively inhibit MM disease in mice than Btz with less neural toxicity due to its longer half-life in bone, which was tested in mice-bearing BR myeloma cells. We also examined overall mouse survival and the pharmacokinetics (PK) of BP-Btz.

**Methods.** 1) NSG mice received intra-tibial injection of 5T.BR (= Btz-resistant 5TMG1-GFP mouse myeloma cells, which we generated) cells and were treated with an equi-molar dose of Btz (0.6 mg/kg) or BP-Btz (1.243 mg/kg) intravenously and assessed tumor burden by measuring GFP intensity using IVIS, bone volume using microCT, and neural damage using electron microscopy (EM). 3) Overall survival was determined in mice-bearing U266 human myeloma cells. 4) PK was evaluated in C57BL/6J WT mice as levels of bone Btz or ubiquitinated proteins by LC-MS/MS, or Western blot.

**Results.** Figure 1. BP-Btz reduces tumor burden, bone destruction, and neural damage in mice-bearing BR 5TMG1-GFP mouse myeloma cells

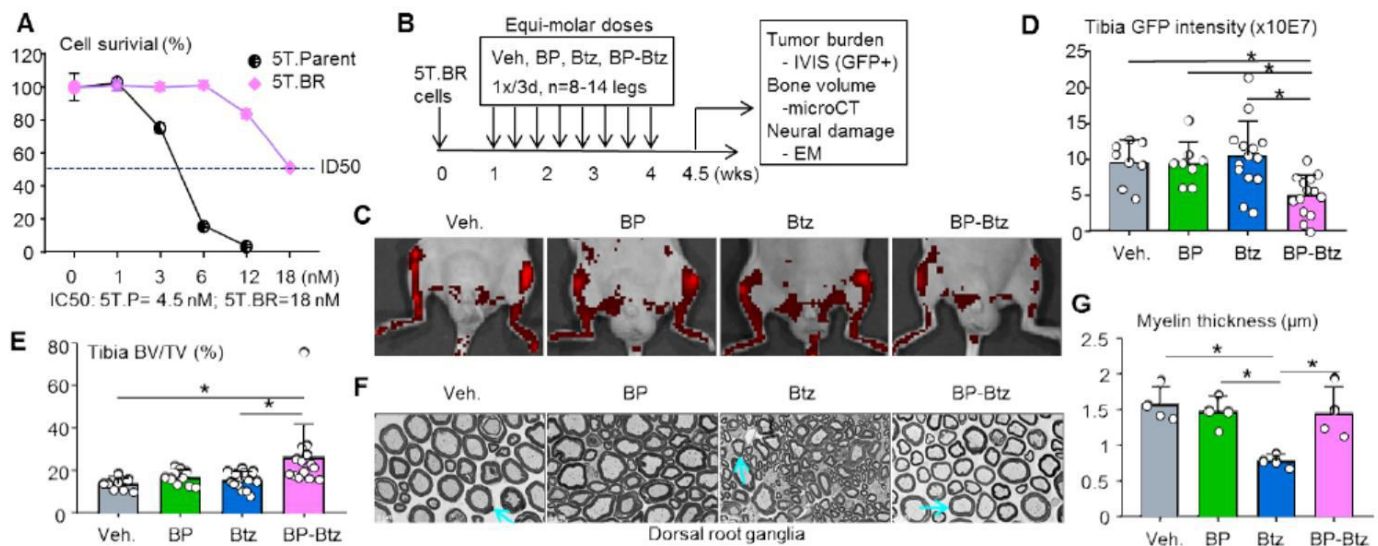


**Figure 1.** (A) 5T.Parent and 5T.BR cells were treated with different doses of Btz. Living cells were identified using a CCK8 kit. (B) Mice received intra-tibial injection of 5T.BR cells and were treated with Btz or BP-Btz for 8 cycles. (C) Representative IVIS images of legs. (D) Tumor burden by GFP intensity. (E) Bone volume by microCT. (F) EM images of cross sections showing changes in myelin thickness and myelinated axons (blue arrows). (G) Myelin thickness measured on EM images. n=4-7 mice/group. Data are mean ± SD. One way ANOVA with Turkey's test. \*p<0.05

Figure 2. BP-Btz increases survival of mice-bearing U266 human myeloma cells, and has longer half-life in bone than Btz.

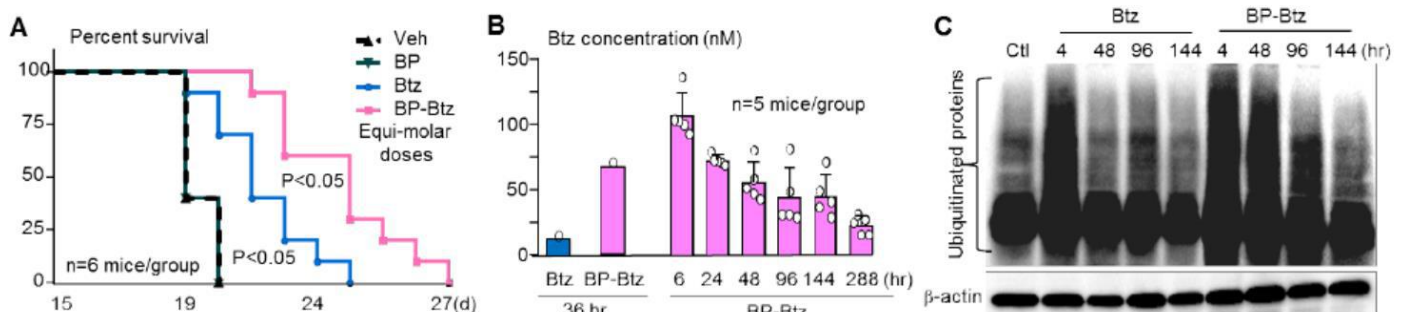


**Figure 2.** (A) Kaplan-Meier curve for mice that received intra-tibial injection of U266 human myeloma cells and were treated with BP, Btz and BP-Btz for 6 cycles, starting on day 10. (B) Btz levels in bones (epiphysis and metaphysis) of Btz- (36 hr) or BP-Btz-treated (6 to 244 hr) mice by LC-MS/MS. (C) Total ubiquitinated-proteins in bone of mice received Btz or BP-Btz by WB.

**Conclusion.** Bone-targeted Btz decreases MM burden and bone loss more effectively than Btz with less systemic side effects, and overcomes Btz resistance. BP-Btz represents a novel therapeutic agent to treat patients with MM.

**Acknowledgments.** This work was supported by research grants from NIH (AR063650, AR069789, AR043510, AR049994).